Final Report RSC-3458-129

MULTIFREQUENCY REMOTE SENSING OF SOIL MOISTURE

by

Sidney W. Theis

Marshall J. McFarland

Wesley D. Rosenthal

Cheryl L. Jones

February 1982

Supported by:

National Aeronautics and Space Administration

Goddard Space Flight Center

Beltsville, Maryland

Contract NSG-5134

TEXAS A&M UNIVERSITY
REMOTE SENSING CENTER
COLLEGE STATION, TEXAS

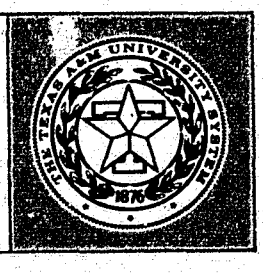

Final Report RSC-3458-129

MULTIFREQUENCY REMOTE SENSING OF SOIL MOISTURE

By

Sidney W. Theis
Marshall J. McFarland
Wesley D. Rosenthal
Cheryl L. Jones

Remote Sensing Center
Texas Engineering Experiment Station
Texas A&M University System
College Station, Texas 77843

February 1982

Supported by:

National Aeronautics and Space Administration
Goddard Space Flight Center
Beltsville, Maryland

Contract NSG-5134

TABLE OF CONTENTS

Page

LIST OF FIGURES

LIST OF TABLES

PREFACE

The final report of Project RSC-3458, "Measurement of Soil Moisture Trends with Airborne Scatterometers" is divided into three volumes. The first volume deals primarily with the work completed by Dr. Sidney Theis relating multispectral (visible through microwave) information to soil moisture trends in bare and vegetated fields. The second volume deals primarily with the work of Dr. Wesley Rosenthal in relating the same multispectral data sets to agricultural crop classification and biomass estimation. The third volume by Ms. Cheryl Jones, details field work, aircraft schedules, data processing and calibrations, and the final data sets.

ABSTRACT

Monitoring soil moisture changes by remote means requires timely and repetitive sensor coverage. This dictates that the sensor must have all-weather capabilities. Microwave sensors have this capability. Until recently, microwave remote sensing of soil moisture has been limited to determining the best single sensor with the maximum sensitivity to soil moisture. Visible/near-infrared sensors have been developed that estimate biomass and discriminate between crops. Vegetation over a particular area does not change as rapidly as surface soil moisture. Therefore the absence of all-weather capabilities is not a severe limitation when visible/near-infrared biomass estimates are combined with microwave sensors to estimate soil moisture.

Multifrequency sensor data from NASA's C-130 aircraft were used 1) to determine which of the all-weather microwave sensors demonstrated the highest correlation to surface soil moisture over optimal bare soil conditions, and 2) to develop and test techniques which use visible/infrared sensors to compensate for the vegetation effect in this sensor's response to soil moisture. Soil moisture and aircraft data were collected at two agricultural areas: Guymon, Oklahoma in 1978 and Dalhart, Texas in 1980.

The L-band passive microwave radiometer was found to be the most suitable single sensor system to estimate soil moisture over bare fields. In comparison to other active and passive microwave sensors the L-band radiometer 1) was influenced least by ranges in surface roughness, 2) demonstrated the most sensitivity to soil moisture differences in terms of the range of return from the full range of

soil moisture, and 3) was less sensitive to errors in measurement in relation to the range of sensor response to soil moisture than the active microwave systems. L-band emissivity related more strongly to soil moisture when moisture was expressed as percent of field capacity. The perpendicular vegetation index (PVI) as determined from the visible/infrared sensors was found useful as a measure of the vegetation effect on the L-band radiometer response to soil moisture. A linear equation was developed to estimate percent field capacity as a function of L-band emissivity and the vegetation index. The prediction algorithm improves the estimation of moisture significantly over predictions from L-band emissivity alone.

INTRODUCTION

Estimation of soil moisture over large areas is useful in meteorology, hydrology, and agriculture. In meteorology, atmospheric models require information about the energy flux at the earth's surface. The two types of energy exchanged at the surface are sensible heat and latent heat. Sensible heat absorbed and released by the soil is for the most part, a small component of the surface energy balance. When latent heat is considered, some measurement of soil wetness is needed in order to relate actual evaporation to potential evaporation rates (Priestley and Taylor, 1972). In hydrology, real-time estimates of soil moisture condition at the beginning of a storm event would improve the ability to estimate runoff and provide flood warnings that would save both lives and property. In agriculture, a time history of surface soil moisture can be used to determine the severity and areal extent of drought conditions as well as inputs into soil moisture profile models needed to estimate agricultural yields. This information is useful to monitor the food supply for the growing population of the world.

Until the advent of the computer and space age technology there was no reasonable way to handle the volume of data required to map soil moisture estimates over an area as large as the United States, much less on a global basis. Conventional soil moisture measurement techniques are very time-consuming and therefore measurements are not widely or regularly obtained over most of the United States. The spatial variations of soil moisture make it difficult to extrapolate conventional point measurements to represent an integrated value over

a large area. These restrictions have led to research in developing remote sensing techniques to estimate soil moisture. The remote sensing approach to soil moisture estimation requires a new scale of thought. Sensing devices, particularly when satellite mounted, integrate many of the micro-scale variations that have been noticeable in point measurements. However, these remotely sensed measurements may actually give the operational user more meaningful information than point measurements, when used with a new set of models which use remote sensor inputs (Blanchard, 1979).

To monitor surface soil moisture by remote means, timely and repetitive sensor coverage is required. Soil moisture changes rapidly in the near-surface layers. After an irrigation or rain, the soil surface dries out within a few days in clear sunny weather (Taylor and Ashcroft, 1972). This dictates that the sensor must have all-weather capabilities. Visible and infrared sensors do not meet the all-weather criterion because the short wavelengths in this region of the spectrum are attenuated and many times completely masked by cloud cover. Microwave sensors with wavelengths greater than 4 cm are not hindered by cloud cover or lack of sunlight. Also, longer wavelengths penetrate into the soil medium to a certain extent (Lundien, 1966). This provides microwave sensors with two potential advantages over visible and infrared sensors: 1) all-weather capability, and 2) the ability to gather information about the subsurface as well as surface moisture conditions.

At visible and infrared frequencies, the sensor response contains information only about a very thin layer at the air-soil interface (Ulaby, 1974). However, this does not mean that visible and infrared

sensors are not valuable tools for large area soil moisture monitoring. Techniques using visible/infrared data have been developed that discriminate between crop types and estimate biomass, leaf area index, and percent cover (Richardson and Wiegand, 1977 and Rouse et al., 1973). Jackson et al. (1981b) suggested the use of vegetative biomass estimates from visible/near-infrared measurements in combination with microwave sensors to determine soil moisture. Vegetation over a particular area does not change as rapidly as surface soil moisture. Only three or four scenes in the visible and near-infrared wavelength region of the spectrum may be necessary to classify the vegetation during a season. Therefore the absence of all-weather capabilities is not a severe limitation when visible/infrared biomass estimates are combined with microwave sensors estimates of soil moisture.

Three basic terrain parameters affect microwave sensors: 1) soil moisture, 2) roughness, and 3) vegetation. The frequency and incident angle determine the scale of roughness to which microwave sensors are sensitive. The influence of vegetation is also dependent upon frequency and incident angle. Until recently, research in microwave remote sensing of soil moisture has been limited to determining the best single sensor which maximizes sensitivity to soil moisture while minimizing the effects of roughness and vegetation. However, the optimum frequency and incident angle may change for each agricultural region with different tillage practices and types of crops that are grown.

Active microwave investigations at the University of Kansas have identified the 4.25 GHz active microwave with incident angles near 10 degrees as the one sensor that can measure soil moisture over all

terrain conditions (Ulaby and Batlivala, 1976; Ulaby et al., 1978). However, data presented by Ulaby et al. (1977) showed a 3 dB shift in the sensor response and a reduction in sensitivity caused by roughness. Active microwave has also shown promise in crop classification when used at large incident angles where the effects of roughness and vegetation dominate (Bush and Ulaby, 1978; Schwarz and Caspall, 1968; Ellermeier et al., 1967).

Passive microwave sensors are also affected by the terrain parameters. Numerous investigations, such as Newton (1977), Schmugge (1978, 1980a, 1980b, and 1980c), and McFarland (1976) have demonstrated the sensitivity of passive microwave sensors to soil moisture. Lee (1974) and Newton (1977) demonstrated that surface roughness influences this sensitivity to soil moisture. The effect of vegetation on passive microwave response was identified in studies such as Lee (1974) and Kirdiashev et al. (1979).

Very few investigations have combined the responses from various sensors to estimate soil moisture. Using L-band passive microwave system, Newton (1977) used the response from two polarizations at one incident angle to infer the roughness contribution on the microwave response at a different incident angle. Investigations which combine microwave sensors with sensors from other regions of the spectrum have not been performed because concurrent data have not been available.

The attention of this study is focused on investigating techniques which infer soil moisture over agricultural lands from a combination of aircraft-mounted sensing devices. The sensors included visible, infrared, and microwave. Multi-sensor data over a wide range of frequencies and incident angles are available only from NASA's C-130

aircraft. Two of the most comprehensive soil moisture experiments using this aircraft were performed jointly by Texas A&M University and the University of California at Santa Barbara at sites in Guymon, Oklahoma and Dalhart, Texas. These data were used in this study

1) to determine which of the all-weather microwave sensors demonstrates the highest correlation to surface soil moisture over optimal bare soil conditions.
2) to develop and test techniques which use visible/infrared sensors to compensate for the vegetative effect in the microwave sensors' response to soil moisture.

It is hypothesized that the final technique would have the potential for estimating soil moisture over a variety of agricultural crops with only remote sensing inputs. These techniques could then be expanded to larger areas with a satellite mounted sensor package.

PHYSICS OF MICROWAVE INTERACTIONS

There is some conceptual difficulty in relating to the microwave portion of the spectrum. Visible and near-infrared sensors are extensions of our eyes. Thermal sensors can be identified with walking barefoot over hot pavement or cool, lush grass. However, we cannot put our hand on a surface and feel the parameters which influence microwave response. The emission, transmission, scattering, and absorption of microwave radiation are governed by the same physical laws that govern radiation in the visible and infrared portions of the spectrum. Microwave energy penetrates through the atmosphere and clouds with minimal attenuation, giving the microwave sensors all-weather capabilities. Since microwave energy has longer

wavelengths, they are affected by parameters below the surface as well as those on the surface. This affords the opportunity to gather information about the soil volume itself.

The ability of microwave sensors to detect soil moisture is based upon the difference in dielectric constant of dry soil and of water. It is common practice to express the dielectric constant, κ, in terms of the dielectric constant of free space, κ_0:

$$\kappa_r = \kappa_0 \kappa \tag{1}$$

where κ_r is a dimensionless complex function expressed by

$$\kappa_r = \kappa_r' - j\kappa_r'' \tag{2}$$

where κ_r' is the relative permittivity, κ_r'' is related to conductivity, and j denotes the complex portion of the function. The magnitudes of both κ_r' and κ_r'' are much greater for water than for dry soils and air space at microwave frequencies. In a dry soil, the value of κ_r' is typically between 3 and 5, whereas the value of κ_r' is about 80 for water (Schmugge et al., 1974).

Investigations such as those by Cihlar and Ulaby (1974), Hoekstra and Delaney (1974) and Newton (1977) have presented the relationship between permittivity (κ_r' and κ_r'') and moisture content for several different soil-texture types and frequencies. An example of the texture effects at 1.4 GHz is presented in Fig. 1 (Newton, 1977). Both the sand and clay soils have approximately the same value of κ_r' at 0% moisture. The function of κ_r' for each soil has two regions separated at a "transition" value of water content. For sand

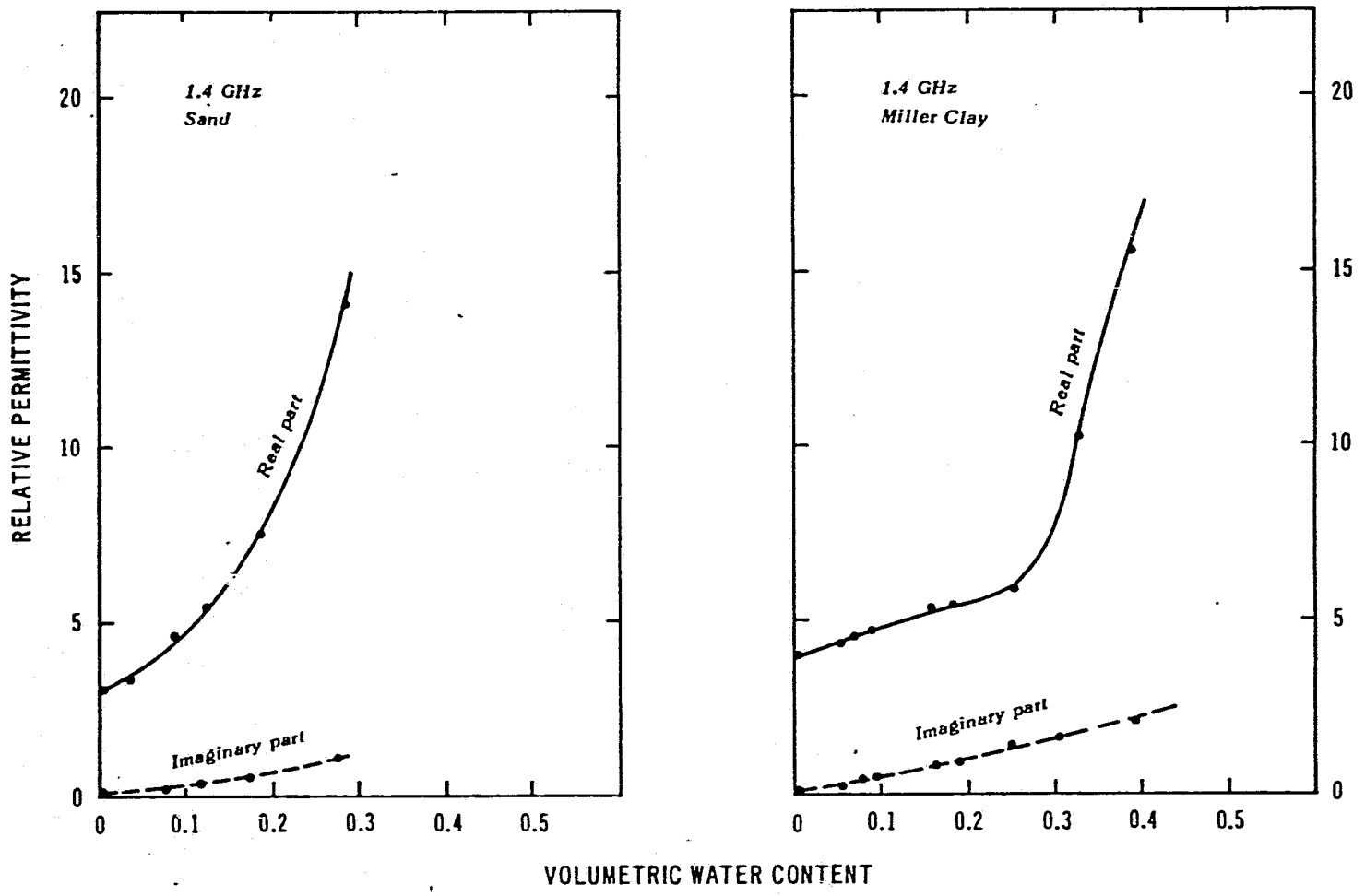

FIG. 1 The relationship between relative permittivity and volumetric water content at 1.4 GHz for (a) sand and (b) Miller clay. From Newton (1977).

the transition value is approximately 3% moisture content in contrast to 20% for the clay. Newton (1977) attributes the change of κ_r' below the transition zone with the increase of the tightly bound or hygroscopic water content. As more water is added, the more loosely bound pore water causes a larger effect (slope). This shift agrees with the established principle that with increasing clay content there is an increasing percentage of tightly bound unavailable water (Brady, 1978). Newton (1977) concludes that the dielectric properties are directly related to availability of soil water to vegetation independent of soil type. It is important to note that κ_r is a function of frequency.

Microwave sensors are of two basic types, active and passive. Active microwave sensors (radar and scatterometers) illuminate the target with microwave energy and measure the amount of energy returned to the antenna. Passive microwave sensors (radiometers) measure the amount of microwave energy that the target emits.

The terrain-sensor interaction processes in microwave remote sensing are governed by the target geometry and dielectric properties. These properties depend upon their relation to the sensor parameters (Cihlar and Ulaby, 1974). Sensor parameters include frequency, incident angle, and polarization as well as whether the sensor is active or passive. The ability of microwave sensors to detect soil moisture is obtained from the direct relationship between microwave response and the dielectric properties of the soil (Hoekstra and Delaney, 1974). As the soil moisture changes, its dielectric properties also change. This causes a corresponding change in the microwave response.

Target geometry refers to the slope, aspect, degree of roughness, and type and extent of vegetative cover (biomass). The effects of target parameters are all integrated into one microwave response. Consequently, it is difficult to relate physical measurements of target parameters to the effects they have on microwave responses. This is further complicated because these effects are also a function of the sensor parameters (Rouse et al., 1969).

Active Microwave

Radar return is that portion of the transmitted energy which returns to the radar receiver. The radar cross section, σ, or alternately the radar cross section per unit area, (scattering coefficient) σ^0, depends upon the properties of the target. Thisparameter contains all the information about the illuminated terrain that a radar is capable of sensing. The scattering cross section, σ_m, for a single point scatterer is related to the radar return, by inverting the radar equation and solving for σ_m (Rouse et al., 1969):

$$\sigma_m = \frac{P_r}{P_t} \frac{(4\pi)^3 D_m^4}{G_m^2 \lambda^2} \qquad (3)$$

where:

σ_m = scattering cross section for a single point scatterer (m^2)

P_r = received signal power (watts)

P_t = transmitted signal power (watts)

D_m = slant range distance to the mth scatterer (m)

λ = wavelength of the transmitted signal (m)

G_m = antenna gain (dimensionless)

The average scattering coefficient per unit area for many scatterers is a dimensionless real number whose magnitude is a function of the terrain parameters. Since σ^0 is dimensionless it can be analyzed in dB and expressed as a function of terrain parameters:

$$\sigma^0 = f(\lambda, \theta, \phi, P, \kappa, \Gamma) \tag{4}$$

where

θ = angle of incidence relative to nadir

ϕ = aspect angle

P = polarization of the incident wave

κ = complex dielectric constant

Γ = index of surface roughness.

An analytical expression for σ^0 is not readily obtainable without simplifying assumptions (Rouse et al., 1969).

In the following discussion, a perfectly smooth surface at the air-soil interface is assumed to facilitate the understanding of the relationship of σ^0 to soil moisture. Under these conditions the Fresnel reflection coefficient, r, can be defined. This coefficient relates the magnitude and phase of the reflected electric and magnetic fields to those of the incident fields of a plane wave which strikes the interface. The parameter of interest is the power reflection coefficient, R:

$$R = r^2 = \frac{Pr}{P_t} \tag{5}$$

$$R_H = \frac{[(p-\mu)^2 + q^2]}{[(p+\mu)^2 + q^2]} \tag{6}$$

$$R_V = \frac{[(\mu\kappa_r' - p)^2 + (\mu\kappa_r'' - q)^2]}{[(\mu\kappa_r' + p)^2 + (\mu\kappa_r'' - q)^2]} \quad (7)$$

where H and V represent horizontal and vertical polarization and $\mu = \cos\theta$. The parameters p and q are given by:

$$p = \frac{1}{\sqrt{2}} \{[(\kappa_r' + \mu^2 - 1)^2 + \kappa_r''^2]^{1/2} + (\kappa_r' + \mu^2 - 1)\}^{1/2} \quad (8)$$

$$q = \frac{1}{\sqrt{2}} \{[(\kappa_r' + \mu^2 - 1)^2 + \kappa_r''^2]^{1/2} - (\kappa_r'' + \mu^2 - 1)\}^{1/2} \quad (9)$$

The sensitivity of R to the complex dielectric constant is not readily apparent from these equations. Using approximate values of κ_r from Fig. 1b and equation (6), R_H for a range of look angles is presented in Fig. 2. Small incident angles show the most sensitivity to changes in soil moisture. The term "look angle" is synonymous with incident angle.

The Fresnel approach addresses only smooth or specular return from the surface with no subsurface contribution or depolarization. The energy is reflected as from a mirror, with the angle of incidence equal to the angle of reflection. Spectral reflection is seldom present in natural terrain except for areas with smooth water surfaces. At the other extreme, isotropic scatterering is when the scattering coefficient is independent of the angle of incidence. The "degree of roughness" of the terrain, a relative quantity, dictates the extent of scattering which forms the reradiation pattern. Examples of specular and isotropic scattering along with an intermediate case are presented in Fig. 3.

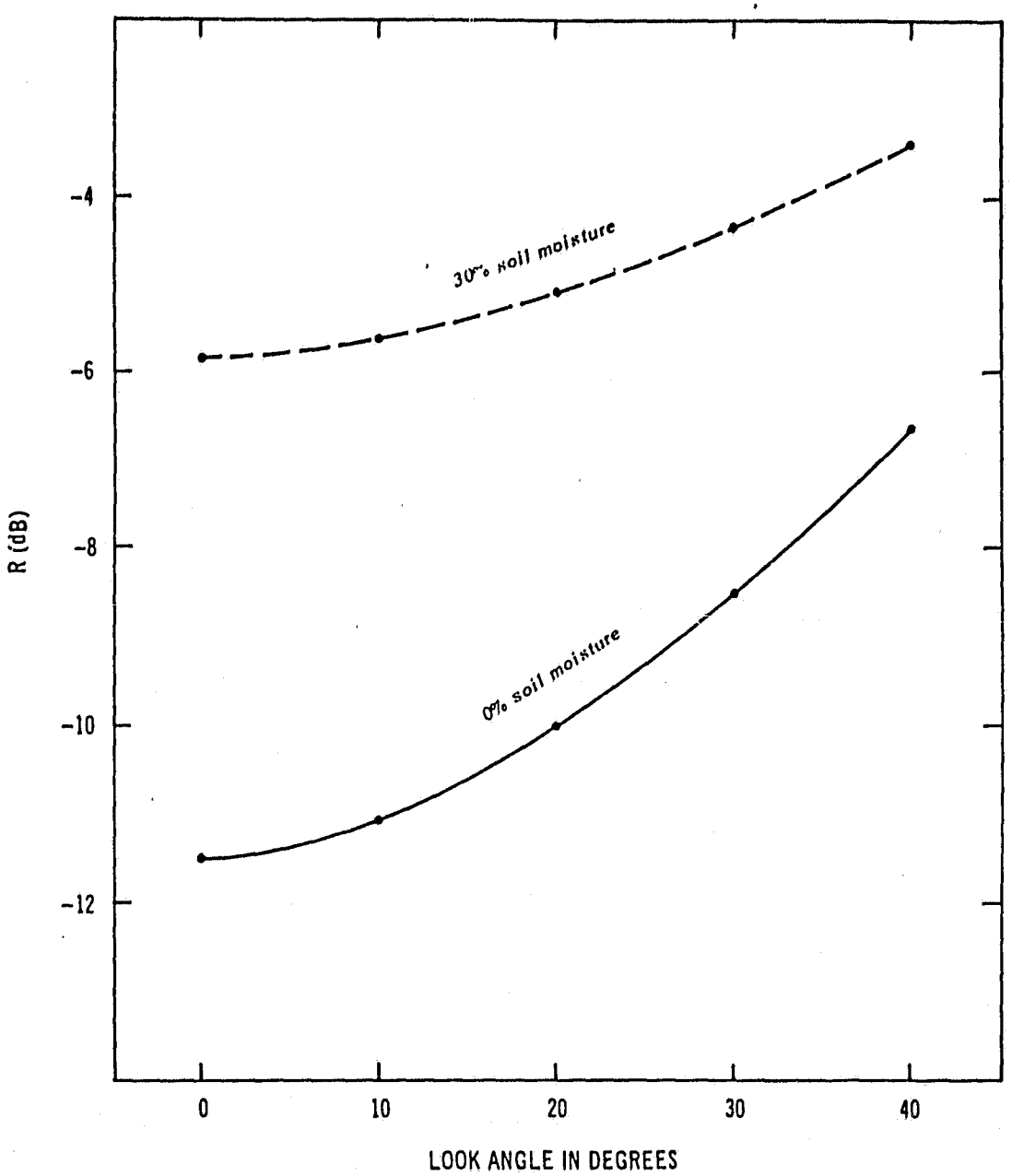

FIG. 2 Relationship between power reflection coefficient (R_H) and look angle for 0% and 30% soil moisture.

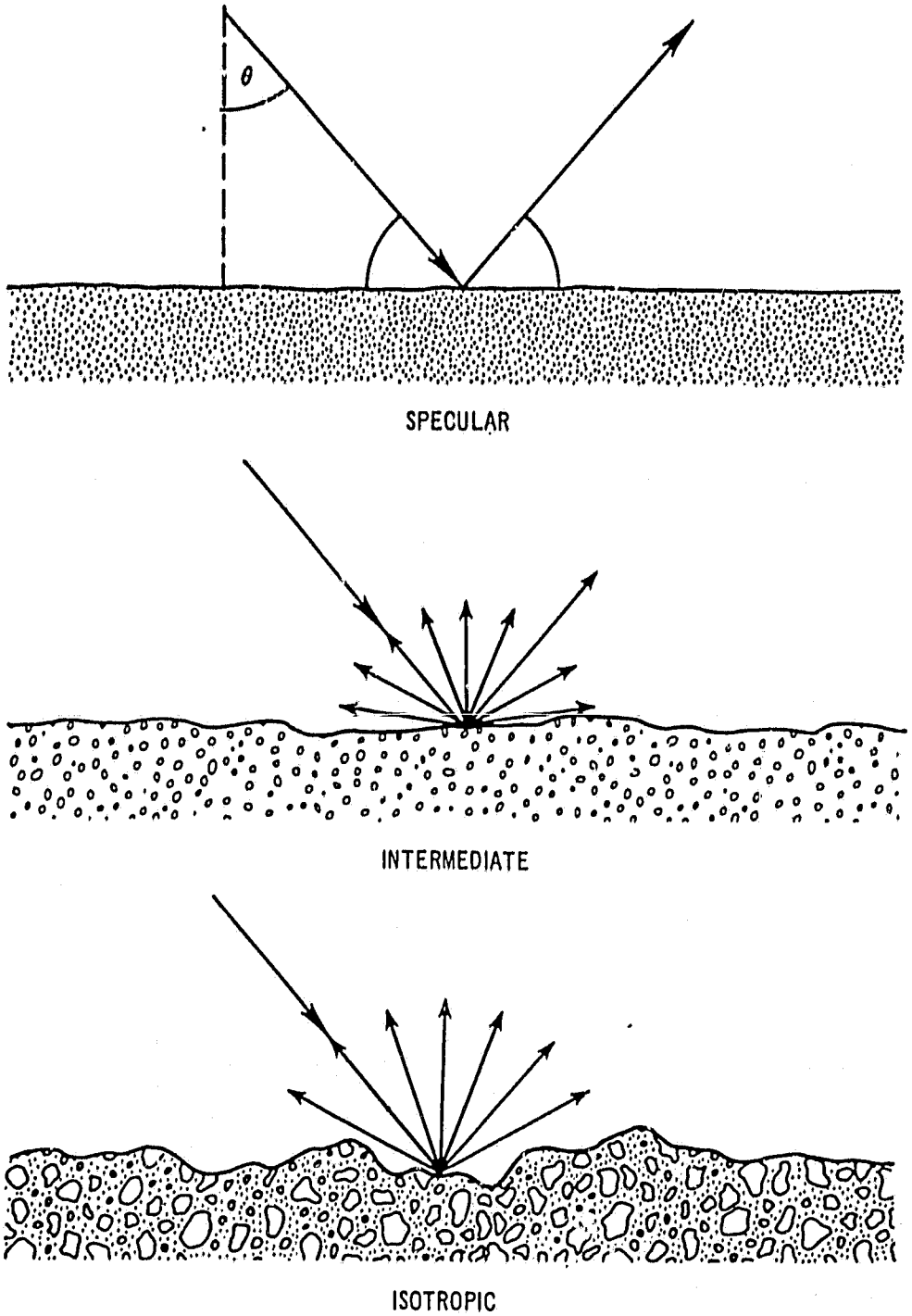

FIG. 3 Examples of spectral and isotropic scattering along with an intermediate case. Incident angle is defined by θ.

A large number of scattering theories have been developed by Barrick (1968), Kodis (1966), Fung (1966), Beckmann (1965), Semenov (1966), Beckmann and Spizzichino (1963), Leader and Dalton (1972), Rouse (1972) and Blanchard (1977). The authors have modeled the effects of surface roughness, subsurface contribution, and depolarization. These modeling efforts have had varying degrees of success for particular terrain roughnesses but no one theory works universally over all scales and distributions of roughnesses and subsurface conditions.

Vegetation effects further complicate the dependency of σ^0 on soil moisture. Vegetation scattering models have been developed by Peak (1959a), Du (1969), and Waite and Cook (1974) with varying degrees of success. The physical phenomena of radar scattering is very complex and not well understood. The scope of this study does not allow in-depth investigations of radar reflectivity theory. Such a study must be done on small, controlled surface areas with accurate measurements of roughness, vegetation, and soil dielectrics. However, it is important to recognize the impact of scattering from surface roughness and vegetation on the scattering coefficient in the attempt to relate the scattering coefficient to soil moisture.

Passive Microwave

Since the microwave emission of a soil originates in the soil volume and propagates outwardly, it is reasonable to examine the emission process within the volume separately from the modifying effects of surface roughness and vegetative cover. The fundamental concepts of microwave radiation are presented here. These concepts are des-

cribed in more detail by Paris (1969 and 1971), Marion (1975), Newton (1977), Hess (1959), and Lintz and Simonett (1976).

The specific intensity of radiant energy emitted by a blackbody is expressed by Planck's radiation law:

$$B_{bb} = \frac{2h\nu}{\lambda^2} [\exp(h\nu/CT)-1]^{-1} \quad (10)$$

where

B_{bb} = specific intensity of radiant energy emitted in a particular frequency range that passes through an element of area in an interval of time and surrounded by a solid angle (watts m^{-2} $steradian^{-1}$ Hz^{-1})

C = Boltzmann's constant (1.38×10^{-23} JK^{-1})

T = temperature of the blackbody (K)

λ = wavelength (m)

h = Planck's constant (6.623×10^{-34} Js)

ν = frequency (Hz)

At microwave frequencies and surface temperatures typical of Earth, the Rayleigh-Jeans approximation of Planck's equation for thermal radiation from a blackbody applies. A Maclaurin expansion of the bracketed quantity in equation (10) is:

$$\exp(h\nu/CT)-1 = h\nu/CT + h^2\nu^2/2C^2/T^2 + \ldots \quad (11)$$

Equation (10) reduces to the Rayleigh-Jeans approximation

$$B_{bb} = \frac{2CT}{\lambda^2} \quad (12)$$

when the higher order terms in equation (11) are neglected as very small.

The emission from a blackbody is completely random; therefore, the polarized specific intensity of emission (B_p) can be expressed as

$$B_p = \frac{CT}{\lambda^2} \tag{13}$$

since one-half the total intensity of emission would exist in each plane of polarization. Material objects on the earth's surface are not perfect radiators, so they are sometimes referred to as graybodies. The intensity of graybody radiation may be thought of as the intensity radiated by an equivalent blackbody multiplied by an efficiency factor. It is assumed that the form of the emission is the same as that of a blackbody and that the polarized intensity, I_p, is given by

$$I_p = \varepsilon B_p \tag{14}$$

where ε is the polarized emissivity of the gray body.

The polarized brightness temperature, T_{BT}, is defined by

$$T_{BT} = \left(\frac{\lambda^2}{C}\right) I_p \tag{15}$$

which reduces to

$$T_{BT} = \varepsilon T \tag{16}$$

where T is the temperature of the emitting graybody. Simply stated, all objects with temperatures above absolute zero emit electromagnetic energy due to the thermal agitation of charged particles. The radiation intensity is linearly related to the temperature and physical properties of the object.

Various sources contribute to the radiation received by a passive microwave system. The most important contribution for this study is the contribution from the earth's surface (εT_{SURF}). Other major sources include the atmosphere between the antenna and the surface, T_{ATM}, and downward radiation from both sun and the atmosphere that is reflected from the surface to the radiometer, T_{SKY}. For a constant height, frequency, and angle

$$T_{BT} = T_{ATM} + \tau \left((1-\varepsilon)T_{SKY} + \varepsilon T_{SURF}\right) \tag{17}$$

where

T_{BT} = brightness temperature, as seen by the radiometer (K)

τ = atmospheric transmission (dimensionless)

$1-\varepsilon$ = reflectance of the surface (dimensionless)

ε = emissivity of the surface (dimensionless)

T_{SURF} = thermometric temperature of the surface layer (K)

Most studies, including this one, neglect all atmospheric effects (T_{ATM}, $T_{SKY}=0$, $\tau \approx 1$). This simplifies equation (17) to

$$T_{BT} = \varepsilon T_{SURF}. \tag{18}$$

This assumption is valid for the majority of atmospheric conditions, but as shown by Paris (1971), it loses validity in the presence of relatively large particles such as rain drops in the atmosphere.

When applied to a soil this simple approach to microwave emission assumes a semi-infinite soil medium with a smooth surface that is in thermodynamic equilibrium and exhibits blackbody (isotropic) radiation. Peake (1959b) demonstrated that ε is equal to absorptivity. This is the basis for describing the emission from a soil volume, ε_0, in terms of the power reflection coefficient:

$$\varepsilon_0 = 1 - R_p \tag{19}$$

where p denotes polarization and R_p can be calculated from equation (6) or equation (7). In Peake's analysis uniform soil moisture and temperature distributions with depth were assumed. Richerson (1971) and Casey (1972) used an effective Fresnel coefficient from horizontal homogeneous layers to provide for non-uniform moisture profiles. Strogryn (1970) developed a rigorous solution for non-uniform temperature and moisture profiles using Maxwell's equations. Using an approach similar to Strogryn, Tsang et al. (1975) formulated emission from a stratified medium. Numerical results were illustrated and compared with the closed form analytical solutions.

Radiative transfer techniques (Newton, 1977; Burke and Paris, 1975) provided a simpler alternative to the general formulation of Stogryn (1970). The soil volume was modeled as a horizontally stratified media with each layer consisting of non-scattering homogeneous soil. Soil moisture and temperature were assumed constant in each

layer. This approach lends itself to physical interpretation and is not computationally difficult.

In nature, the soil surface is seldom perfectly smooth and without vegetation. The remainder of this section examines the influence of surface roughness and vegetation upon the passive microwave response to soil moisture.

Surface roughness modifies the microwave emission from a soil volume. Choudhury et al. (1979) modeled roughness by modifying equation (19) with a roughness parameter, h:

$$\varepsilon = \varepsilon_0 + \Delta\varepsilon \tag{20}$$

where

$$\Delta\varepsilon = R_p(1 - e^{-h}) \tag{21}$$

Using both 1.4 GHz and 10.6 GHz radiometers, Lee (1974) and Newton (1977) reported measurements of bare, smooth, and rough soil surfaces that demonstrated that increased surface roughness decreases the sensitivity of the emission to changes in soil moisture, and that for dry soils the emission is approximately independent of surface roughness. Using these same frequencies, Blinn and Quade (1974) obtained measurements for both raked and smooth sand. From their results, the 10.6 GHz frequency was affected much more by that specific scale of roughness than the 1.4 Ghz frequency. This indicates that the "sensed" roughness is a function of wavelength. For a smooth field Newton (1977) reported a 100 K change in T_{BT} in going from wet to dry soils. This sensitivity was reduced to about 60 K for extremely

rough fields that had been deep plowed to produce large clods. This shows good agreement with the 80 K range of T_{BT} for the moderately rough fields encountered in Phoenix (Schmugge, 1978).

The effects of vegetation on the surface brightness temperature have been modeled by Sibley (1973), Basharinov and Shutko (1978), and Kirdiashev et al. (1979). Experimental results from Lee (1974) support Sibley's model which predicts that the vegetation is essentially an attenuator at low vegetation density and a predominant emitter at high vegetation density. As an attenuator, the vegetation lowers the apparent temperature measurement; as a predominant emitter, it raises the apparent temperature. Lee (1974) used 1.4 GHz and 10.6 GHz frequency radiometers and reported that for 10.6 GHz, thick vegetation had completely masked the soil contribution regardless of surface roughness. In contrast, for the 1.4 GHz frequency, the vegetation generally exhibits an attenuating effect. Therefore, the effect of vegetation on apparent temperature is dependent on frequency, with lower frequencies showing more potential to detect soil moisture through the vegetation.

REVIEW OF PREVIOUS WORK

Active Microwave

Early ground-based measurement programs at Ohio State University (Taylor, 1959 and Cosgriff et al., 1960) and by the Corps of Engineer (Lundien, 1966) investigated radar responses and penetration into a variety of natural and man-made surfaces. Roughness, vegetation, and soil moisture were found to be the general classes of parameters which influenced radar response. Due to the well-developed photographic

interpretation techniques, the greatest excitement in the remote sensing community during the 1960s and early 1970s was created by radar image analysis. Numerous authors presented qualitative image interpretations of the effects of vegetation (Ellermeier et al., 1967; Moore and Simonett, 1967; Morain and Simonett, 1966; Schwarz and Caspall, 1968; and Berger, 1970) and suggested radar as a crop classifier. However, the launching of Landsat redirected vegetative studies away from radar and toward visible/infrared techniques.

MacDonald and Waite (1971) renewed interest in radar's potential for soil moisture detection. Their study was the first to qualitatively discern soil moisture variations in radar imagery at relatively high frequencies and large incident angles. Previous experiments with similar imaging radars had been conducted with soil moisture showing little influence upon radar return even for bare soils (Simonett, 1970). However, MacDonald and Waite (1971) discerned the difference between wet swampy lands and the better drained, relatively drier soils of natural levees. Both these areas were beneath defoliated tree branch cover. Studying flooded low areas in Central Texas, Blanchard et al. (1979) described this phenomena as multiple scattering between the trees and the smooth free water surface.

The University of Kansas has since provided the bulk of research into the dependency of radar response on soil moisture. A description of the truck-mounted Microwave Active Spectrometer (MAS) system is provided in Ulaby et al. (1978). The research using this system identifies C-band radar (4.25 GHz) at incident angles near 10 degrees as the optimum frequency which can estimate soil moisture over all terrain conditions with a minimum of influence from roughness (Ulaby and

Batlivala, 1976; Ulaby et al., 1978). However, sensitivity (approximately 3 dB) to roughness (Ulaby et al. 1977) and vegetation type (Ulaby et al., 1979) is demonstrated at this frequency and incident angle. They found that as soil moisture varies from 0 to 30%, σ^0 changes by approximately 10 dB. Jackson et al. (1981a) reported agreement with the University of Kansas with aircraft mounted radars by illustrating that C-band at 15 degrees incident angle exhibited the best linear correlation with soil moisture. However, the 14 points presented exhibited a sensitivity of over 20 dB per 30% moisture range.

Blanchard (1978) presented results from aircraft-mounted radar experiments (13.3 and 1.6 GHz). The influence of roughness and vegetation were minimized at angles between 10 and 20 degrees. At the 10 degree incident angle, the moisture sensitivity increased from 4 dB at 13.3 GHz to 9 dB at 1.6 GHz per 30% soil moisture. This closely agrees with the Kansas data for 4.25 GHz reported by Ulaby et al. (1977) and indicates no significant difference in sensitivity between 4.25 and 1.6 GHz. However, the 1.6 GHz data from Blanchard (1978) does not agree with the low sensitivity shown by Ulaby at 1.1 GHz.

Most radar measurements are accurate to only 3 dB. As mentioned before, roughness has at least a 3 dB effect at the optimum incident angles. The magnitude of these variations along with vegetation effects can significantly mask the effectiveness of radar to quantify soil moisture when applied to a variety of terrains.

Passive Microwave

Many investigators have experimentally shown the sensitivity of truck and aircraft-mounted passive microwave radiometers to soil moisture variations. Poe et al. (1971) observed that the emissivity of a smooth bare field varied from 0.5 for very wet soil to greater than 0.9 for dry soil. Blanchard (1972) and Blinn and Quade (1972) reported decreasing T_{BT} with increasing moisture content. The rates ranged from 1.5 to 4.8 K per one percent change in moisture content depending on frequency and soil type. This range is supported by Basharinov et al. (1974), who reported a slope of approximately 3-4 K per one percent moisture change for the 1-3 cm wavelength range. A comparison of aircraft observation of T_{BT} over agricultural fields around Phoenix in 1973 (Schmugge et al., 1974) and 1975 (Schmugge, 1976; Choudhury et al., 1979) demonstrated that these results are repeatable. Recent controlled truck-mounted experiments by Newton (1977) and Wang et al. (1980) agree closely with the previous findings.

Schmugge (1980a) developed a relationship between soil texture and field capacity

$$FC = 0.30 - 0.0023 \times SAND + 0.005 \times CLAY \qquad (22)$$

where:

FC = field capacity (for use with volumetric soil moisture)

SAND = percent sand

CLAY = percent clay.

He determined that passive microwave response should be related to percent field capacity instead of soil moisture by volume. Percent field capacity may, in some applications, be more important than absolute water content.

The sensitivity of radiometers to soil moisture has also been demonstrated from space. McFarland (1976) showed a definite relationship between the Skylab 21 cm brightness temperatures and an antecedent precipitation index (API). The soil moisture index (API) was calculated from rain gage data within the 110 km footprint. Eagleman and Lin (1976) also related Skylab 21 cm data to soil moisture variations as determined by water budget models. The 1.55 cm Electrically Scanning Microwave Radiometer (ESMR) response was correlated to moisture indices (McFarland and Blanchard, 1977; Theis 1979; Schmugge et al., 1977). This shorter wavelength radiometer demonstrated the potential to detect soil moisture during periods of the year when the agricultural fields were essentially bare.

Visible/Infrared Biomass Models

Reflected solar radiation is the primary source of energy for visible/infrared sensors. Different materials possess different spectral reflective properties unique to that material. Due to Fresnel reflectance at air/water interfaces within leaves, radiation at the near- and middle-infrared frequency is strongly reflected (Gates, 1980). This reflectance increases with increasing biomass. This phenomenon has been the basis for classification of vegetation and estimating biomass. Two biomass estimation models are presented here.

Richardson and Wiegand (1977) developed the perpendicular vegetation index (PVI). This graphical approach presented in Fig. 4 plots two Landsat bands against each other; MSS5(0.6-0.7 μm) and MSS7 (0.8-1.1 μm). As soil reflectance properties change, the two bands change together to form the soil line. PVI was calculated using the Pythagorean theorem;

$$PVI = \sqrt{(Rgg5 - Rp5)^2 + (Rgg7 - Rp7)^2} \qquad (23)$$

where Rp is the reflectance values of an individual band and Rgg is the corresponding soil reflectance for the Landsat bands. PVI is the perpendicular distance from the soil background line to the plotted radiance values.

The Transformed Vegetation Index (TVI) has been used as a rangeland biomass estimator (Rouse et al., 1973);

$$TVI = \sqrt{\frac{(MSS7 - MSS5)}{(MSS7 + MSS5)} + 0.5} \qquad (24)$$

The ratioing under the radical is a standard practice to remove the scene to scene variations of sun angle and atmospheric optical density difference. The 0.5 was added to prevent the term under the square root from becoming negative. PVI was used in this study because it was developed for agricultural crop lands and may be used as both a crop classifier and biomass estimator.

Sensor Combinations

Very few investigations have combined responses from various sensors to estimate soil moisture. Newton (1977) used the difference

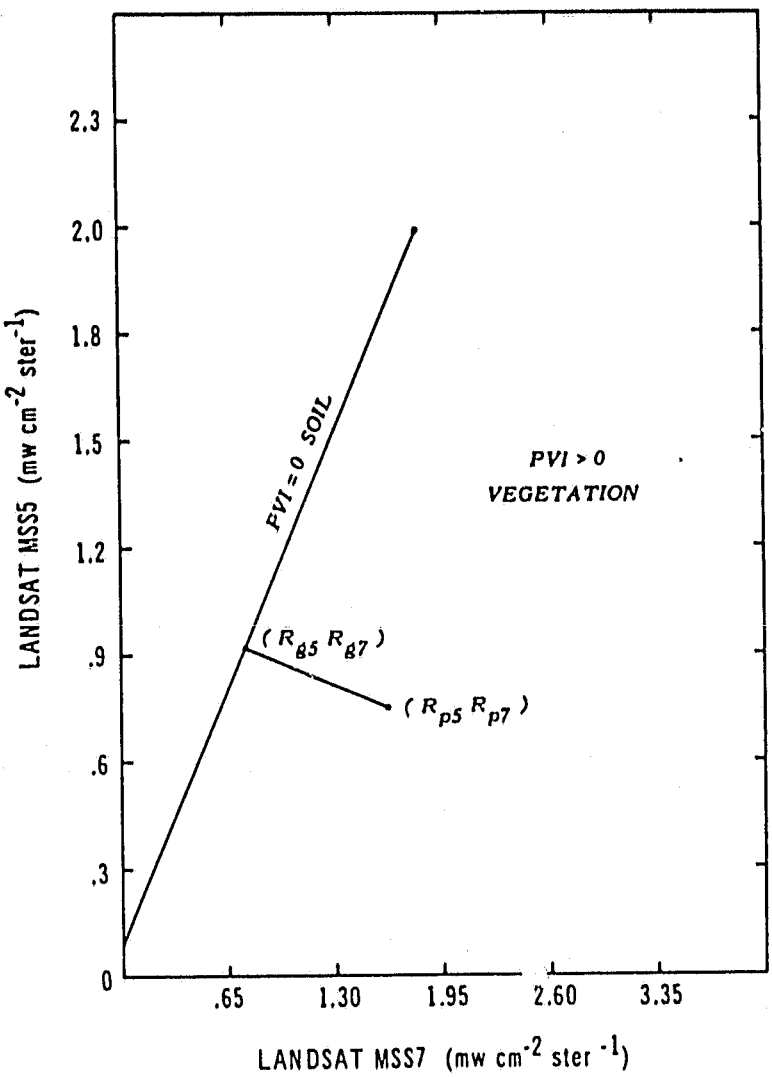

FIG. 4 Diagram illustrating the principle of the perpendicular vegetation index (PVI) model. A perpendicular from candidate plant coordinates (Rp5, Rp7) intersects the soil background line at coordinates (Rg5, Rg7). A PVI=0 indicates soil, and a PVI>0 indicates vegetation. From Richardson and Wiegand (1977).

in the horizontally and vertically polarized L-band radiometer at 35 degree incident angle as a parameter to infer roughness. This parameter was used in combination with the L-band emissivity at 20 degree incident angle as an estimate of soil moisture over various roughnesses.

Jackson et al. (1981b) developed a model to predict emissivity of a scene from surface temperature, soil moisture, and vegetative biomass inputs. Encouraging results were obtained for wet biomass values below 1300 g/m^2. Beyond this, the sensitivity is probably too low for the model to be of use. These results support the need for biomass estimations (possibly obtained from visible/infrared sensors) as an indicator of vegetation effect on bare soil emission. Jackson could not investigate this because visible/infrared data were not taken simultaneously with the microwave data. The data collected for this study were used to develop sensor combination techniques to estimate soil moisture by remote means.

DATA COLLECTION AND PROCESSING

Multisensor data over a wide range of frequencies are available only from NASA's C-130 aircraft. The C-130 collected all sensor data used in this study. Aircraft and soil moisture data were collected near Dalhart, Texas in August 1980 and near Guymon, Oklahoma in August, 1978. These areas were chosen because each had relatively homogeneous soils, reasonably low relief, a variety of crops, and the availability of irrigation. The Texas and Oklahoma Panhandle areas were initially surveyed in one mile square sections with boundaries of the sections oriented North-South and East-West. Aircraft flight

lines were also orientated in these directions to make it possible for the pilot to fly one half mile over the fields that were sampled and thus allow adequate sampling by the sensors over each field. Agricultural practices usually dictate one crop per quarter section which is also the area irrigated by one center pivot sprinkler system. For this study a field was defined as one half of a quarter section with the long axis of the field parallel to the aircraft flight line. The half quarter section provided an area large enough for sufficient coverage with aircraft line sensors and small enough for an adequate ground sampling network.

Experiment Site Descriptions

Guymon

Sampled fields were located under four flight lines approximately 20 km southwest of Guymon, Oklahoma (Fig. 5). The soil type was generally a silty clay (35% clay, 35% silt, and 30% sand) with many areas having caliche ($CaCO_3$) near the surface. The crop types were alfalfa, and milo, with some fallow fields. The milo fields were chosen with some fields having rows perpendicular and some parallel to the flight lines. The field conditions are summarized in Table 1.

Dalhart

The sampled fields were chosen under two flight lines approximately 20 km northwest of Dalhart, Texas (Fig. 6). The soil type of the surface 30 cm was a sandy loam (75% sand, 10% silt, and 15% clay). The 22 fields sampled were almost equally divided into irrigated and non-irrigated fields. The irrigated fields included millet and mature corn. Pasture, wheat stubble, and disked wheat stubble comprised the non-irrigated fields.

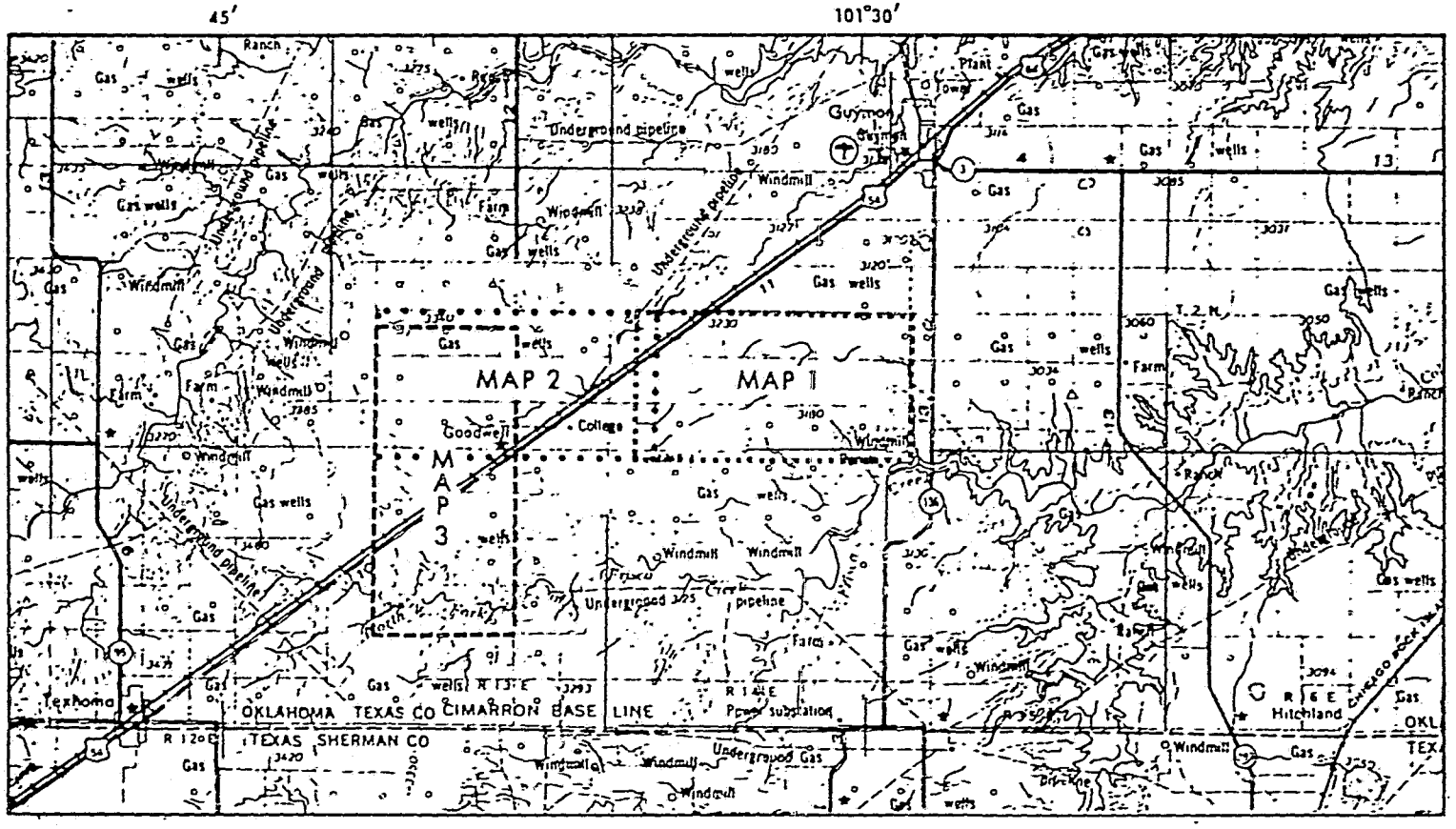

GUYMON AREA MAP

INDEX TO FIELD MAPS

Approximate scale 1 : 250,000

FIG. 5 Guymon field maps. a) Area map of Guymon showing relative locations of each field map.

GUYMON, OKLAHOMA 1978

LEGEND FOR FIELD MAPS 1,2 & 3

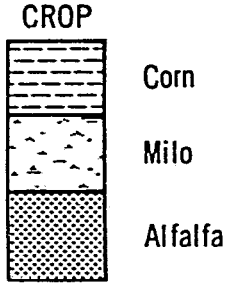

Consult field notes for row crop orientation to aircraft flight lines.

Prepared by the Texas A&M University Remote Sensing Center. Base data compiled from USGS topographic maps, R.S.C. team field notes and NASA contracted aerial photography collected August 2-17, 1978.

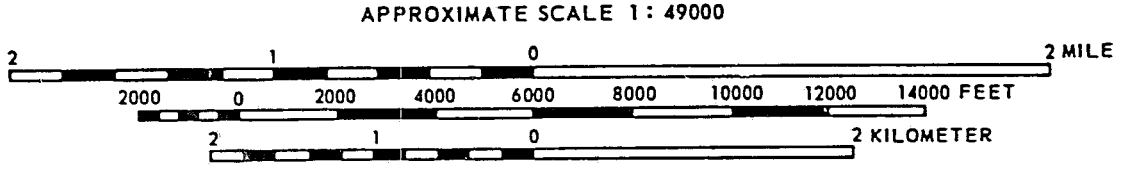

FIG. 5b Legend for Guymon, Oklahoma field maps.

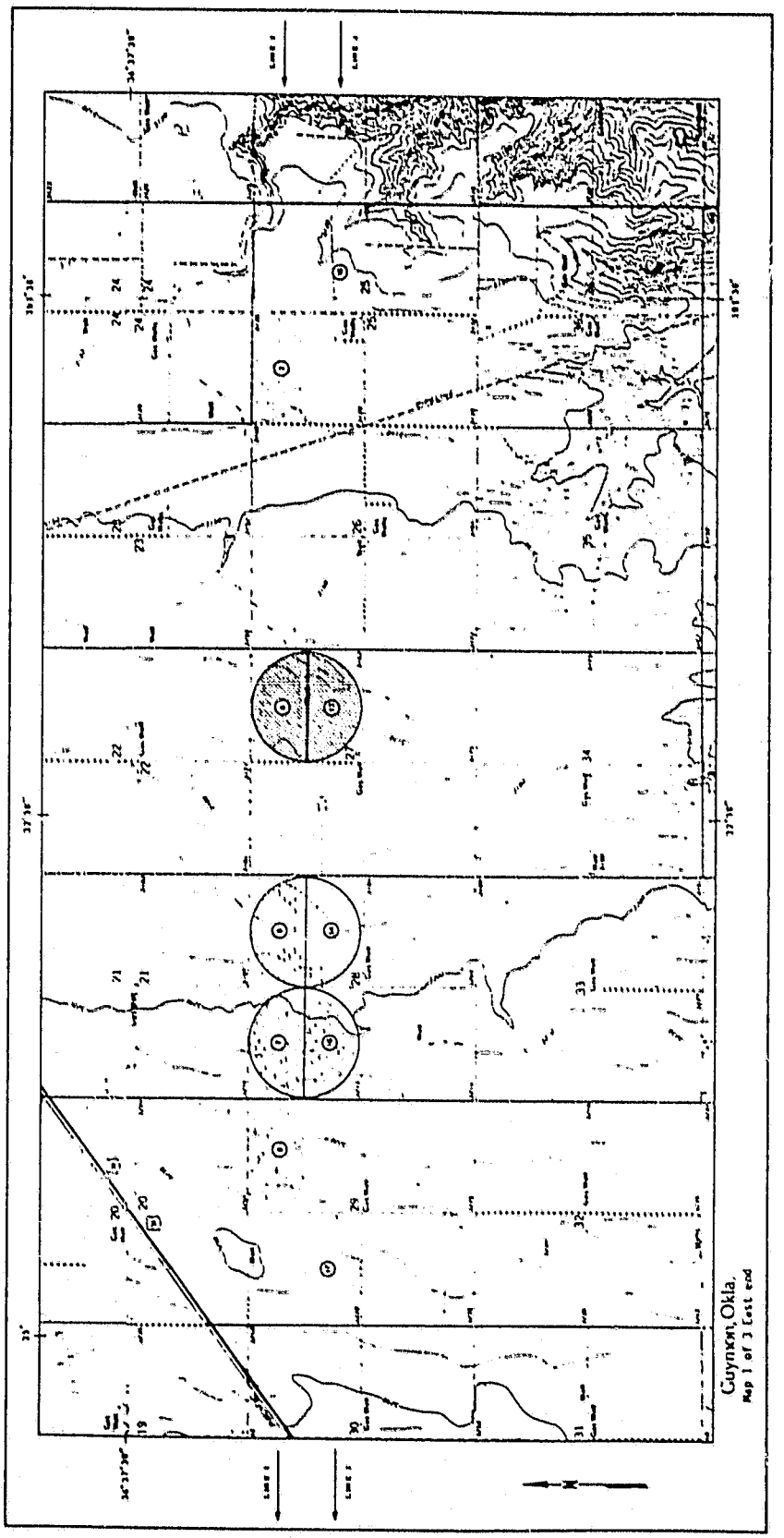

FIG. 5c Locations of sample fields at Guymon.

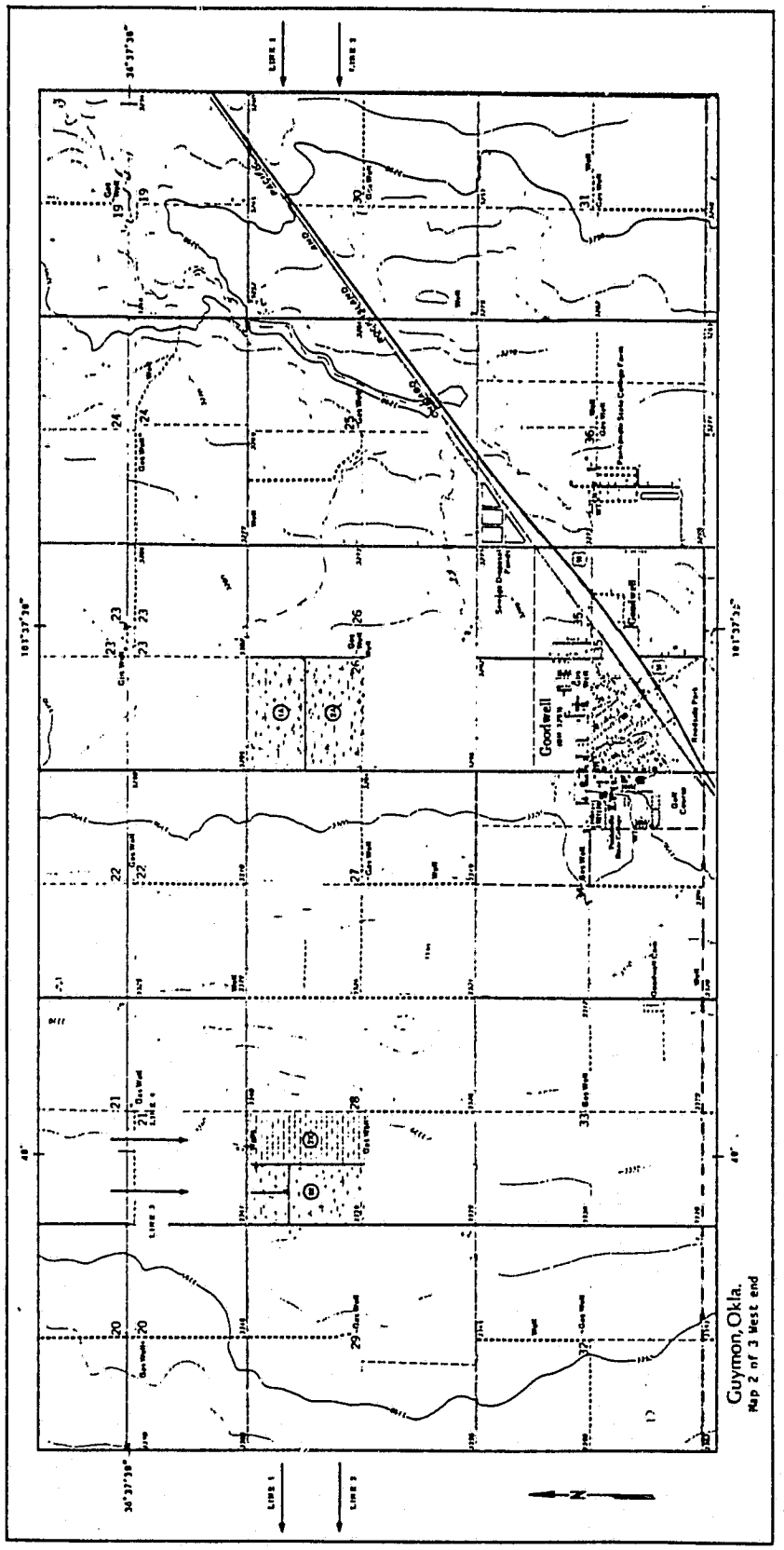

FIG. 5d Locations of sample fields at Guymon.

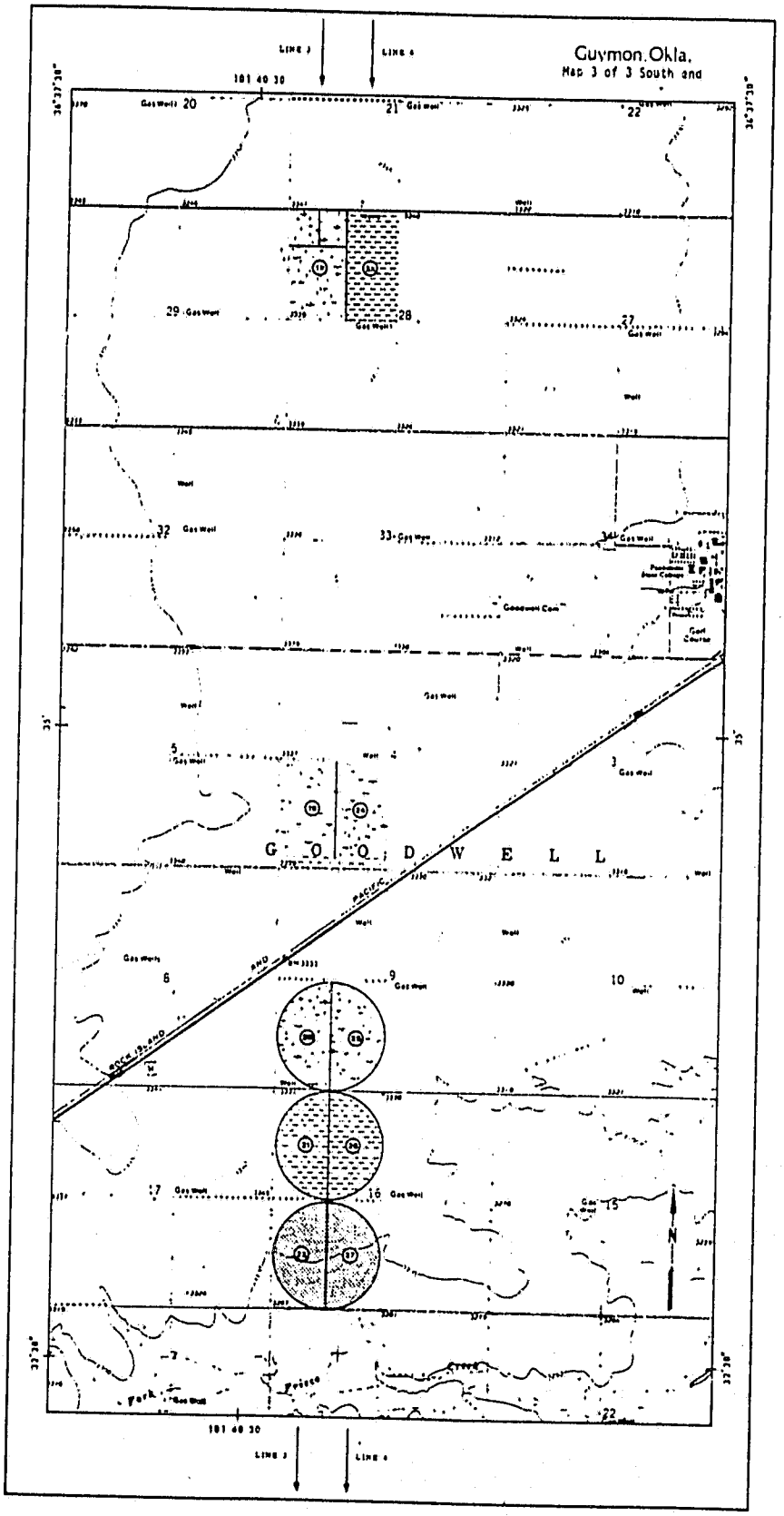

FIG. 5e Locations of sample fields at Guymon.

Table 1. Surface Conditions of Guymon Fields

Condition	Fields Numbers
Summer Fallow (bare)	2, 10, 17, 21, 26
Sprinkler Irrigated August 1	14
Sprinkler Irrigated August 14	6
Listed August 17	2X
Circular Irrigated Alfalfa	4, 13, 22, 27
Milo	
Circular Irrigated	
23 cm tall, drilled	7, 15
90 cm tall perpendicular rows	20, 25
Furrow Irrigated	
90 cm tall parallel rows	8, 1X, 1a, 2a
90 cm tall perpendicular rows	18, 24

Table 2. Surface Conditions of Dalhart Fields

Condition	Field Numbers
Bare	
Wheat stubble	17,18
Disked stubble	19,20,21,22
Mulched stubble (with weeds)	13,14
Half disked, half burned stubble	15,16
Corn	1,2,7,8,9,10,11,12
Pasture	5,6
Millet	3,4

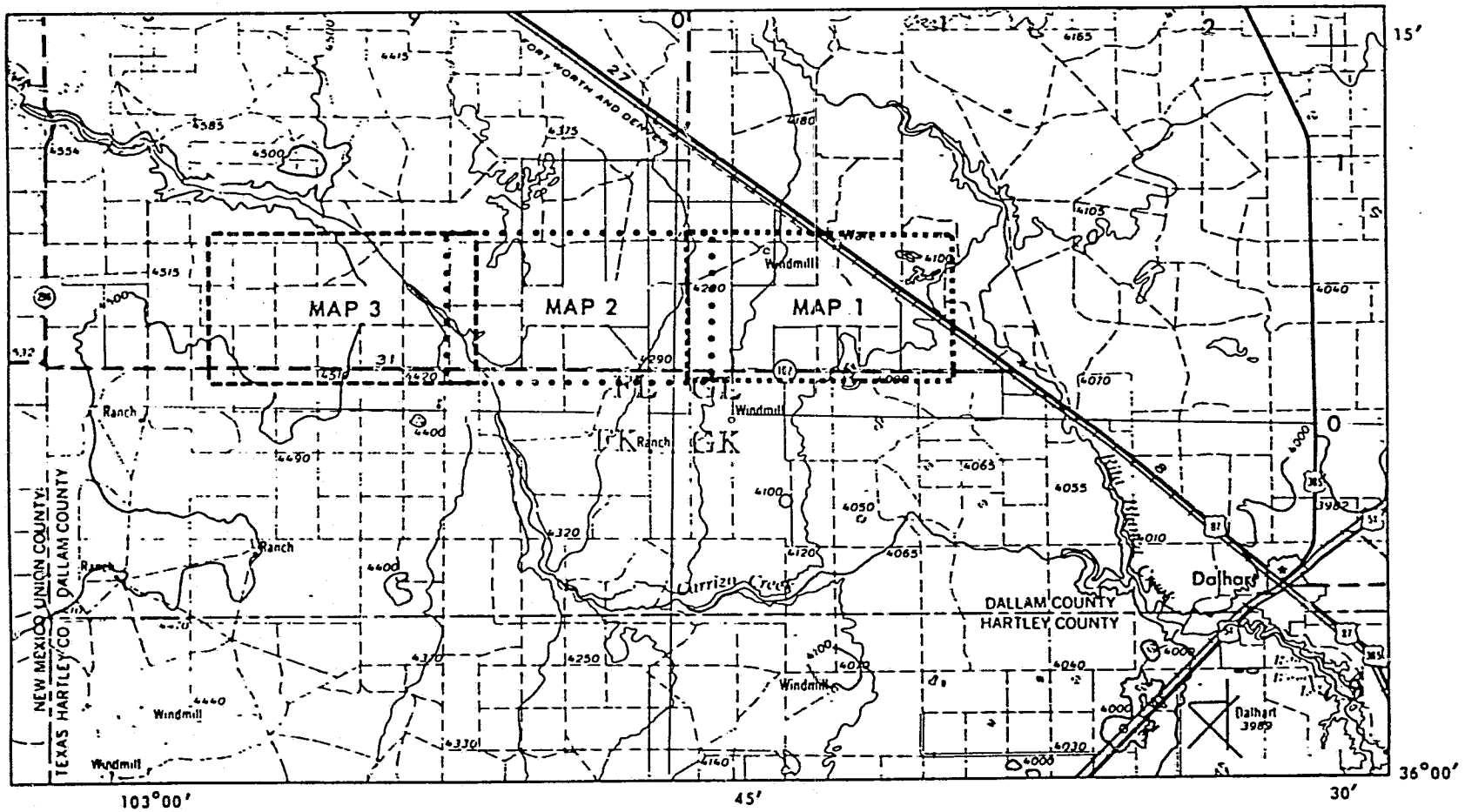

DALHART AREA MAP

INDEX TO FIELD MAPS

Approximate scale 1:250,000

FIG. 6 Dalhart field maps. a) Area map of Dalhart showing relative location of each field map.

DALHART, TEXAS 1980

LEGEND FOR FIELD MAPS 1,2 & 3

CROP

Bare: wheat stubble

disked wheat stubble

mulched wheat stubble

Millet

Milo

Corn

Alfalfa

Pasture

Grazed

— Flight line markers

▲ Corner reflectors

✱ Rain gauges

• Vegetation sample sites

Row direction was east-west for all sample fields with row crops.

APPROXIMATE SCALE 1:49000

2 1 0 2 MILES

2000 0 2000 4000 6000 8000 10000 12000 14000 FEET

2 1 0 2 KILOMETERS

Prepared by the Texas A&M University Remote Sensing Center. Base data compiled from USGS topographic maps, R.S.C. team field notes and NASA contracted aerial photography collected August 14-18, 1980.

FIG. 6b Legend for Dalhart, Texas field maps.

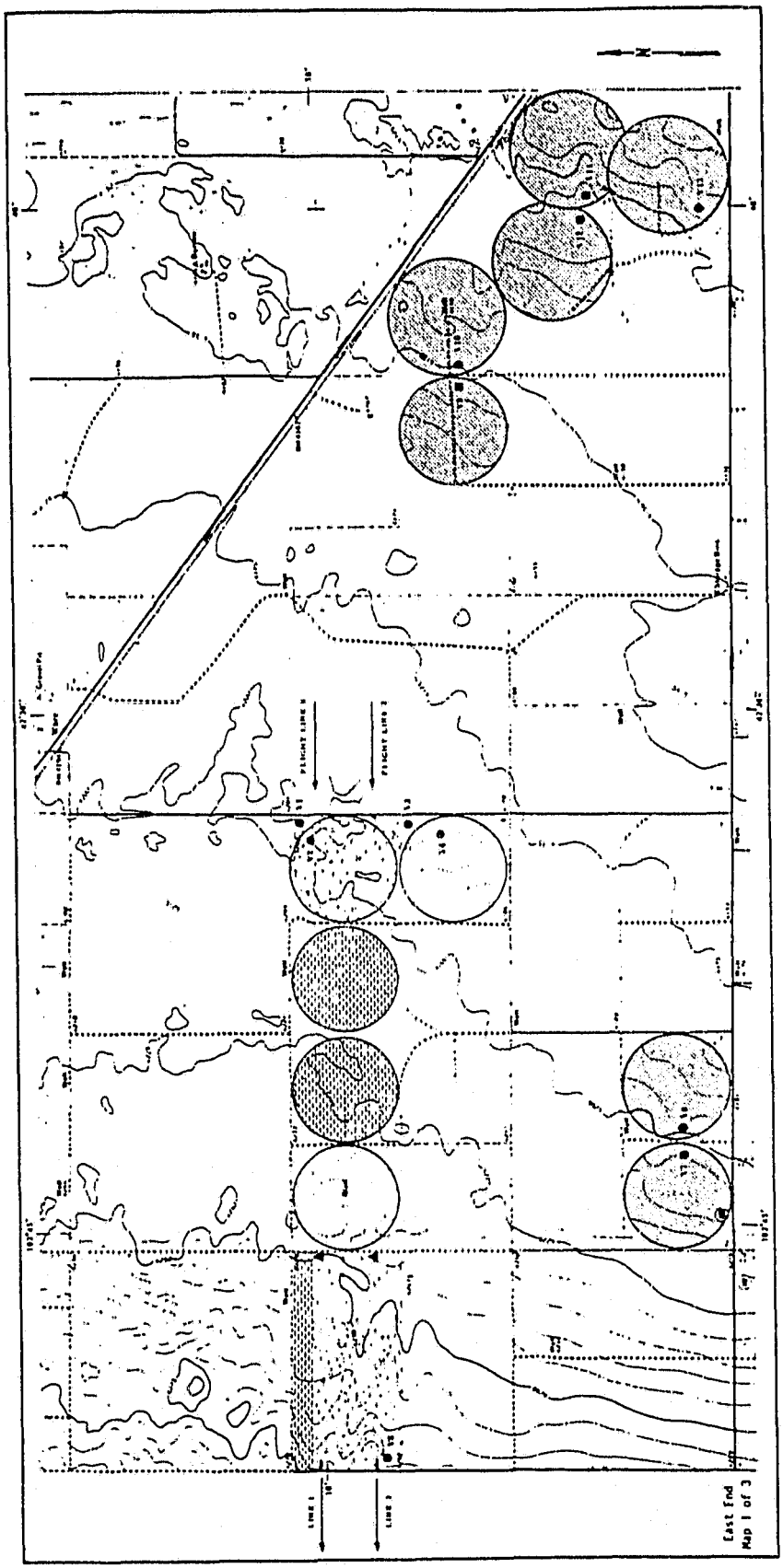

FIG. 6c Locations of sample fields at Dalhart.

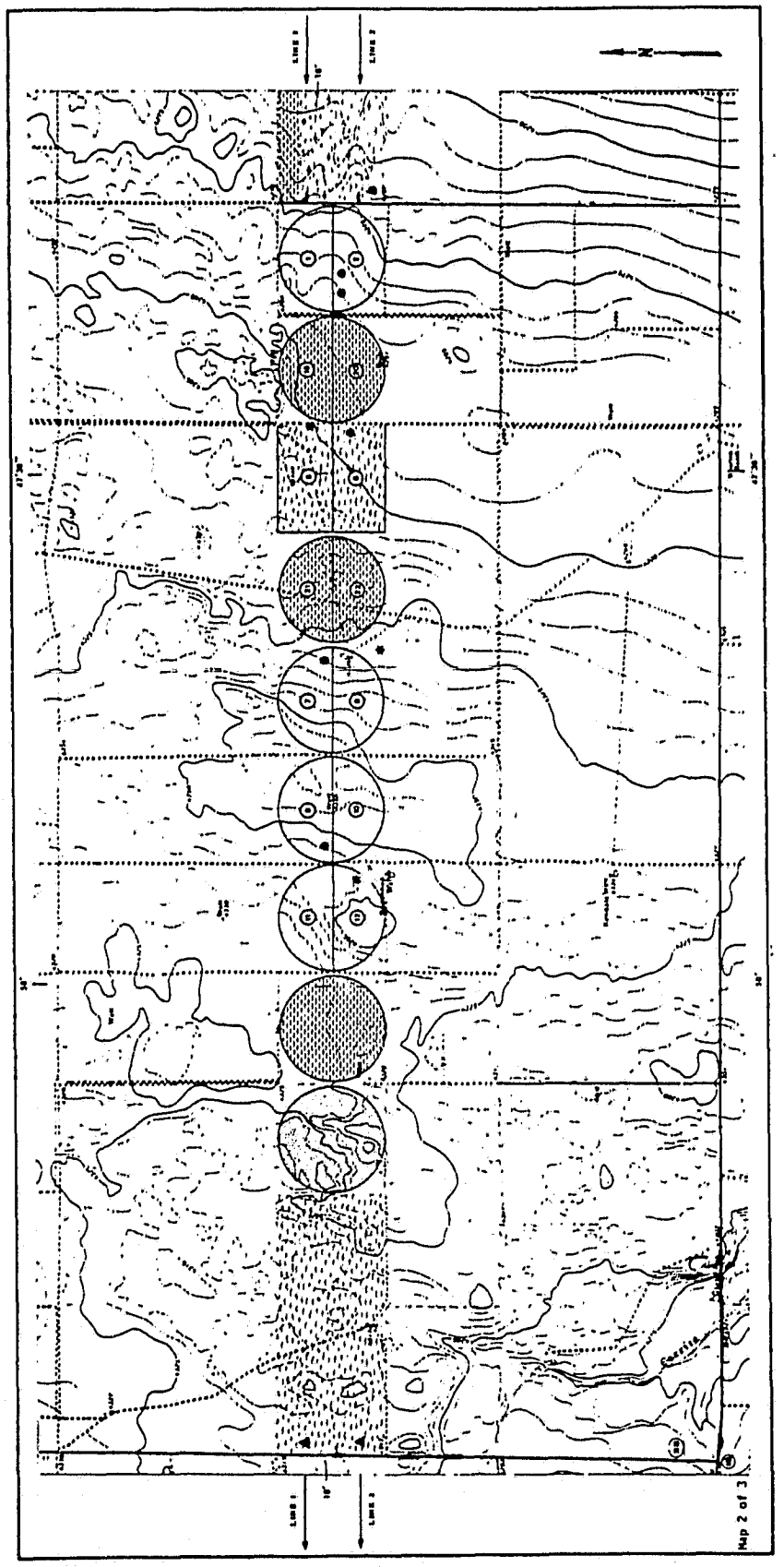

FIG. 6d Locations of sample fields at Dalhart.

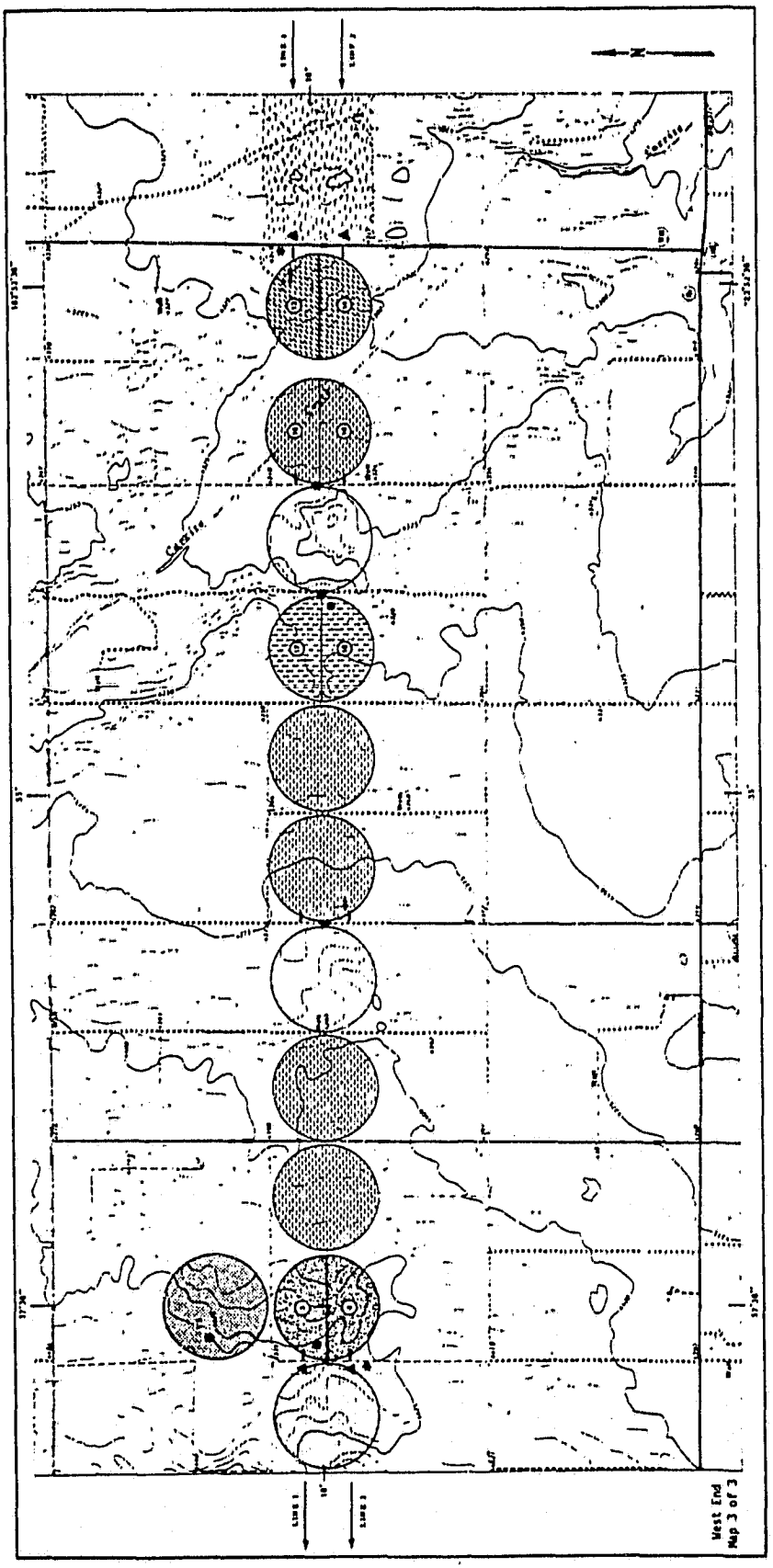

FIG. 6e Locations of sample fields at Dalhart.

The summer of 1980 was extremely dry in the Dalhart area. However, it was fortunate that this area received a one inch rain after the first sampling date. This provided a range of soil moisture conditions. Those fields with vegetation were reasonably uniform in crop cover. All corn fields were in mature stages. Only fields 1 and 2 showed areas of stress especially where some of the sprinkler nozzles were not functioning properly. Field conditions are summarized in Table 2.

Soil Moisture Data

Soil moisture samples were collected at eight points per 32 hectare field (Fig. 7) except in the Guymon fields 6 and 14 which were intensively sampled (37 points). Dalhart sample depths were 0-2 cm, 2-5 cm, 5-15 cm, 0-15 cm, 15-30 cm, 30-45 cm (Fig. 8). The 5-15 cm interval was divided into two samples at Guymon; 5-9 cm and 9-15 cm. Manpower limitations did not allow each field to be sampled during the

To correlate the ground data to aircraft data, the soil moisture values in fields not sampled on flight days had to be extrapolated. To do this, graphs were generated plotting soil moisture versus time. By incorporating precipitation events and irrigation schedules in the graphs, it was possible to produce dry-down curves for each field and point. This method also enabled the estimation of soil moisture for points where values were missing due to pesticide spraying, rain, sample spills, etc. Where the curve for each depth intersected a flight time, the value was recorded as the new gravimetric soil moisture. These values plus the bulk density results were used to calculate the volumetric soil moistures by point. Texture analyses were performed for each field in Guymon and for selected fields in Dalhart.

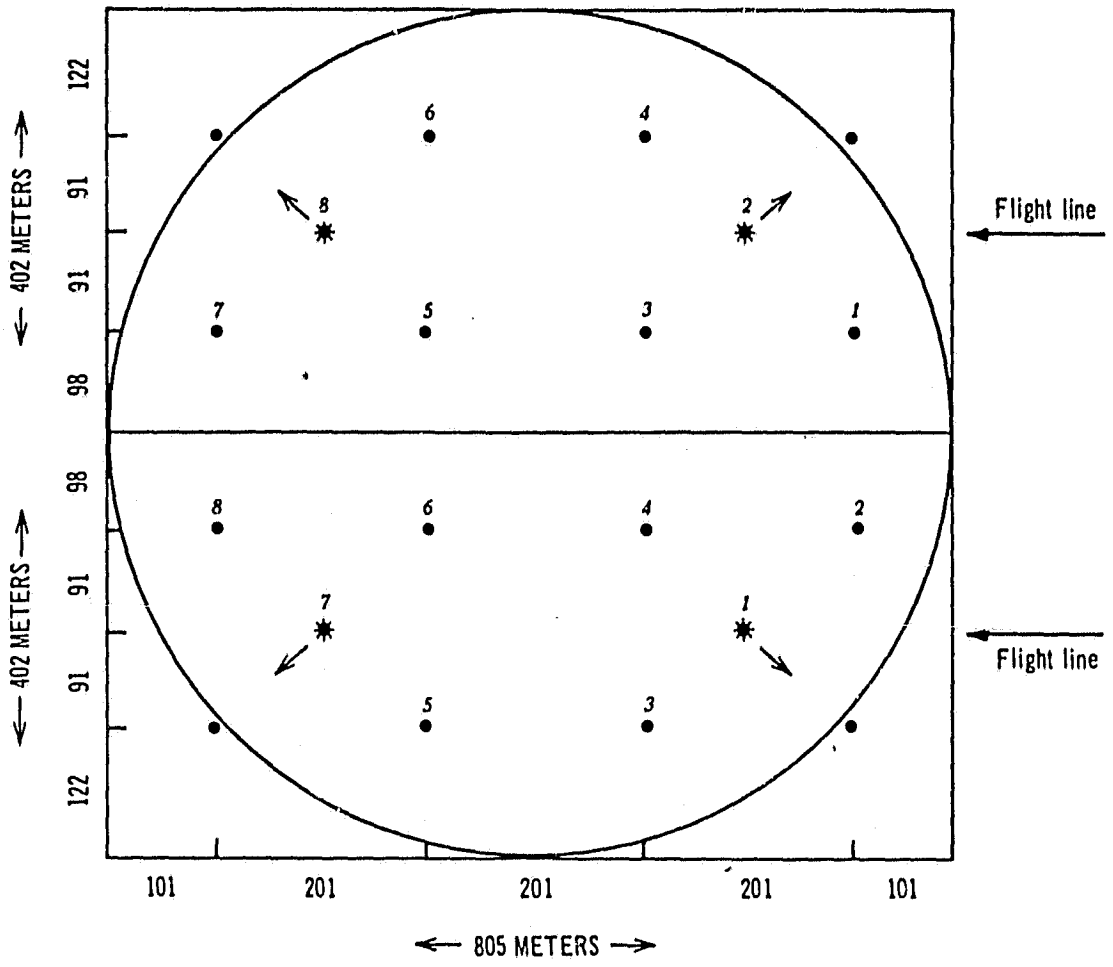

* These points were moved outside the pivot boundary for non-circular fields.

FIG. 7 Sampling pattern for fields at Guymon and Dalhart.

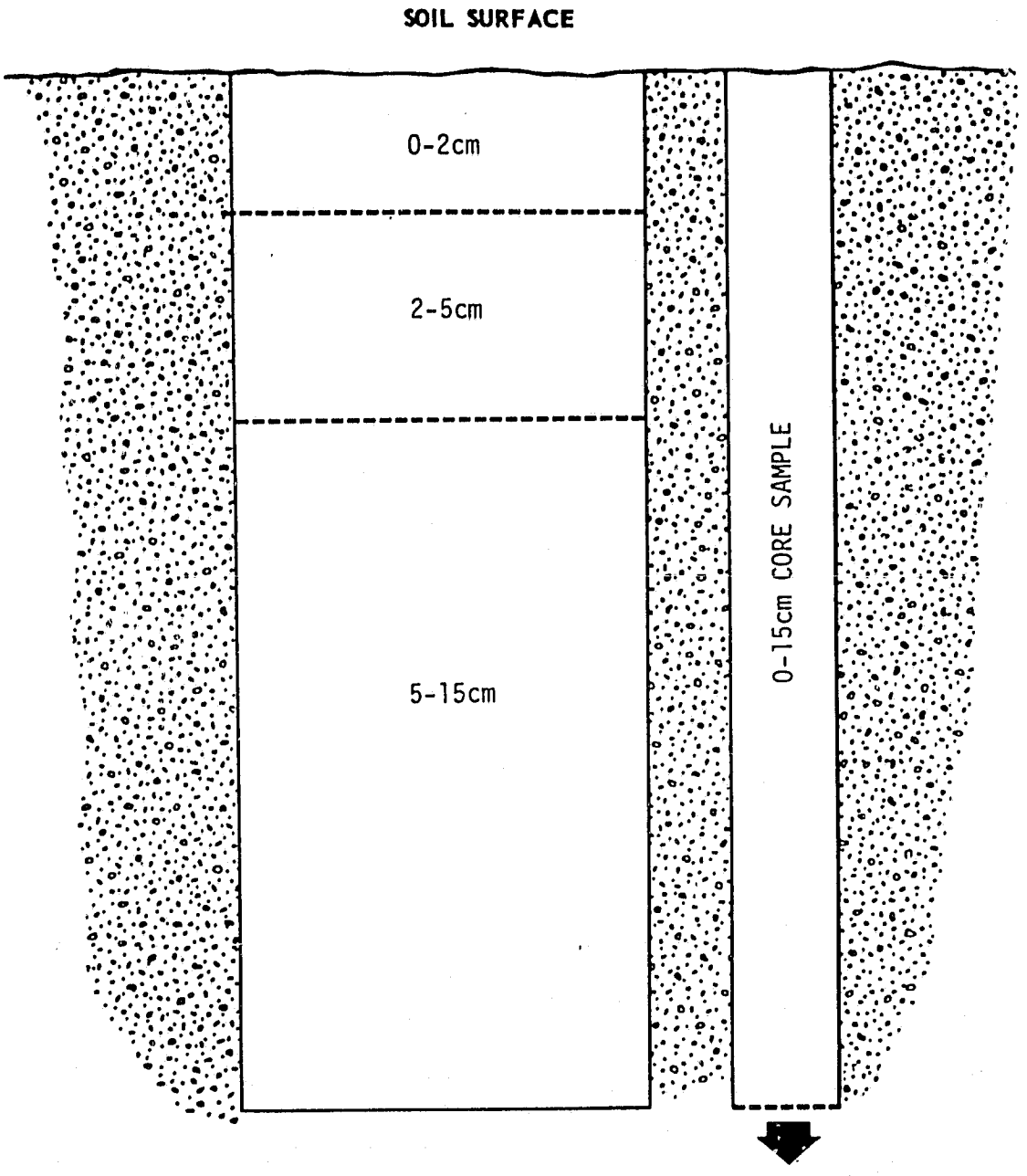

FIG. 8 Soil moisture sampling depths at Dalhart and Guymon. The 15-30 and 30-45 cm core samples were also taken in addition to the above. The 5-15 cm sample was divided into two samples at Guymon; 5-9 cm and 9-15 cm.

Ground tracks of the line sensors were used to determine which sample points fell within the area covered by the sensors. These points were arithmetically averaged by field and termed soil moisture under the line sensors or just soil moisture.

The soil sample processing lab was set up with conventional microwave ovens. As the samples came in from the field, they were weighed with seals and lids on the cups. This weight (measured to a tenth of a gram) was recorded as the wet weight. Lids and seals were then discarded and soil samples dried in the ovens. At regular time intervals two test samples per oven were removed and weighed and returned to the ovens. The weights were plotted on a graph to track the dry-down. When the weight loss of the test samples leveled out to less than a 0.2 gram difference from the previous weighing, they were considered dry. All samples were then removed from the oven and their dry weights recorded. As the preprocessing was completed for a set, the samples were stored for possible future reference.

A programmable calculator was used in the lab to compute gravimetric soil moistures as the final weights were completed. The program automatically subtracted an average lid, seal and cup weight from the gross values. Daily soil moisture charts were kept on each field, point and depth. This system facilitated quality control of the data. If a value was questionable, the sample was located, reweighed and its soil moisture recalculated immediately.

Aircraft Data

Aircraft sensor data were similar for both experiments. The Guymon data were collected on August 2, 5, 8, 11, 14, and 17, 1978. The Dalhart data were collected on August 14, 16 (two flights), and 18

(late afternoon), 1980. The sensor package consisted of 1) seven scatterometer frequencies and polarizations, 2) three passive microwave radiometer frequencies and polarizations, 3) Barnes PRT-5 thermal data, 4) aerial photography, and 5) visible/infrared scanner data. Soil moisture flights were made at an altitude of 500 m. Scatterometer frequencies and polarizations included:

1) 13.3 GHz VV
2) 4.75 GHz HH
3) 4.75 GHz HV
4) 1.6 GHz HH
5) 1.6 GHz HV
6) 0.4 GHz HH
7) 0.4 GHz HV

where VV = vertically polarized transmitted and received

HH = horizontally polarized transmitted and received

HV = horizontally polarized transmitted and vertically received. Eight look angles from nadir were processed: 5, 10, 15, 20, 25, 35, 40, and 45 degrees. Near-nadir (3 degree) passive microwave data were collected at 1) L-band (1.6 GHz) horizontal polarization, 2) C-band (4.75 GHz) vertical, and 3) C-band horizontal polarization. In Dalhart, the eight channels of the NS001 (simulated thematic mapper) bands included:

1) Channel 1: 0.45-0.52 μm
2) Channel 2: 0.52-0.60 μm
3) Channel 3: 0.63-0.69 μm
4) Channel 4: 0.76-0.90 μm
5) Channel 5: 1.00-1.30 μm
6) Channel 6: 1.55-1.75 μm

7) Channel 7: 2.08-2.35 μm

8) Channel 8: 10.4-12.5 μm

In Guymon, five channels from the modular multispectral scanner (M^2S) were processed:

1) Channel 4 0.548-0.583 μm

2) Channel 7 0.662-0.701 μm

3) Channel 8 0.703-0.747 μm

4) Channel 9 0.770-0.863 μm

5) Channel 11 8.000-12.00 μm

The M^2S channels 7, 9, and 11 correspond closely to the NS001 channels 3, 4, and 8, respectively.

Data Processing

Processing procedures for the individual sensors and ground data are given in Appendix A. The procedures included calibration, quality control, data omission, and field average determination. Data omission usually occurred with excessive roll and drift of the aircraft. Once field averages had been calculated for each sensor and their corresponding soil moisture, the ground and aircraft data sets were merged. Further analysis was done on the field averaged data set.

ANALYSIS AND DISCUSSION

Approach

Case studies were first performed to investigate the microwave sensor responses to soil moisture and roughness. Previous studies have related microwave sensor responses to surface soil moisture at near incident angles. Near incident angle scatterometer (active) and

radiometer (passive) microwave data for all available frequencies and polarizations were plotted and regressed against soil moisture (0-2 cm) over essentially bare soils. Regression line slopes and correlation coefficients were used as criteria for evaluating the sensitivity and relative value of each sensor configuration. From this analysis a single microwave sensor, the L-band radiometer, was chosen as the sensor that exhibited the highest potential to quantify soil moisture.

The analysis was then expanded to vegetated fields for this sensor. Linear relations were determined for the L-band response to soil moisture for each crop type. These individual relations were used to obtain predicted values of soil moisture. The correlation between measured and predicted soil moisture over all fields represented the optimum capability of the L-band passive microwave sensor to quantify soil moisture when crops can be accurately classified.

In general, crop type is related to biomass; however, there is a range of biomass within each crop type. A visible/infrared biomass estimator and crop classifier (PVI) was directly combined with the L-band passive microwave data to quantify soil moisture independent of crop type. The direct combination technique was compared to the classification techniques and microwave alone.

Case Studies

Two case studies were performed on the sensor data from Dalhart in order to investigate each microwave sensor's response to particular changes in 1) soil moisture and 2) roughness. Fig. 9 illustrates a

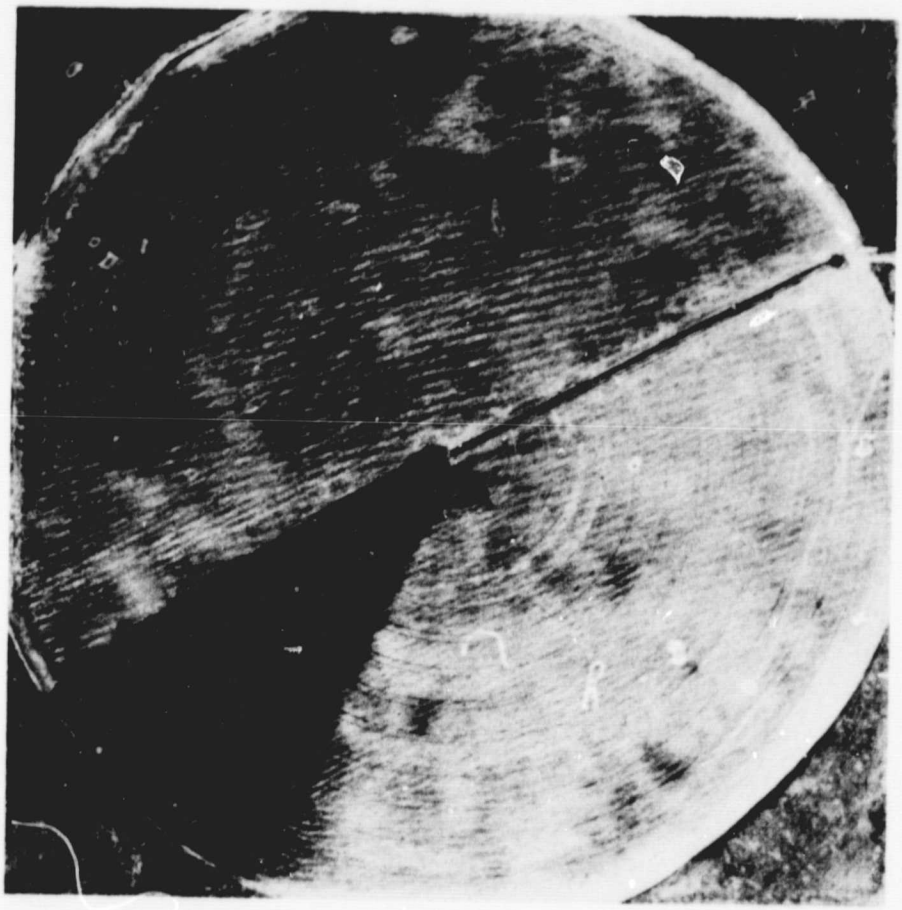

FIG. 9 Photo of case study field. The lower left portion of the field is being actively irrigated.

field being actively irrigated at the time of the data collection. Soil moisture measurements were not available but the field is noticeably wetter (darker) on the left side where it had been irrigated recently. The field had uniform roughness on a scale similar to nearby sample fields. Line plots of each sensor are presented at the same horizontal scale as the photograph in Figs. 10-12. Passive microwave sensor (Fig. 10) exhibited approximately a 25 K sensitivity to the difference in soil moisture while the surface thermal temperature range was approximately 3.5 K. This small thermal response is due to the time of day the data were taken. The flight time was mid-morning but this change in thermal temperature indicates that there was a change in moisture between the two portions of the flight line. The scatterometers at 10 degree incident angle (Fig. 11) exhibited considerable signal noise and a maximum sensitivity of only approximately 5 dB after the noise is smoothed. It is interesting to observe that all the scatterometers exhibit a stronger dependence on soil moisture at 40 degree incident angle (Fig. 12). This is contrary to results from most previous studies.

The second case study involved field 15 at Dalhart. A photo is not presented but the left half portion of this field had been recently disked. The right half was burned wheat stubble (relatively smooth). The field had uniform soil moisture (15 percent by volume). A definite roughness influence is apparent in the passive microwave responses (Fig. 13) that does not readily appear in the 10 degree scatterometer data (Fig. 14). The roughness effect is again apparent in all the 40 degree scatterometer data (Figure 15) with the exception of returns from the 1.6 GHz HV, 0.4 GHz HH, and 0.4 GHz HV scatterometers.

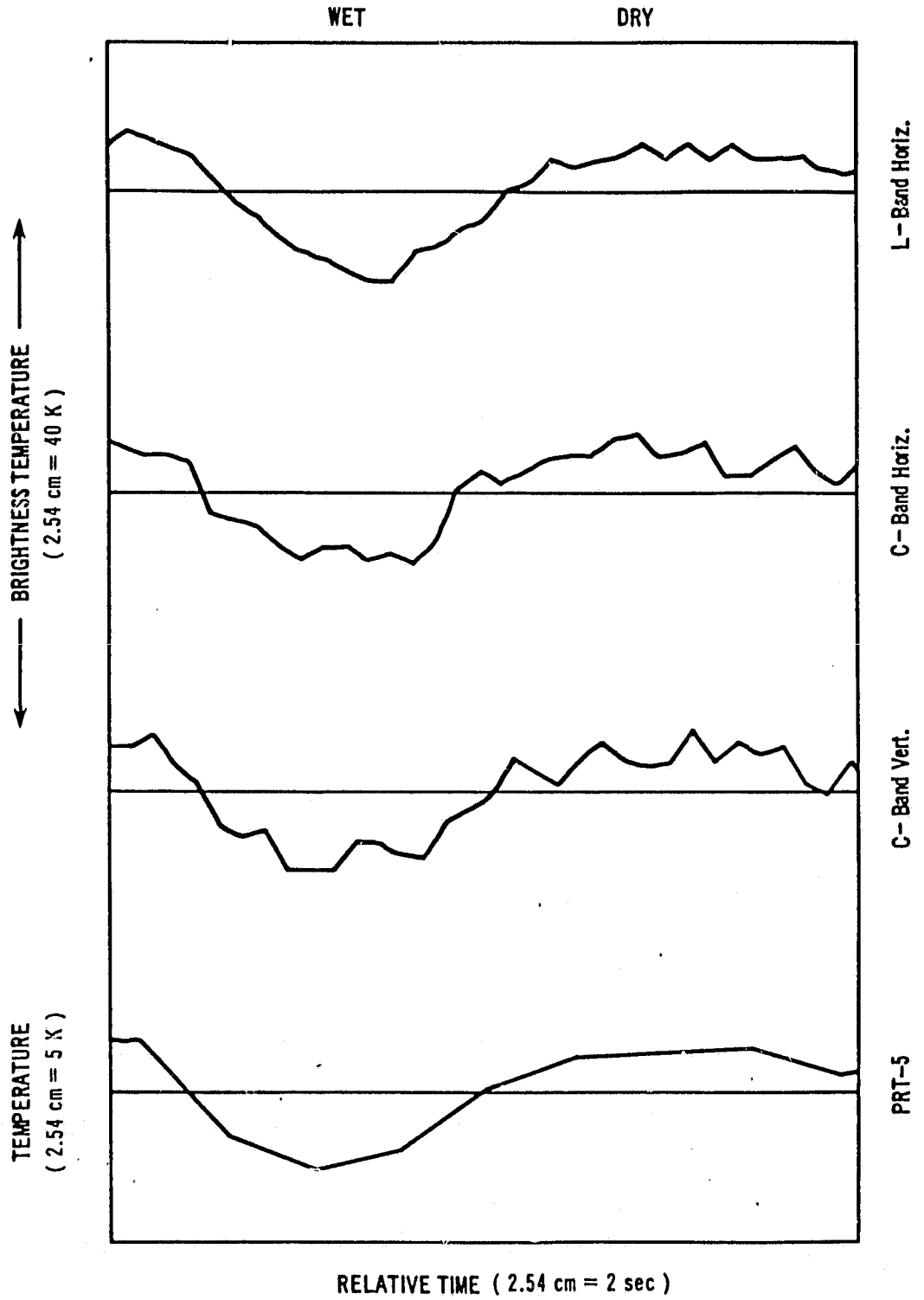

FIG. 10 Line plots (sensor response vs. time) of field in Fig. 9 for L- and C-band radiometers and PRT-5.

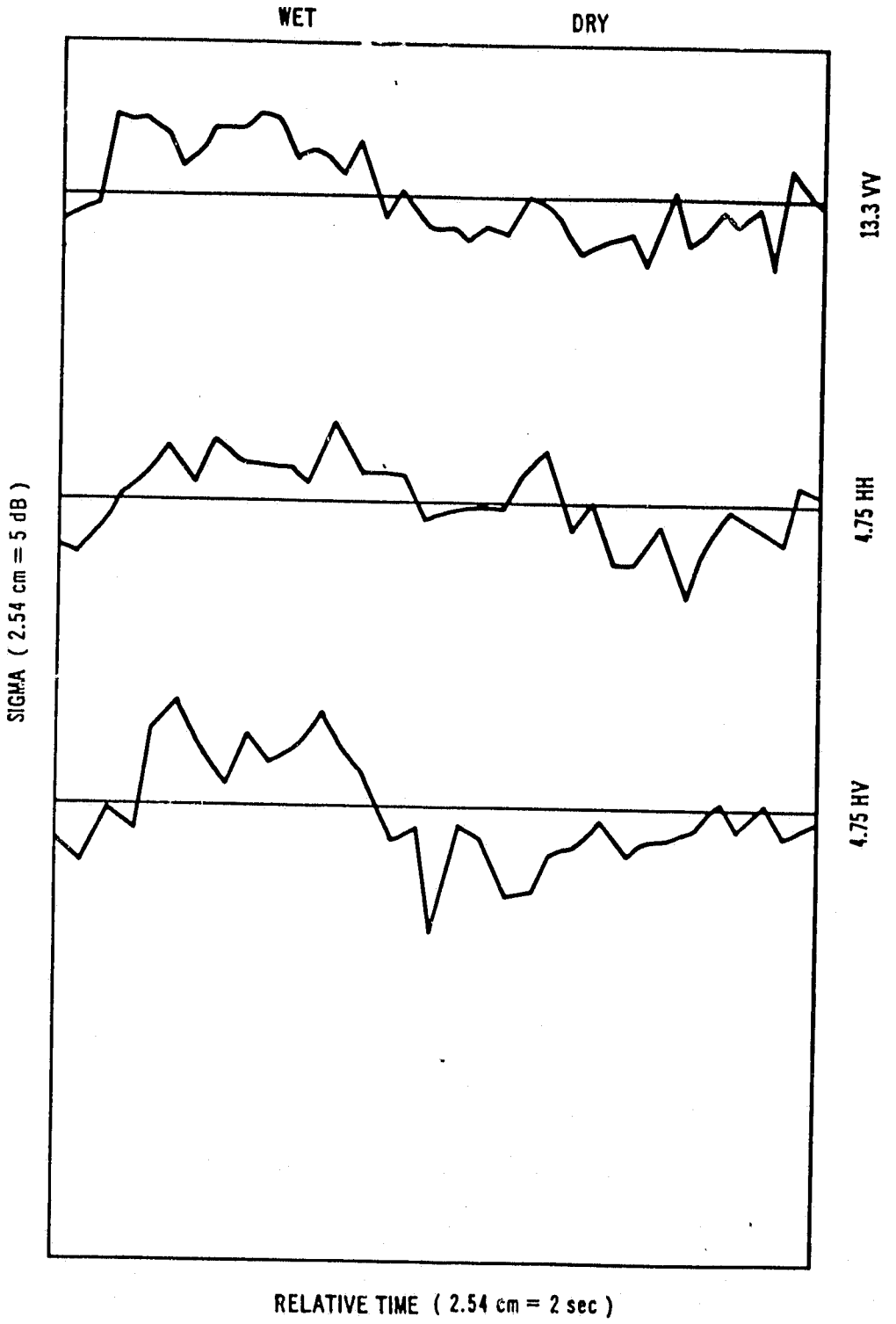

FIG. 11a Line plots (sensor response vs. time) of field in Fig. 9 for 13.3 GHz VV, 4.75 GHz HH, and 4.75 GHz HV scatterometers at 10 degree incident angle.

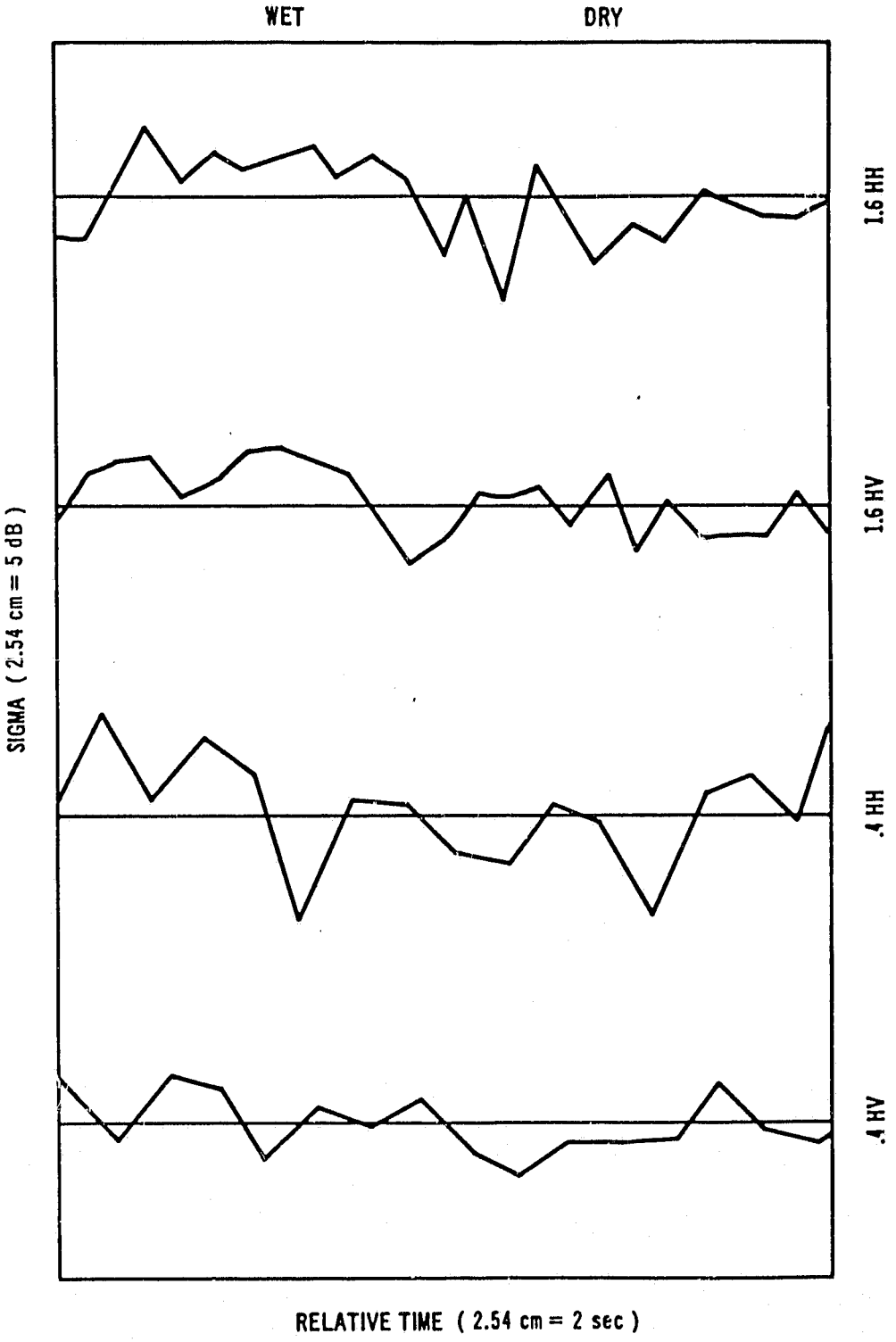

FIG. 11b Line plots (sensor response vs. time) of field in Fig. 9 for 1.6 GHz HH, 1.6 GHz HV, 0.4 GHz HH, 0.4 GHz HV scatterometers at 10 degree incident angle.

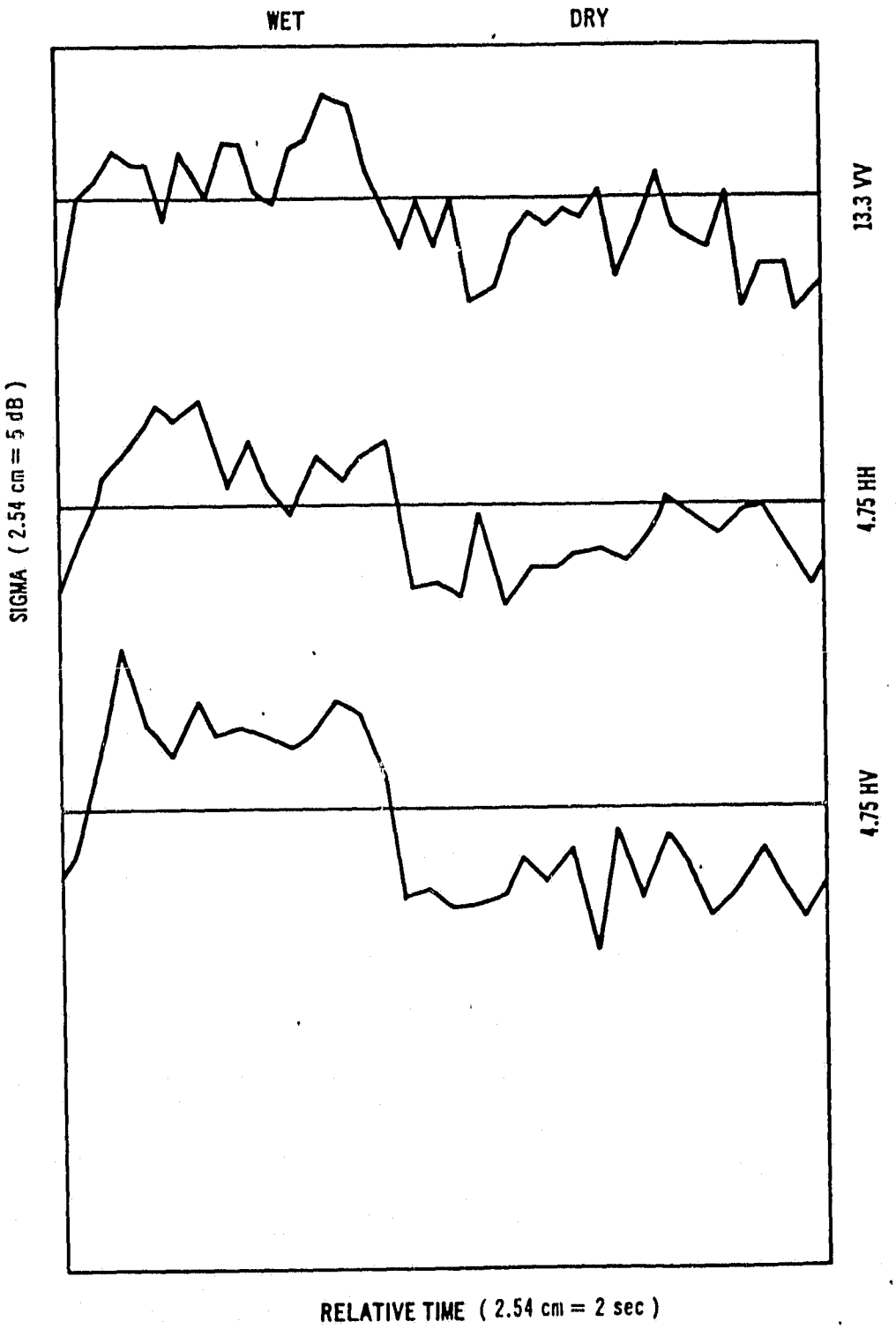

FIG. 12a Line plots (sensor response vs. time) of field in Fig. 9 for 13.3 GHz VV, 4.75 GHz HH, and 4.75 GHz HV scatterometers at 40 degree incident angle.

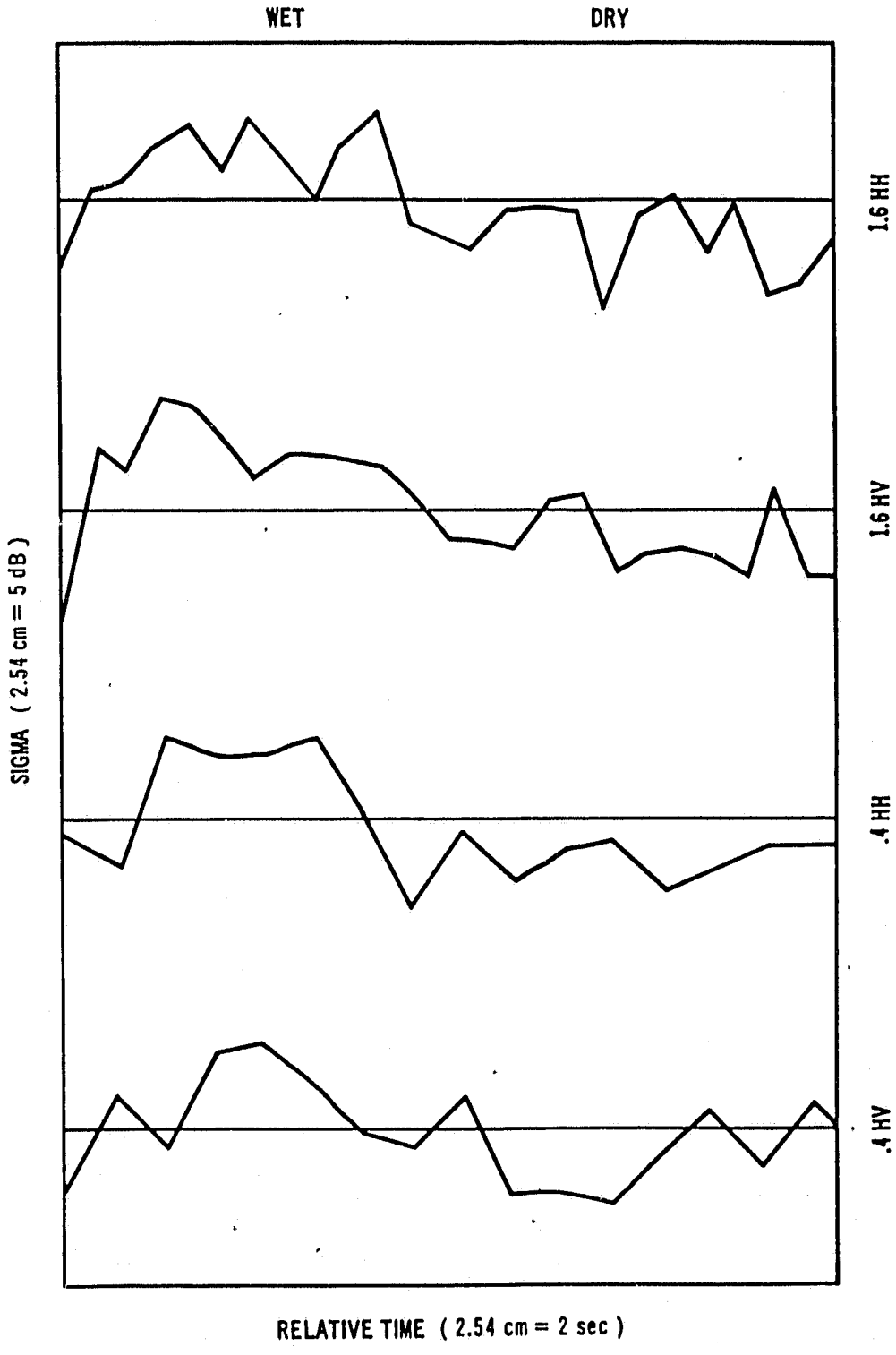

FIG. 12b Line plots (sensor response vs. time) of field in Fig. 9 for 1.6 GHz HH, 1.6 GHz HV, 0.4 GHz HH, 0.4 GHz HV scatterometers at 40 degree incident angle.

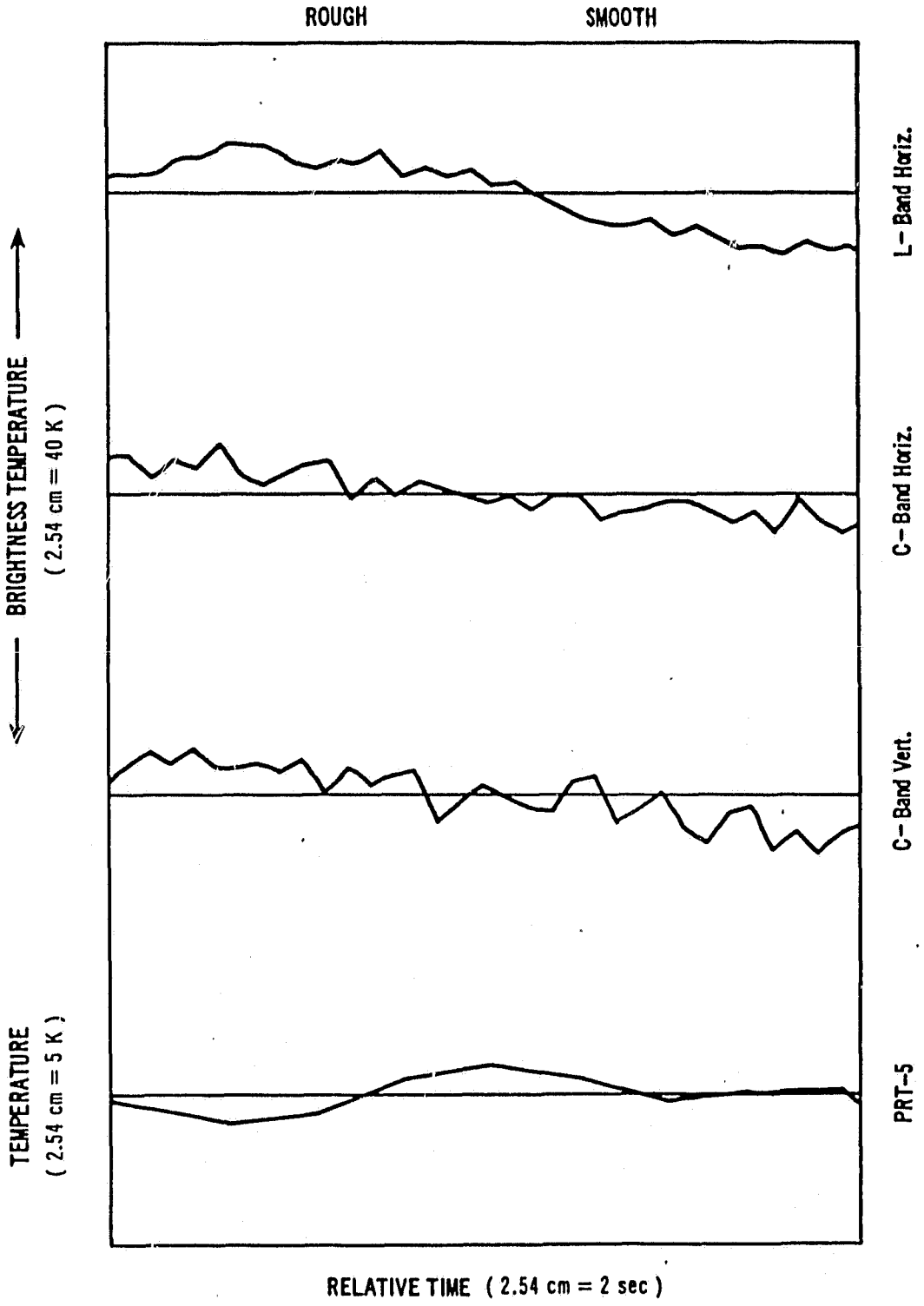

FIG. 13 Line plots (sensor response vs. time) of case study field (rough and smooth) for L- and C-band radiometers and PRT-5.

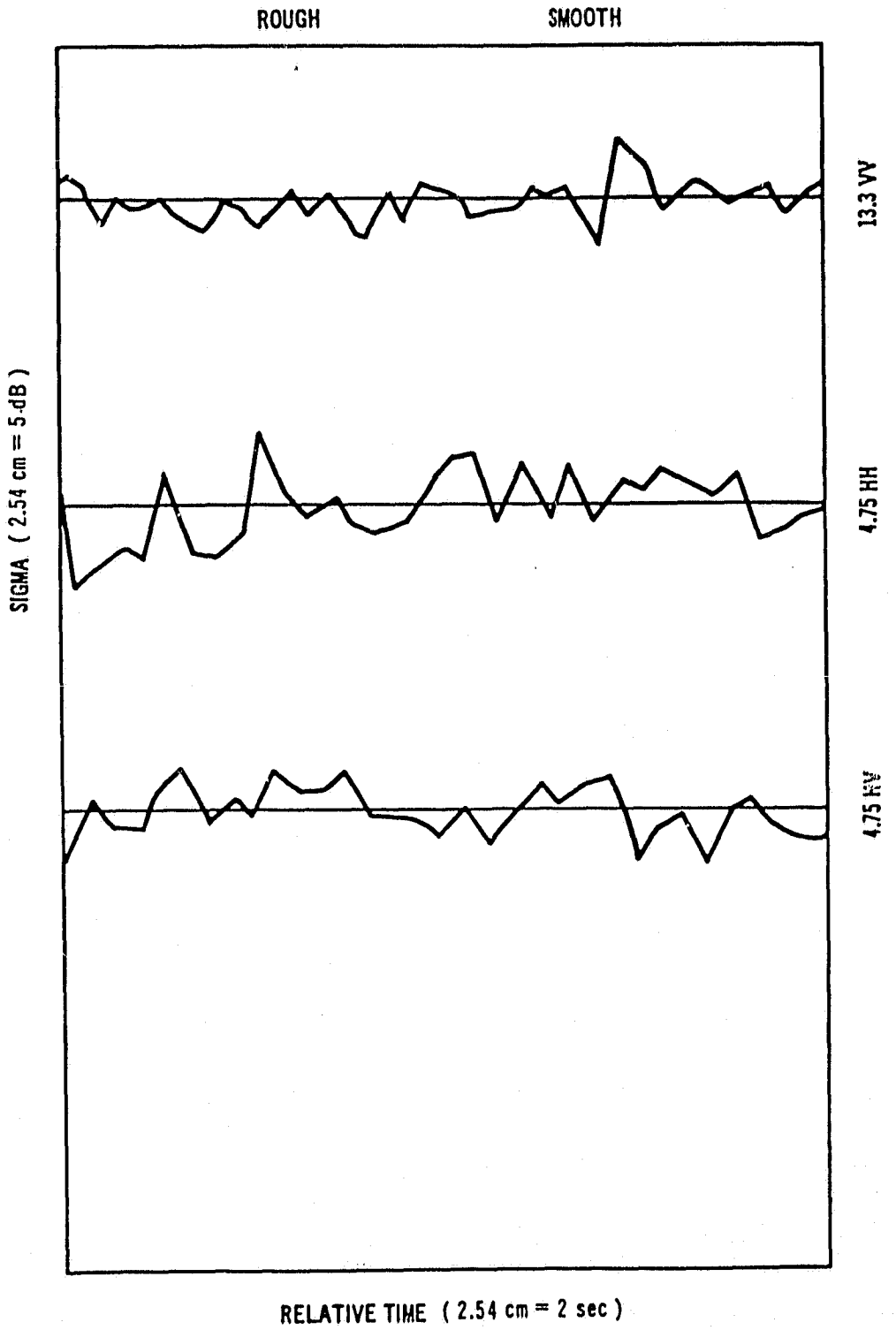

FIG. 14a Line plots (sensor response vs. time) of case study field (rough and smooth) for 13.3 GHz VV, 4.75 GHz HH, and 4.75 GHz HV scatterometer at 10 degree incident angle.

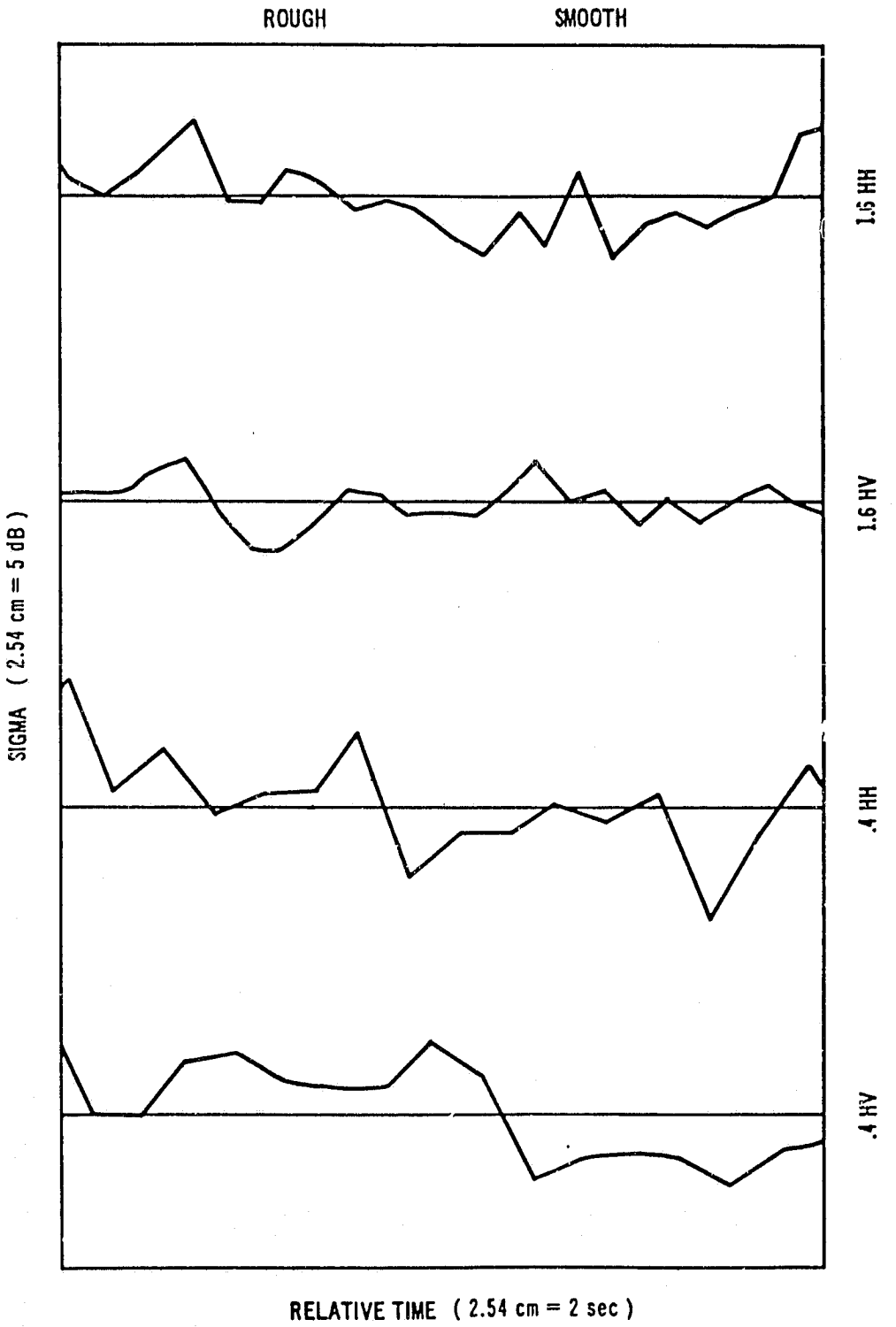

FIG. 14b Line plots (sensor response vs. time) of case study field (rough and smooth) for 1.6 GHz HH, 1.6 GHz HV, 0.4 GHz HH, and 0.4 GHz HV, scatterometer at 10 degree incident angle.

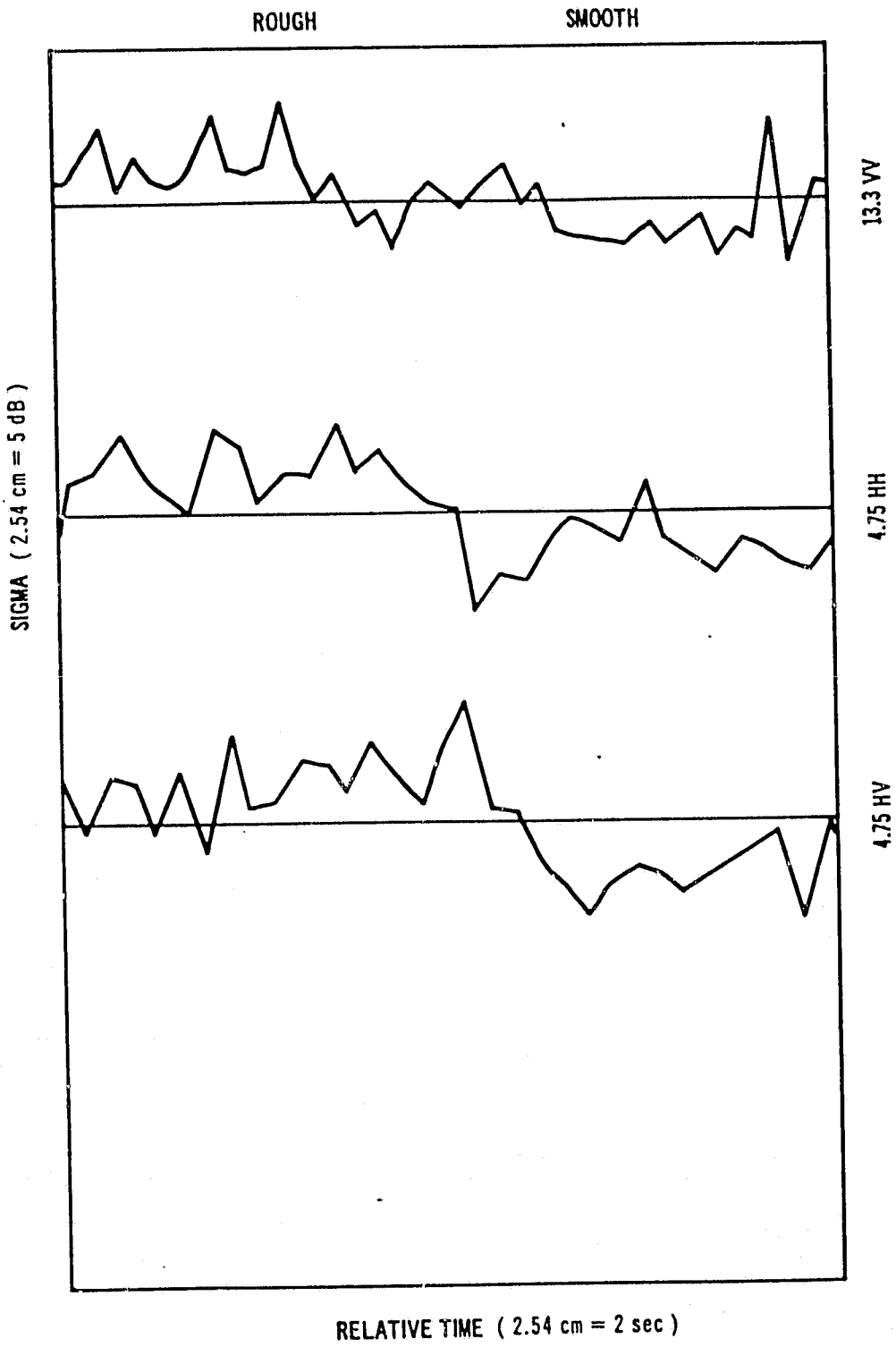

FIG. 15a Line plots (sensor response vs. time) of case study field (rough and smooth) for 13.3 GHz VV, 4.75 GHz HH, and 4.75 GHz HV scatterometer at 40 degree incident angle.

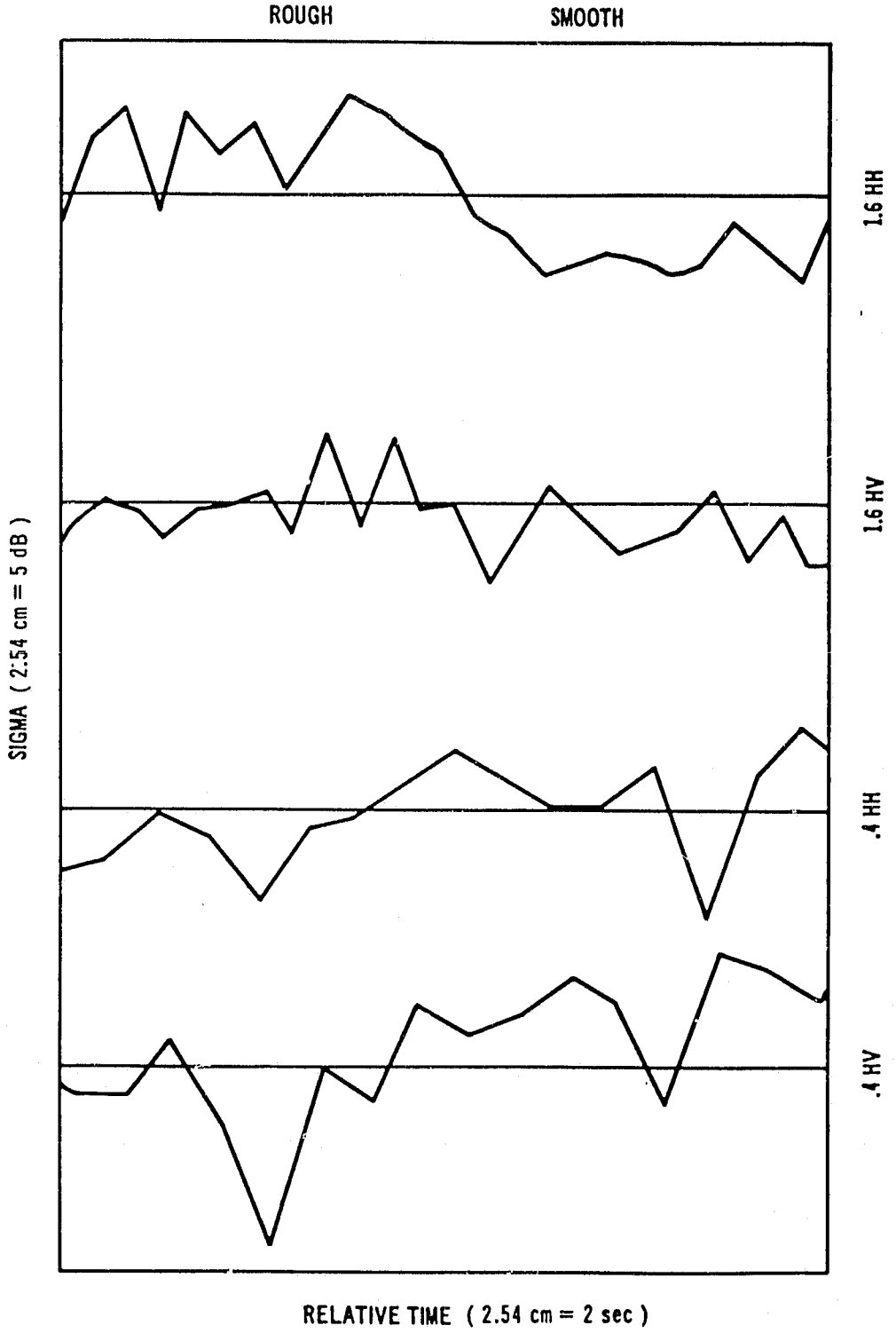

FIG. 15b Line plots (sensor response vs. time) of case study field (rough and smooth) for 1.6 GHz HH, 1.6 GHz HV, 0.4 GHz HH, and 0.4 GHz HV scatterometer at 40 degree incident angle.

Microwave Sensor Responses to Soil Moisture Over Bare Fields

This analysis is presented in two sections (scatterometers and radiometers) to avoid confusion between the active and passive systems. For the same set of fields, plots of sensor responses versus volumetric soil moisture (0-2 cm) are presented for each sensor. The fields selected for these illustrations were all bare with a range of roughness effect due to tillage and surface weathering. There was no quantitative measure of roughness, but it was observed to range from smooth to moderately rough as defined by Newton (1977).

Scatterometers

As mentioned before, previous investigations indicated that the scatterometer's highest potential for detection of soil moisture is around the 10 degree incident angle. Plots of each scatterometer's response at the 10 degree incident angle versus soil moisture in the surface 2 centimeters are presented (Fig. 16-19) to illustrate differences in the data sets. The scatterometer returns at low soil moisture shifted approximately 0 dB, 5 dB, 8 dB and 7 dB for the 13.3, 4.75, 1.6 and 0.4 GHz systems, respectively. These shifts illustrate that the comparison of the two data sets must be approached with caution. Further analysis was conducted for each scatterometer within each data set to minimize the influence of lack of calibration.

Each scatterometer's response versus volumetric soil moisture (0-2 cm) was analyzed for 10, 15, 20, and 40 degree incident angles. The 1.6 GHz HH scatterometer (Dalhart) is illustrated in Fig. 20 as a representative sample of the scatterometer responses. The remainder of the illustrations are in Appendix B. The absence of a direct

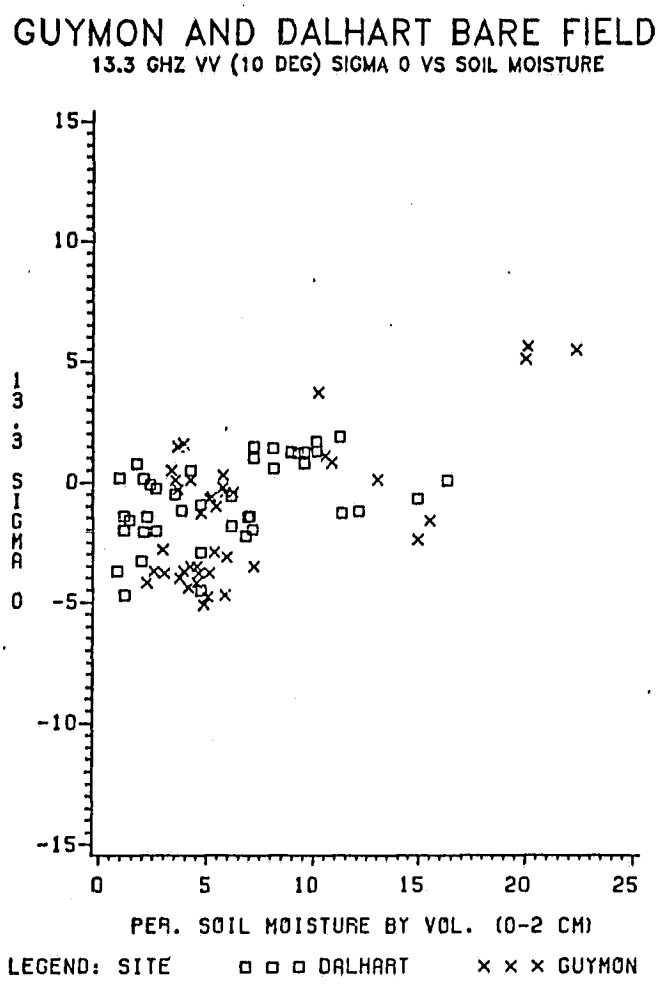

FIG. 16 Scatterplot of 13.3 GHz σ^0 vs. volumetric soil moisture (0-2 cm) for Guymon and Dalhart bare fields.

GUYMON AND DALHART BARE FIELDS

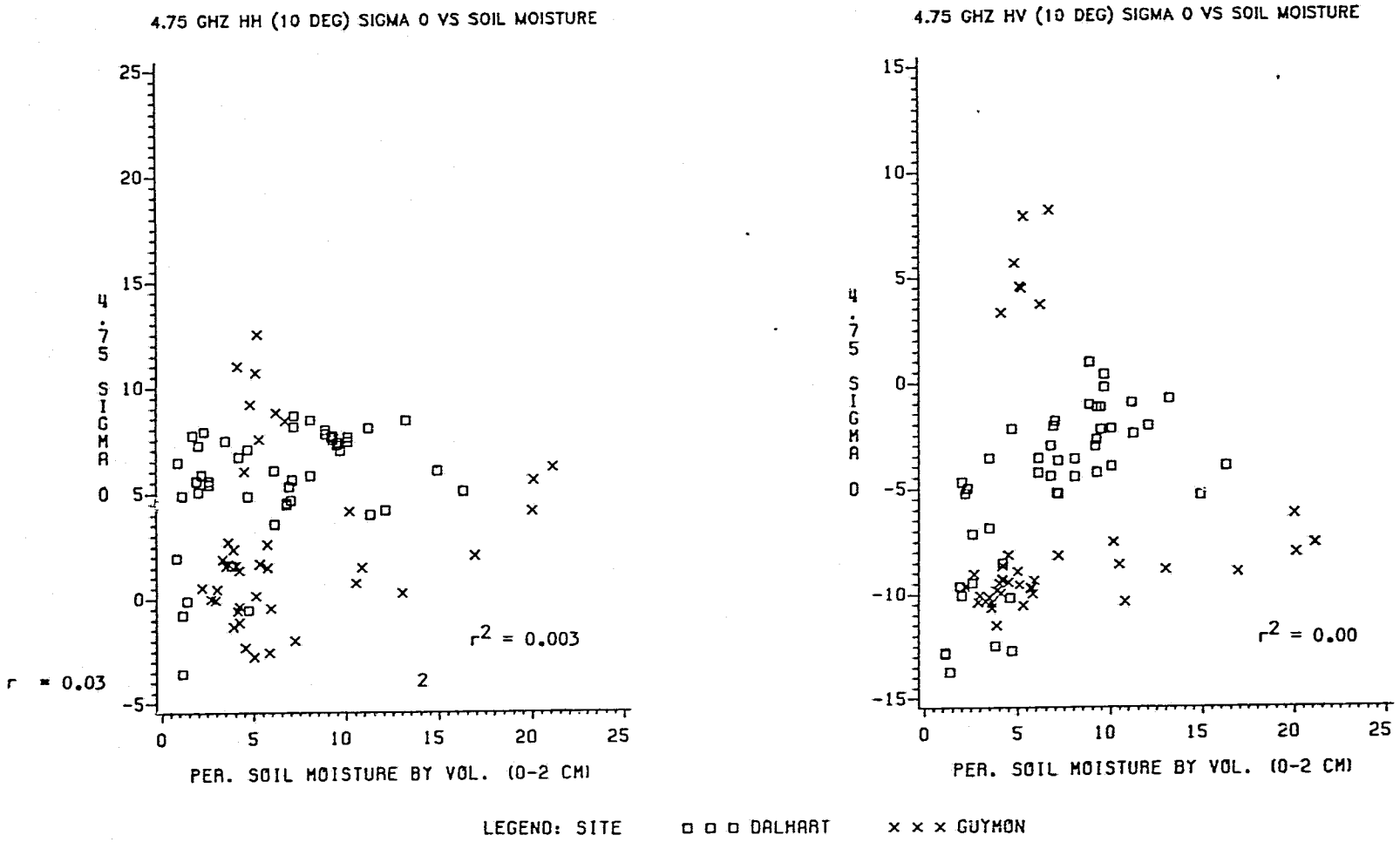

FIG. 17 Scatterplot of 4.75 GHz σ^0 vs. volumetric (0-2 cm) for Guymon and Dalhart bare fields.

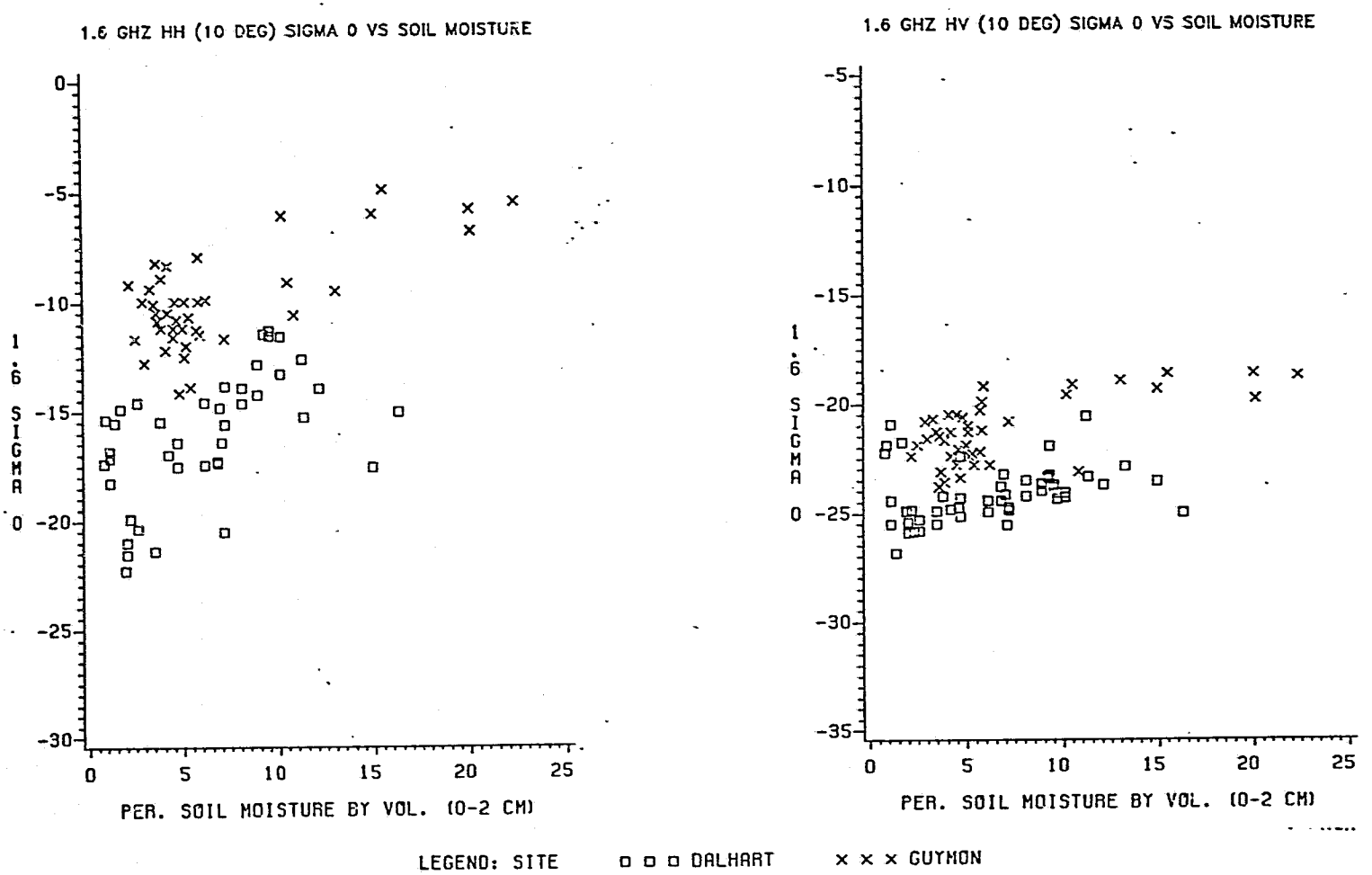

FIG. 18 Scatterplot of 1.6 GHz σ^0 vs. volumetric soil moisture (0-2 cm) for Guymon and Dalhart bare fields.

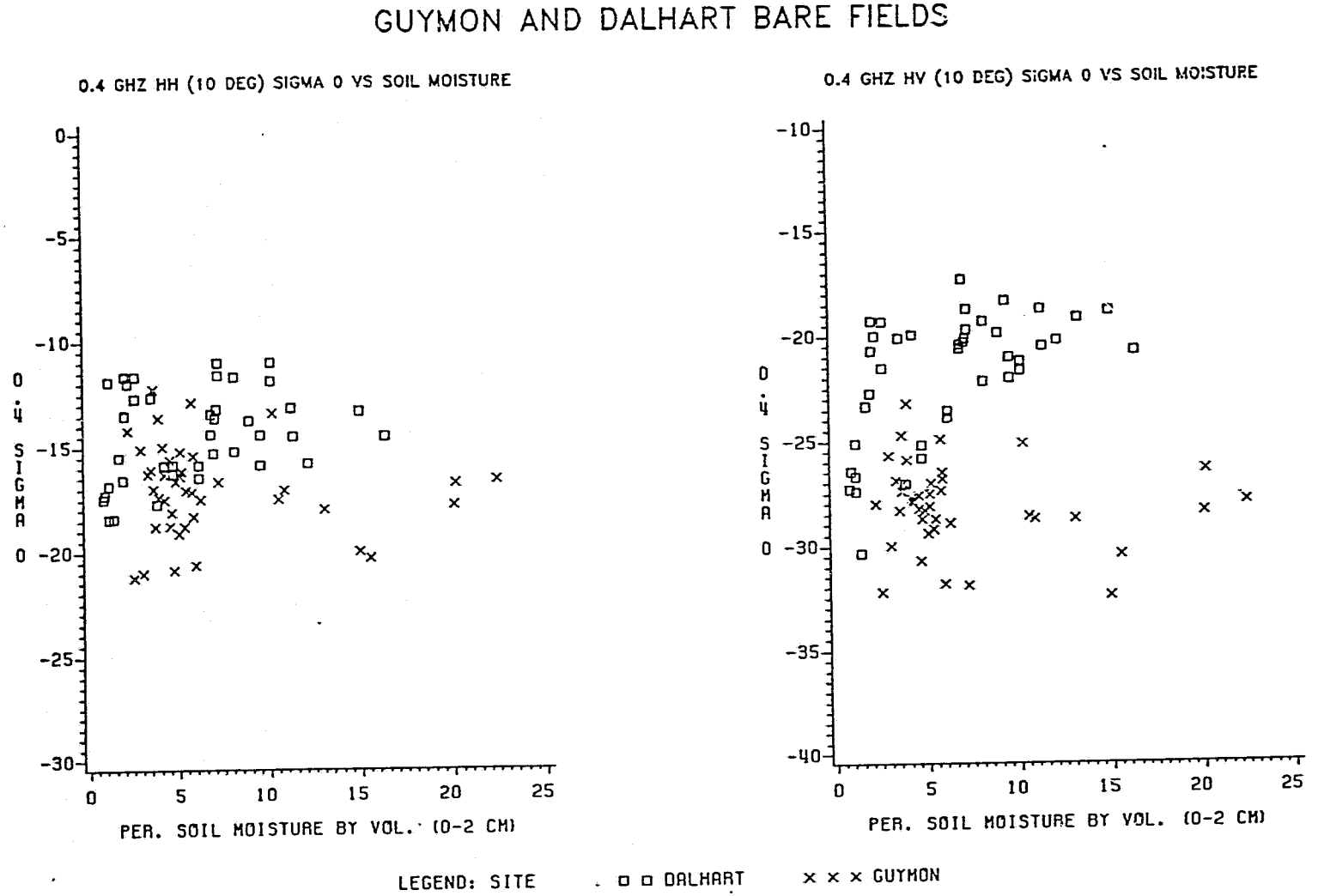

FIG. 19 Scatterplot of 0.4 GHz σ^0 vs. volumetric soil moisture (0-2 cm) for Guymon and Dalhart bare fields.

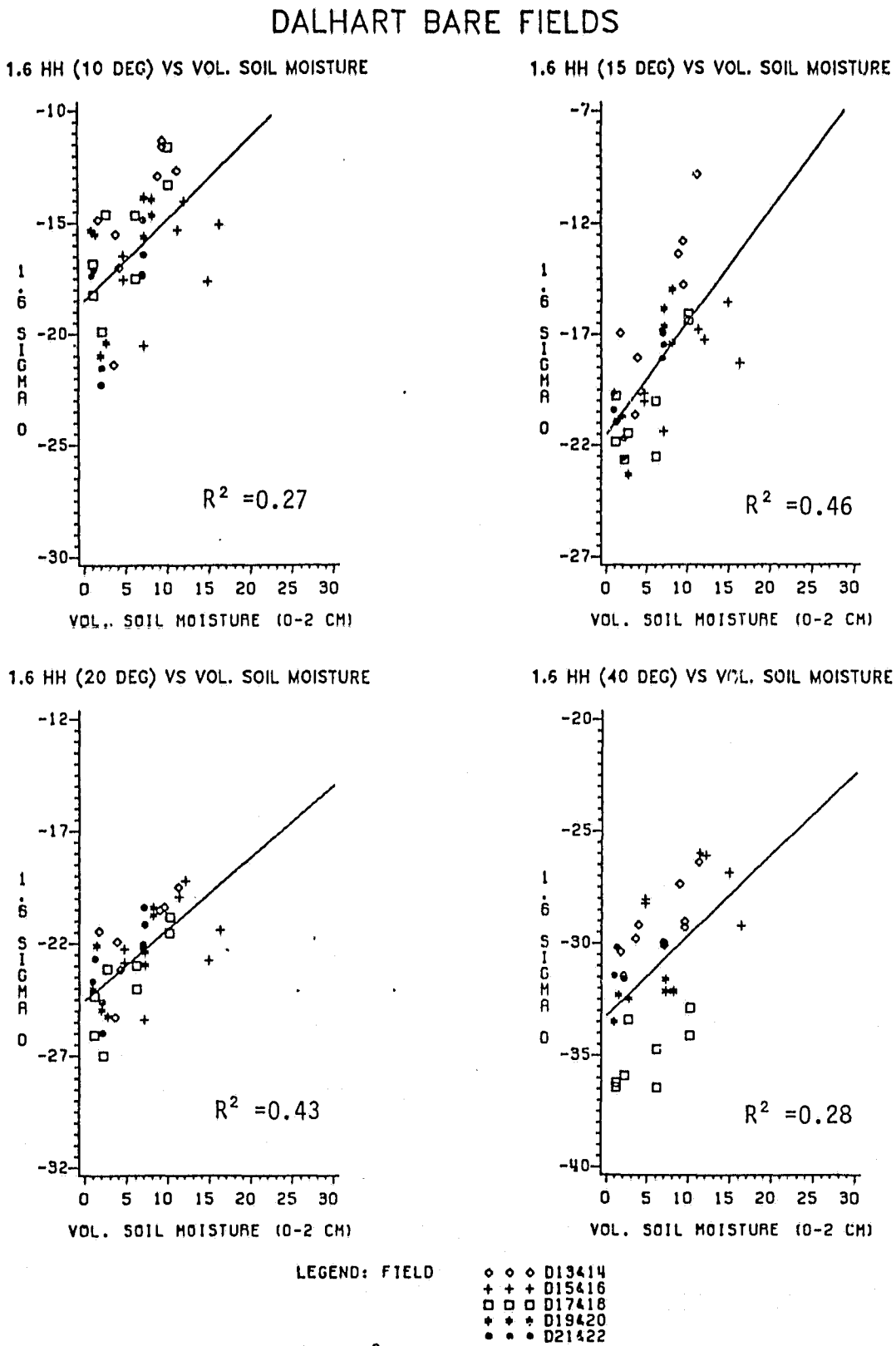

FIG. 20 Dalhart 1.6 GHz HH σ^0 vs. volumetric soil moisture (0-2 cm) at 10, 15, 20, and 40 degree incident angles.

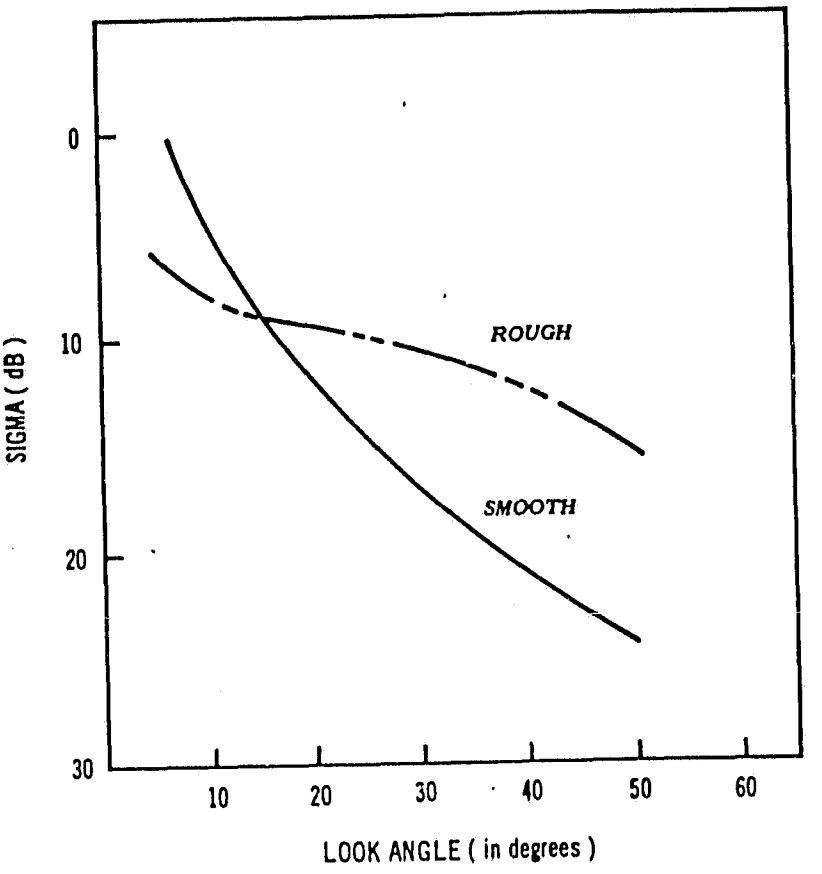

FIG. 21 General effect of uniform roughness upon the relation between σ^0 and look angle.

and soil moisture for all bare fields and each scatterometer (10, 15, 20 and 40 degree incident angles) are compiled in Table 3.

Table 3. Scatterometer R^2 Values for σ^0 versus Volumetric Soil Moisture

	R^2 Values							
	Guymon				Dalhart			
Scatterometer	10°	15°	20°	40°	10°	15°	20°	40°
13.3 VV	0.43	0.47	0.65	0.10	0.20	0.29	0.21	0.22
4.75 HH	0.32	0.35	0.46	0.60	0.13	0.14	0.12	0.03
4.75 HV	0.57	0.36	0.49	0.51	0.45	0.49	0.45	0.36
1.6 HH	0.48	0.58	0.47	0.35	0.27	0.46	0.43	0.28
1.6 HV	0.43	0.59	0.57	0.62	0.02	0.28	0.36	0.17
0.4 HH	0.02	0.11	0.19	0.22	0.08	0.38	0.19	0.07
0.4 HV	0.02	0.00	0.00	0.00	0.29	0.49	0.22	0.17

The largest R^2 value (0.65) obtained for either data set was Guymon's 13.3 GHz VV (20 degree); however, the largest average R^2 value (0.52) was obtained for the 1.6 GHz HH (15 degree). These values will be used in the next section to compare the capability of the scatterometers to detect soil moisture to that of passive microwave radiometers over the same set of fields.

Radiometers

Radiometers provide intensity measurements in terms of brightness temperature (K). By assuming the temperature of the emitting layer to be that sensed by the PRT-5, emissivity can be calculated using equation (18) as

$$\varepsilon = T_{BT}/T_{PRT-5} \qquad (25)$$

For this study the emissivity was used as the measure of the passive microwave response. The data sets were initially analyzed together (Figs. 22-24) to determine if there were calibration problems. No significant calibration problems were evident except in the L-band horizontal emissivity (Fig. 24) where the dry emissivity values were significantly higher at Dalhart; however, the linear R^2 value for this combined data set was 0.71. The radiometer data were further analyzed by comparisons to volumetric soil moisture and percent field capacity for each data set (Figs. 25-27). Both the C-band horizontal and vertical data showed considerable scatter for Dalhart (Figs. 25 and 26). The scatter is related to the differences in the roughness of the field groups. Fields D17&18 appeared "smoother" to the radiometers than fields D15&16. Recall that these two fields also exhibited corresponding differences in relative roughness in the 40 degree incident angle 1.6 GHz HH scatterometer (Fig. 20). The same roughness effect is apparent in the L-band radiometer data but to a lesser degree (Fig. 27). The "sensed" relative roughness did not influence the longer L-band wavelengths as much as it did the C-band wavelengths.

Percent field capacity (PFC) is defined as

$$PFC = VSM/FC \times 100 \qquad (26)$$

where

VSM = measured volumetric soil moisture

FC = Field capacity obtained from texture analysis and equation (22)

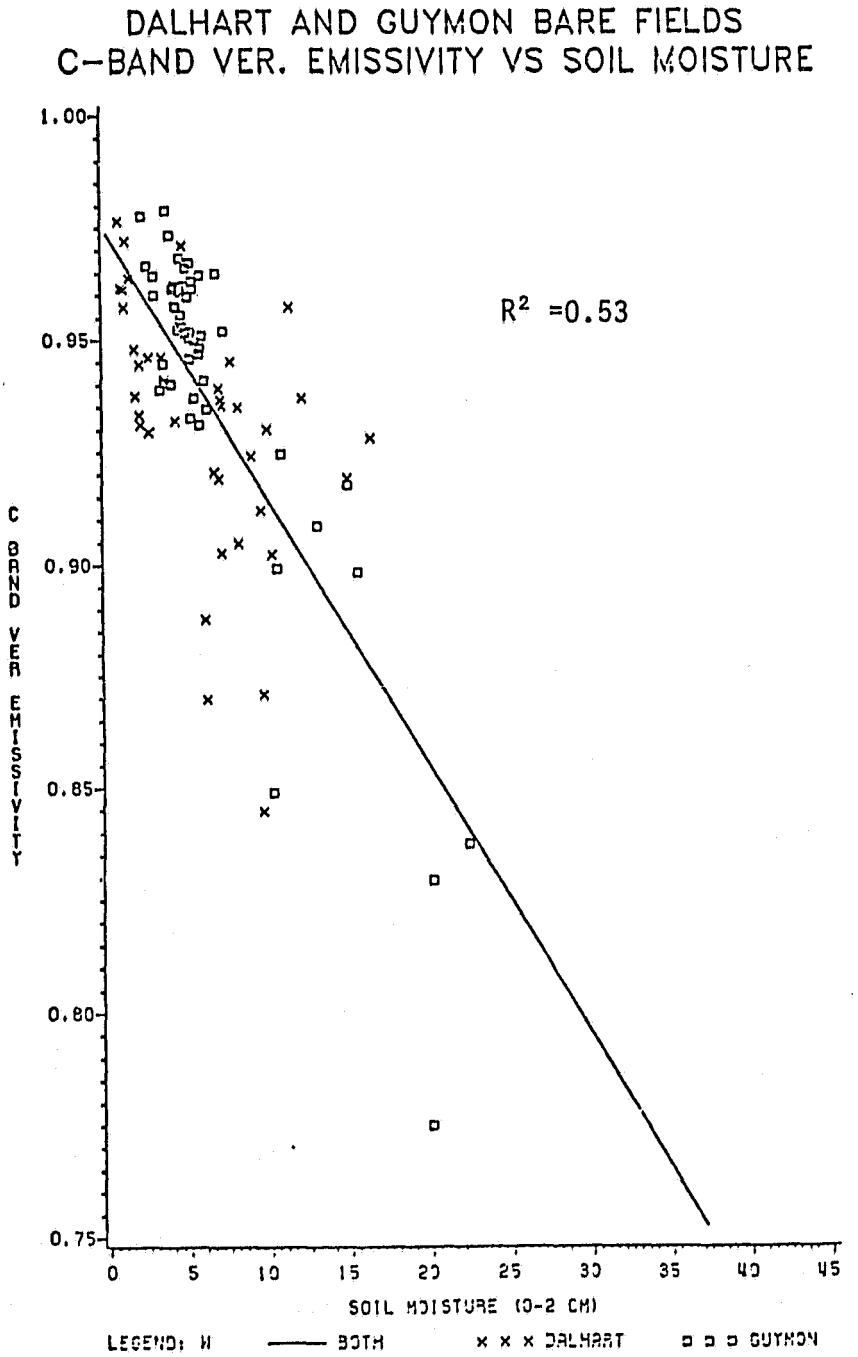

FIG. 22 Scatterplot and regression line for C-band (vertical polarization) emissivity vs. volumetric soil moisture for Dalhart and Guymon bare fields analyzed together.

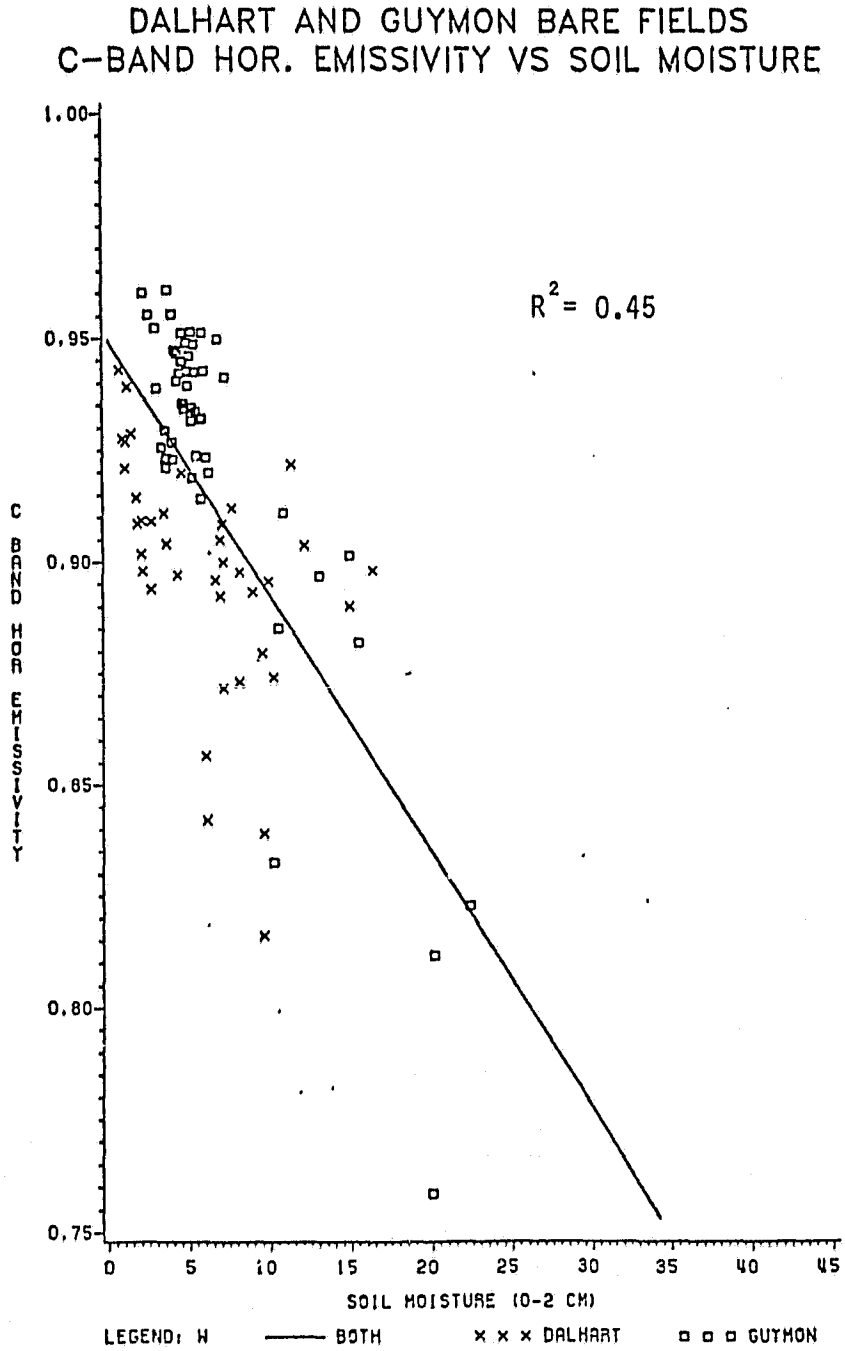

FIG. 23 Scatterplot and regression line for C-band (horizontal polarization) emissivity vs. volumetric soil moisture for Dalhart and Guymon bare fields analyzed together.

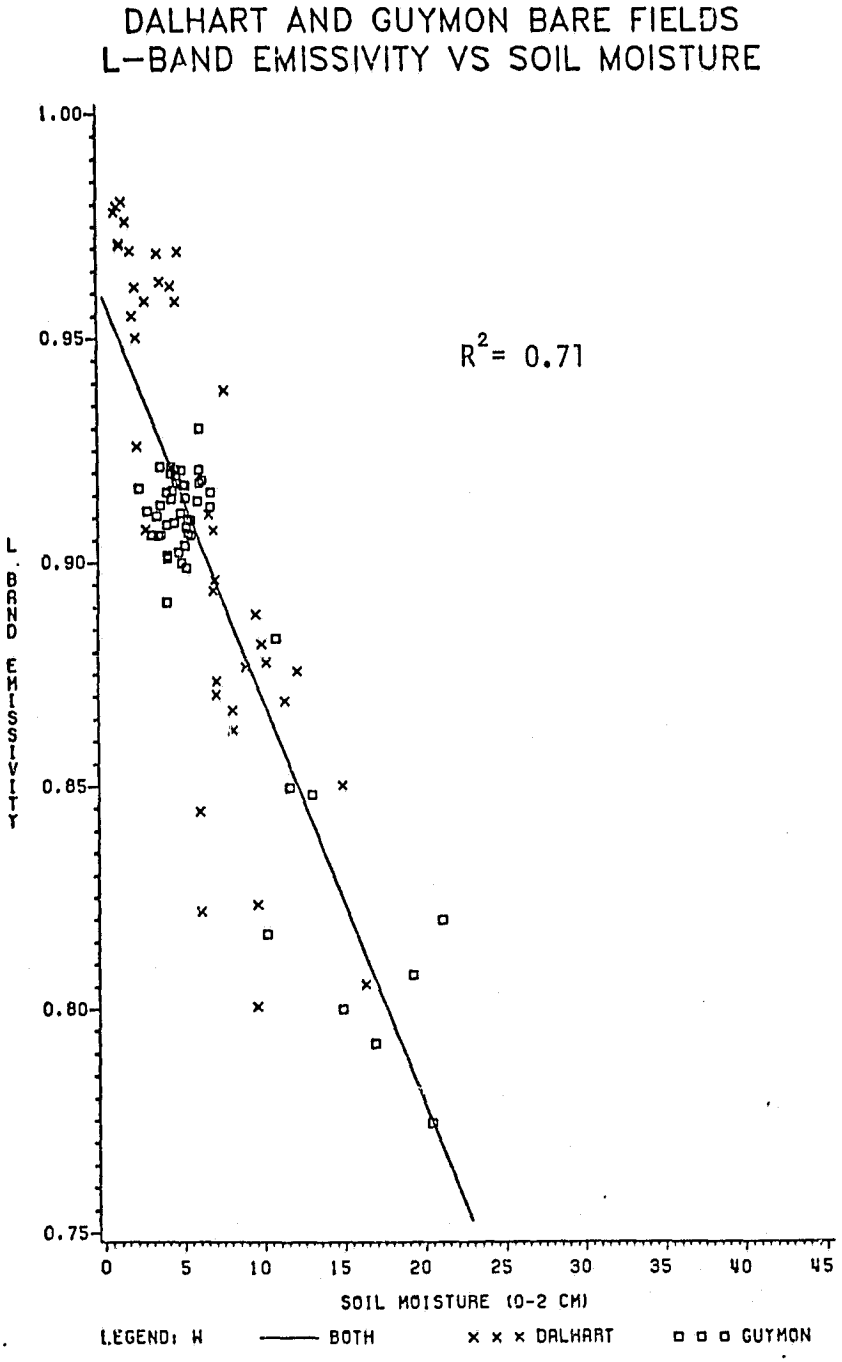

FIG. 24 Scatterplot and regression line for L-band (horizontal polarization) emissivity vs. volumetric soil moisture for Dalhart and Guymon bare fields analyzed together.

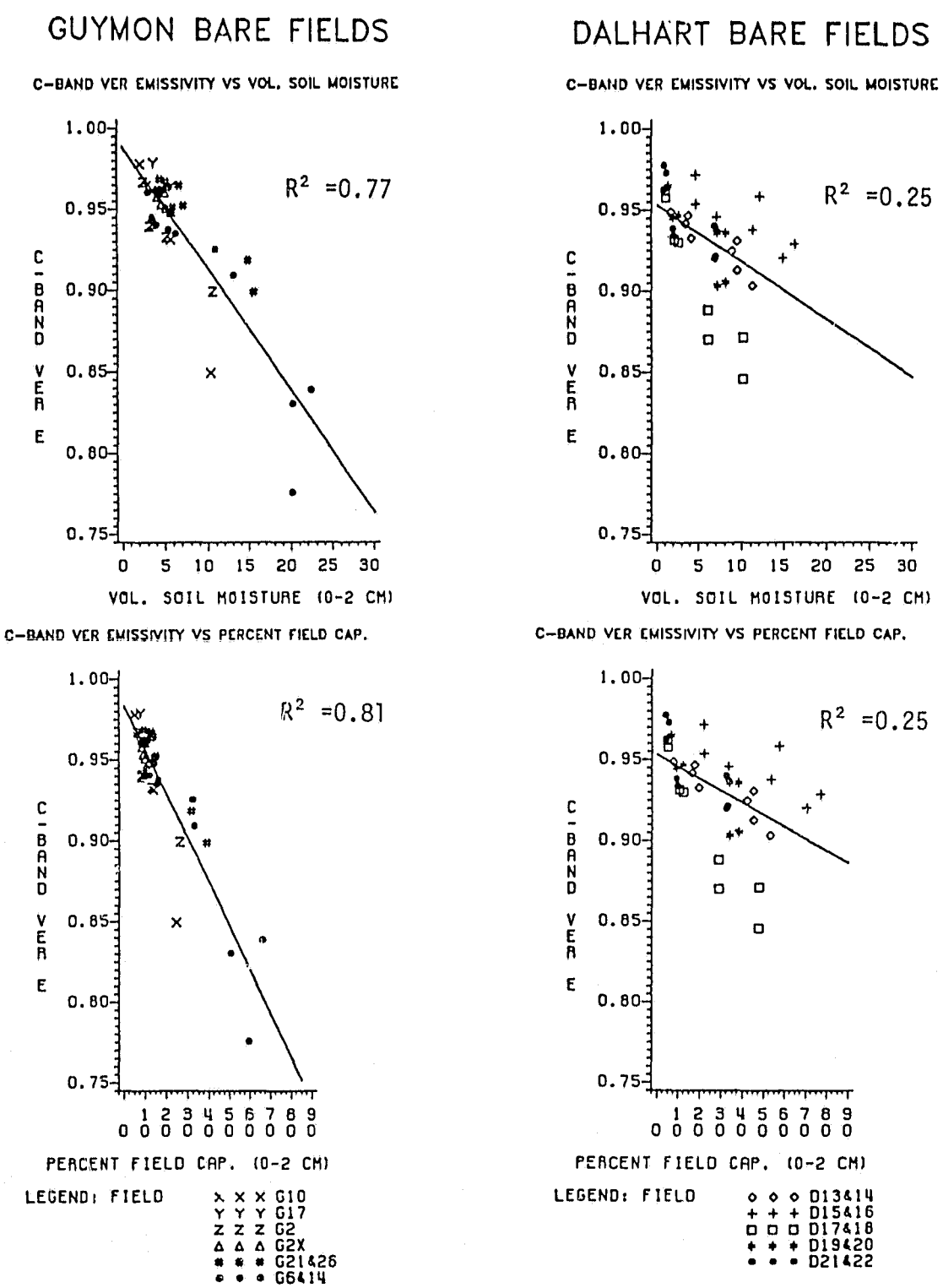

FIG. 25 C-band (vertical polarization) response to volumetric soil moisture and percent field capacity for Guymon and Dalhart bare fields analyzed separately.

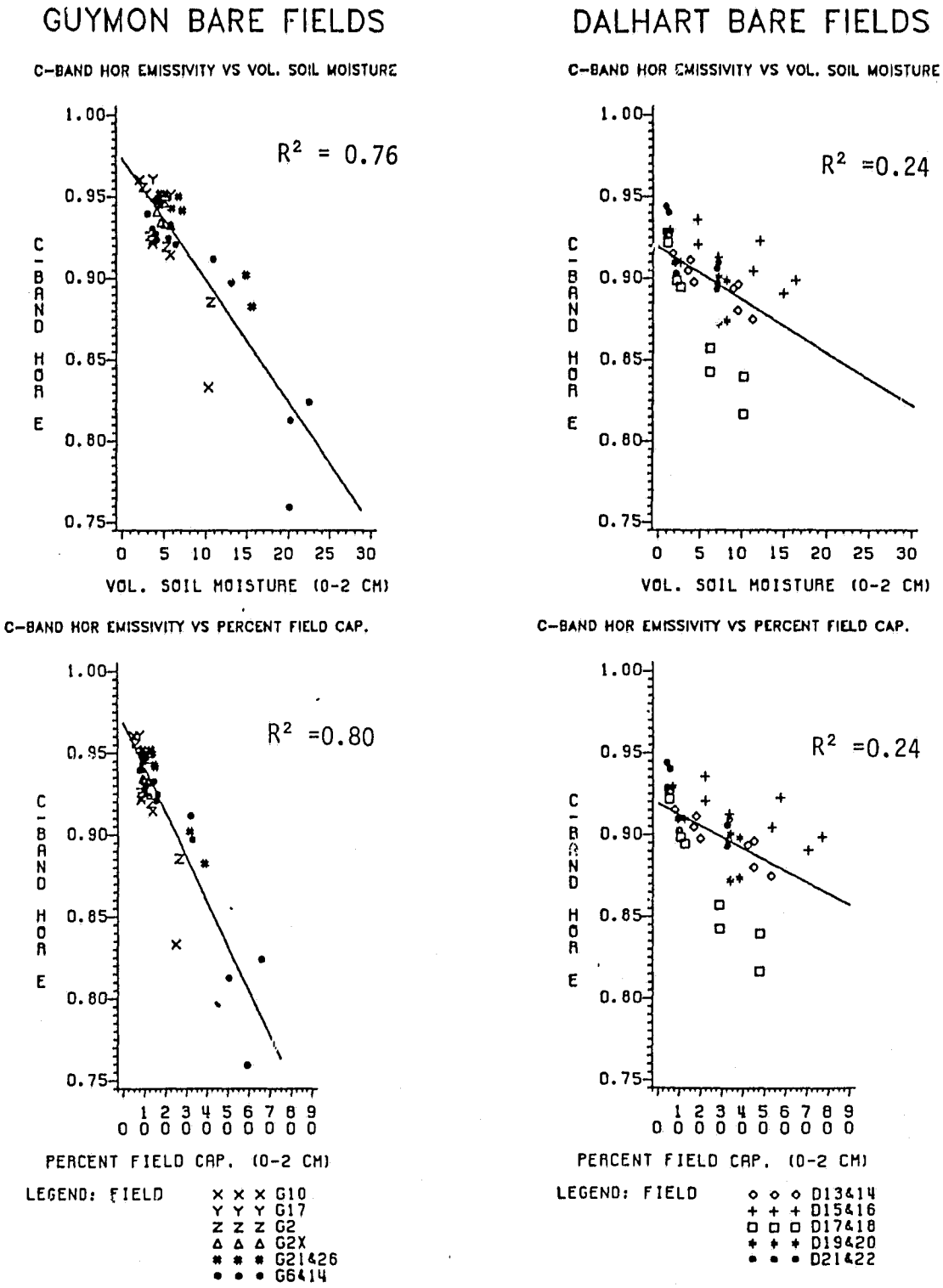

FIG. 26 C-band (horizontal polarization) response to volumetric soil moisture and percent field capacity for Guymon and Dalhart bare fields analyzed separately.

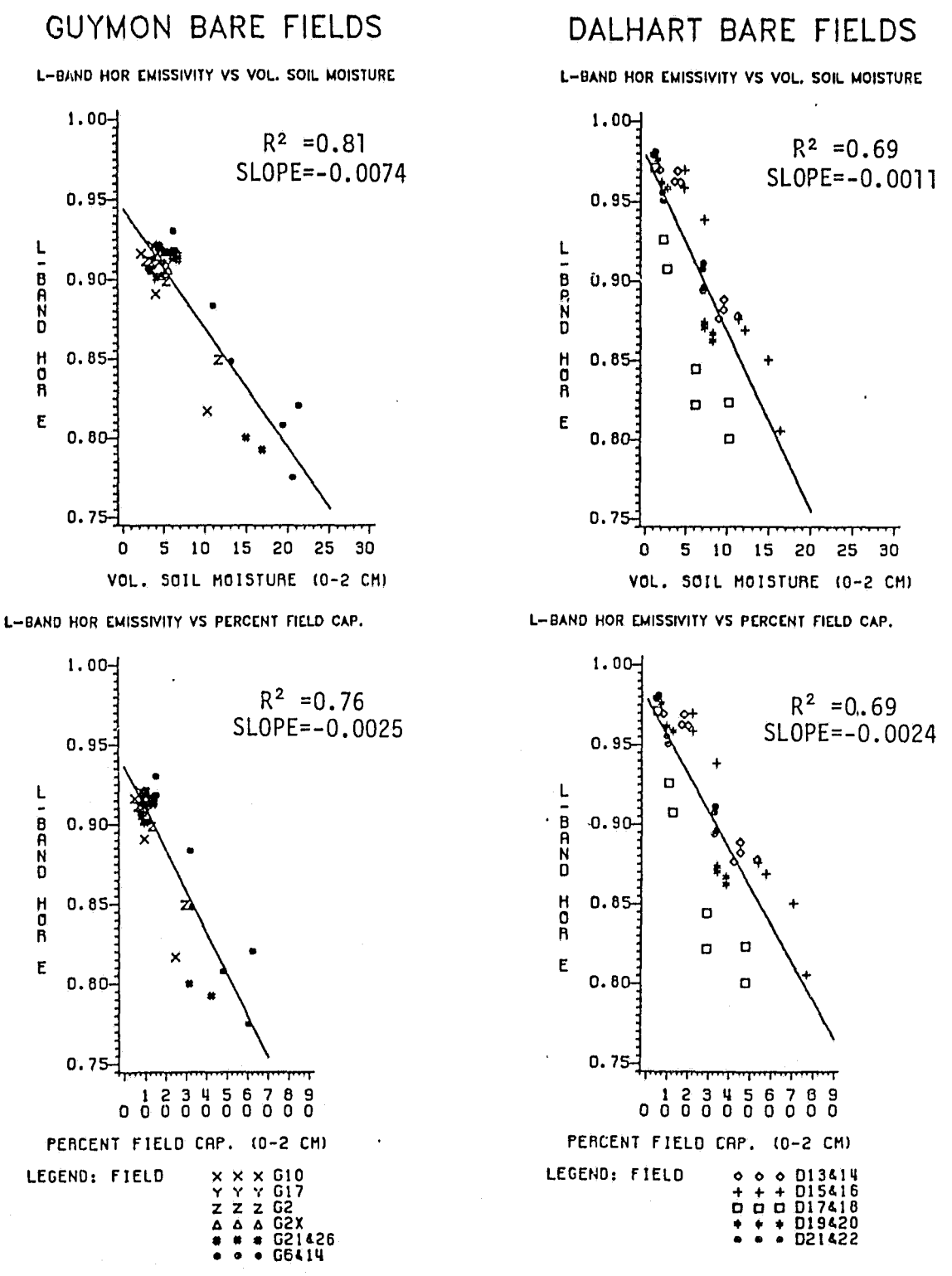

FIG. 27 L-band (horizontal polarization) response to volumetric soil moisture and percent field capacity for Guymon and Dalhart bare fields analyzed separately.

The difference in soil texture between the Guymon and Dalhart test sites is better identified in the L-band radiometer measurements since the effect of roughness, which could be confused with texture effects is reduced at this frequency. Guymon had a much higher clay content than Dalhart. The slopes of the regression lines are different at Guymon and Dalhart when ε is related to volumetric soil moisture (-0.0074 and -0.0011, respectively). In contrast, they are almost identical when ε is related to percent field capacity. This supports the hypothesis that passive microwave responses should be analyzed as a function of percent field capacity. After consideration of the field capacity plots it is evident that the calibration problem with L-band was magnified in the percent field capacity plots because it was not offset by the texture effect. The difference in the intercept between data sets is 0.043. This correction was added to the Guymon data set for all further analyses. The correction was added to Guymon because the L-band antenna used in collecting that data set was deteriorating and replaced between the times of the Guymon and Dalhart experiments. The deterioration tended to reduce the passive microwave response at Guymon (Blanchard, 1981).

The one inch rainfall which occurred at Dalhart provided an opportunity to relate the roughness "sensed" by L-band radiometers with that sensed by L-band scatterometers. This was not possible in Guymon because the irrigated bare fields (G6&14) provided only one field with a sufficient moisture range to establish the relative roughness effects. The σ^0 intercept values at 0 percent moisture, $\sigma^{0'}$, were obtained for each of the Dalhart bare field groups from the 1.6 GHz HH (40 degree) scatterometer (Table 4).

Table 4. σ_0' Values for Each Field Group in Dalhart

Field	σ_0'
D13&14	-30.8
D15&16	-28.7
D17&18	-36.2
D19&20	-32.6
D20&21	-31.5

This "roughness" was considered to influence both the intercept and the slope of the ε vs percent field capacity relationship. The linear equation:

$$\varepsilon = A + B * PFC \tag{27}$$

was modified by

$$A = A1 + A2 * \sigma_0' \tag{28}$$

$$B = B1 + B2 * \sigma_0' \tag{29}$$

$$\varepsilon = A1 + (B1\ 8\ PRF) + (B2 * PFC * \sigma_0') + (A2 * \sigma_0') \tag{30}$$

The resulting equation when applied to bare fields in the Dalhart data set is:

$$\varepsilon = 1.212 + (0.00165*PFC) + (0.000145*PFC*\sigma^{0'}) + (.00681 \times \sigma^{0'}) \tag{31}$$

with R^2 value = 0.93 and F value = 158.5. The significant increase in R^2 values indicates that scatter in the L-band radiometer is indeed due to difference in relative roughness as sensed by the 1.6 HH (40 degree) scatterometer. From the case study and comparison of R^2

values, the L-band radiometer shows the strongest relationship to soil moisture over the same set of bare fields than any other microwave sensor. Therefore, L-band radiometer data were used in all further analyses.

L-band Emissivity Response to Soil Moisture over all Crop Types

No significant difference in ε response to moisture could be discerned when certain "near bare" fields were included in the classification of bare fields. These included Guymon's 23 cm tall milo fields (7 and 15) and Dalhart's pasture (5 and 6) and millet (3 and 4). This indicates that for L-band, attenuation of the soil emission is insignificant for these fields. For this experiment the crop types were classified and generally can be rank-ordered from lower to higher biomass:

1) bare soil
2) alfalfa
3) milo
4) corn

Four fields of alfalfa were sampled at Guymon. Fields 4 and 13 and fields 22 and 27 were pairs of adjoining fields. During the 18 day experiment the alfalfa was irrigated and matured. Fields 22 and 27 were harvested before the last flight day. These two fields were on a steep hillside; consequently, the effective incident angle was increased from 3 degrees to greater than 10 degrees. An increase in effective incident angle in the horizontal polarization causes a decrease in emissivity (Newton, 1977). The decrease was observed in Fig. 28a where the values of ε for fields G22&27 were generally shifted downward from the values for fields G4&13. A realistic

correction of 0.02 (Newton, 1981) was added to the emissivity for fields G22&27 with a resulting increase in the significance of the linear relationship between ε and PFC (Fig. 28b) (R^2 values increased from 0.49 to 0.67). All milo fields considered in this study were at the Guymon site while all corn fields were at the Dalhart site. The linear analysis of the milo fields (Fig. 29) showed a strong relationship between ε and PFC (R^2 value = 0.69). The same analysis for corn fields (Fig. 30) yielded a much weaker relationship (R^2 value = 0.08) due to:

1) Corn masked or attenuated the emissivity from the soil, thus destroying the response to soil moisture differences.
2) The difference of biomass depending on the field group varies markedly within the corn classification.

The influence of different biomass within the corn fields is noted when PVI values are compared to regression lines for individual field groups. Fields D7&8 and D11&12 had PVI values greater than 4.5. These fields were combined into field D>4.5. Regression lines for the three subclasses of corn are presented in Fig. 31. The relatively flat slope for the combined data for high biomass corn fields (D>4.5) indicates that as PVI values approach 4.5 the measured emissivity is virtually insensitive to the soil moisture under the corn. To illustrate the need to compensate for vegetation, emissivity was plotted versus percent field capacity for all fields combined with the resulting R^2 values of 0.09 (Fig. 32).

Most previous studies have modeled emissivity as the dependent variable while using soil moisture and biomass as independent variables (Jackson et al., 1981b; Choudhury, 1981). Choudhury used the model

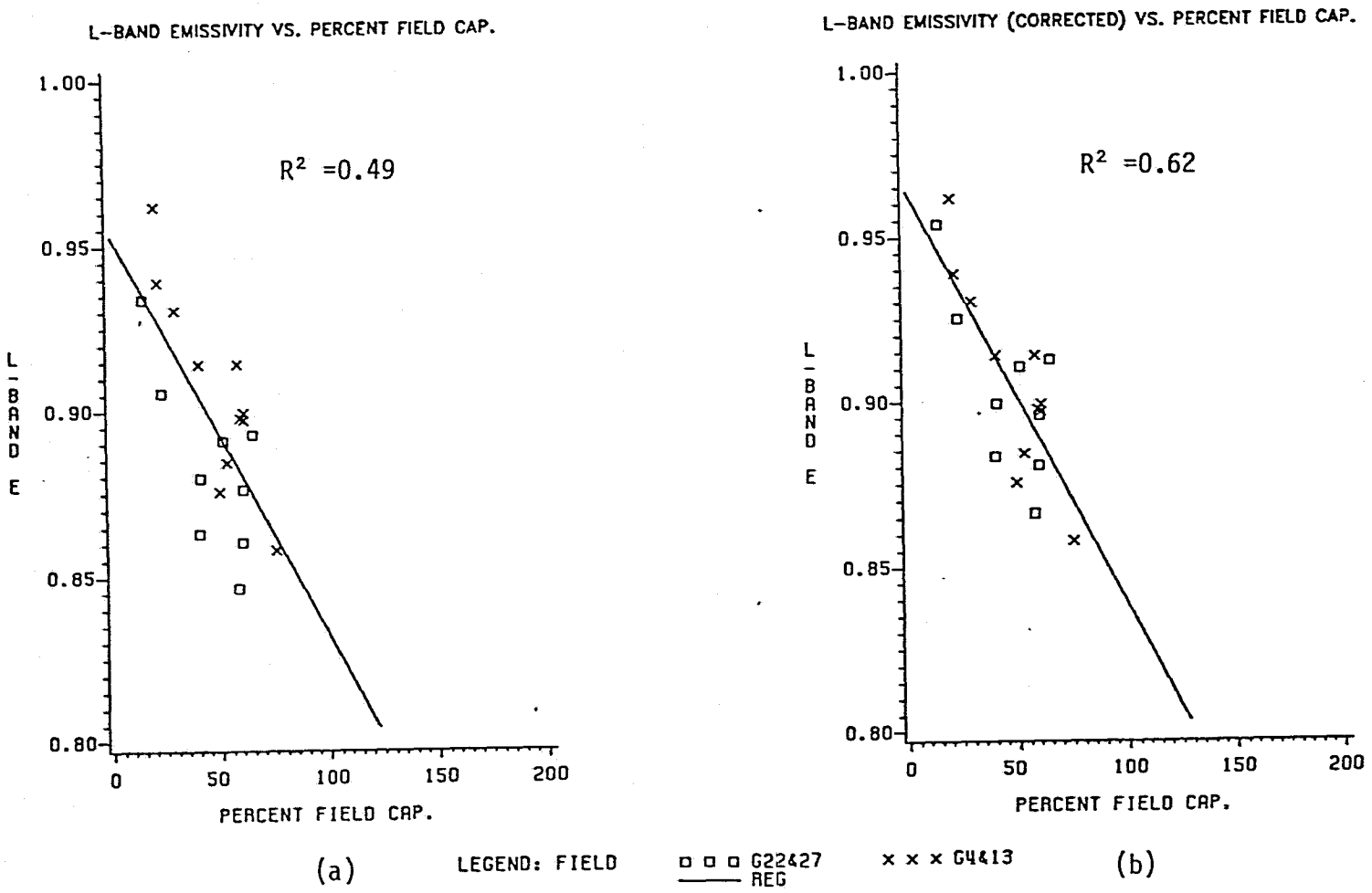

FIG. 28 Scatterplot and regression lines for L-band emissivity vs. percent field capacity for alfalfa fields with a) uncorrected and b) corrected emissivity values.

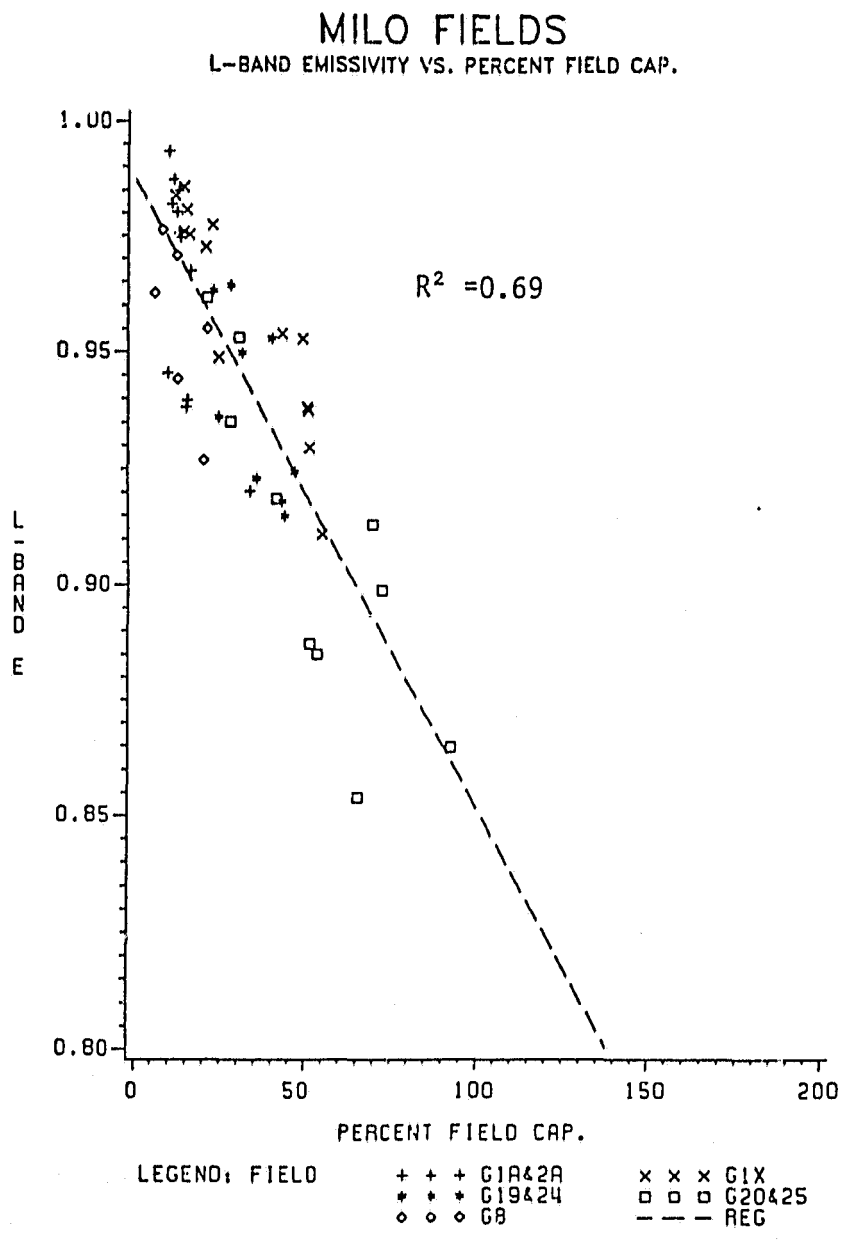

FIG. 29 Scatterplot and regression line for L-band emissivity vs. percent field capacity for Milo fields.

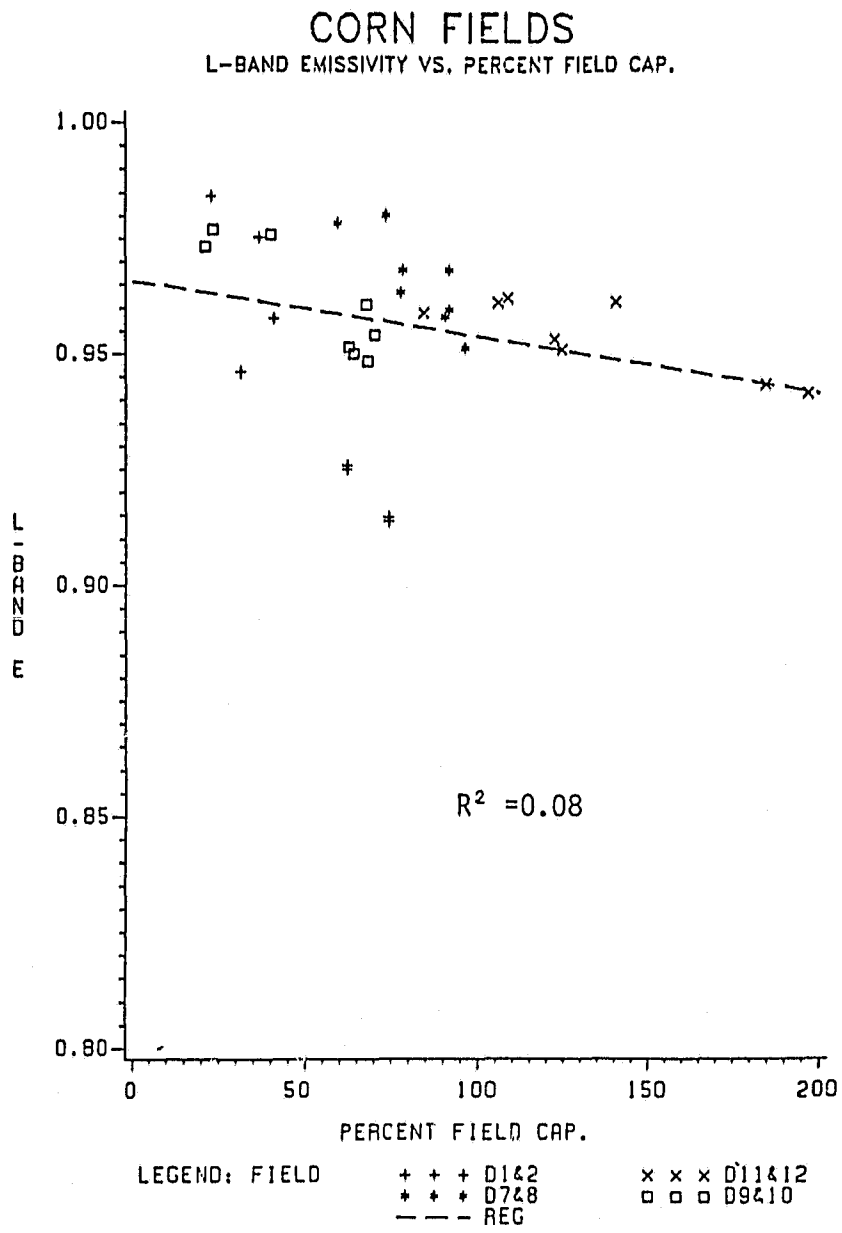

FIG. 30 Scatterplot and regression line for L-band emissivity vs. percent field capacity for Corn fields.

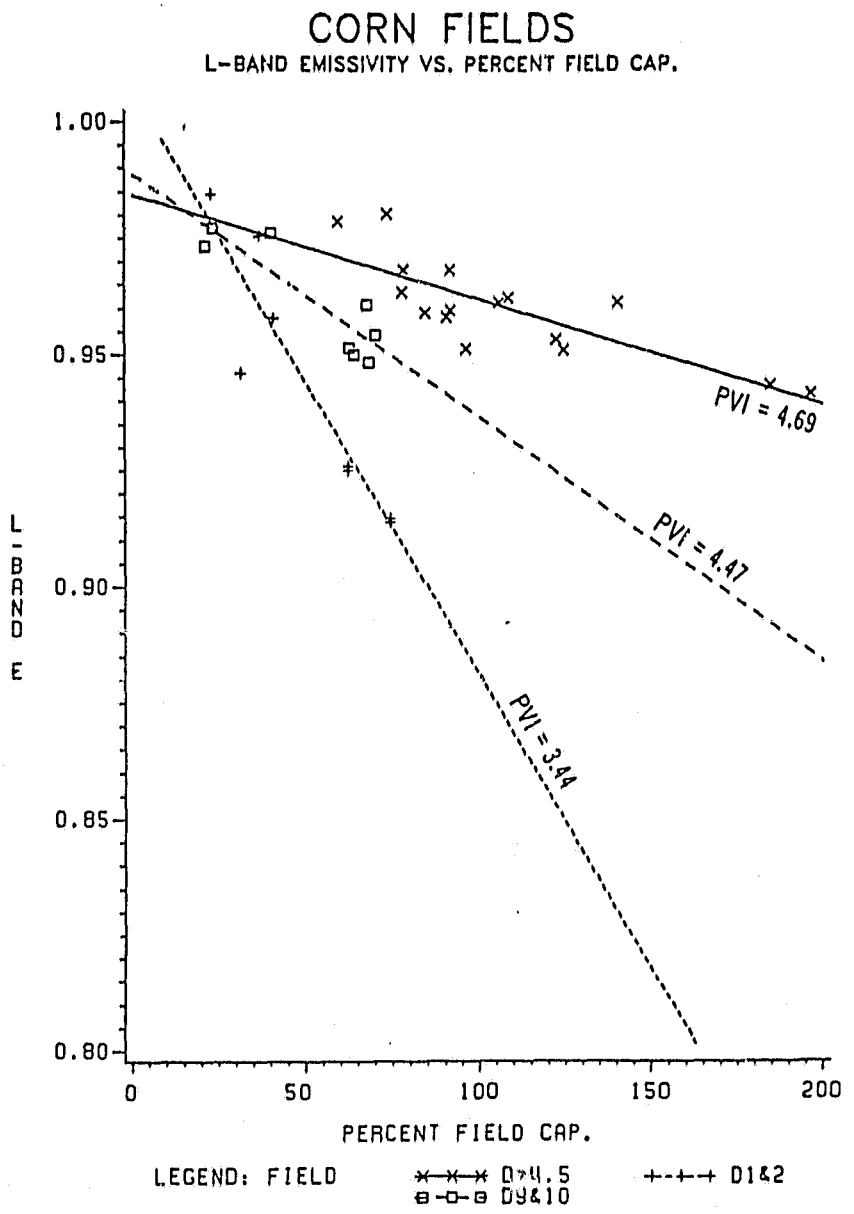

FIG. 31 Scatterplot and regression lines with corresponding PVI values for L-band emissivity vs. percent field capacity for individual fields of corn.

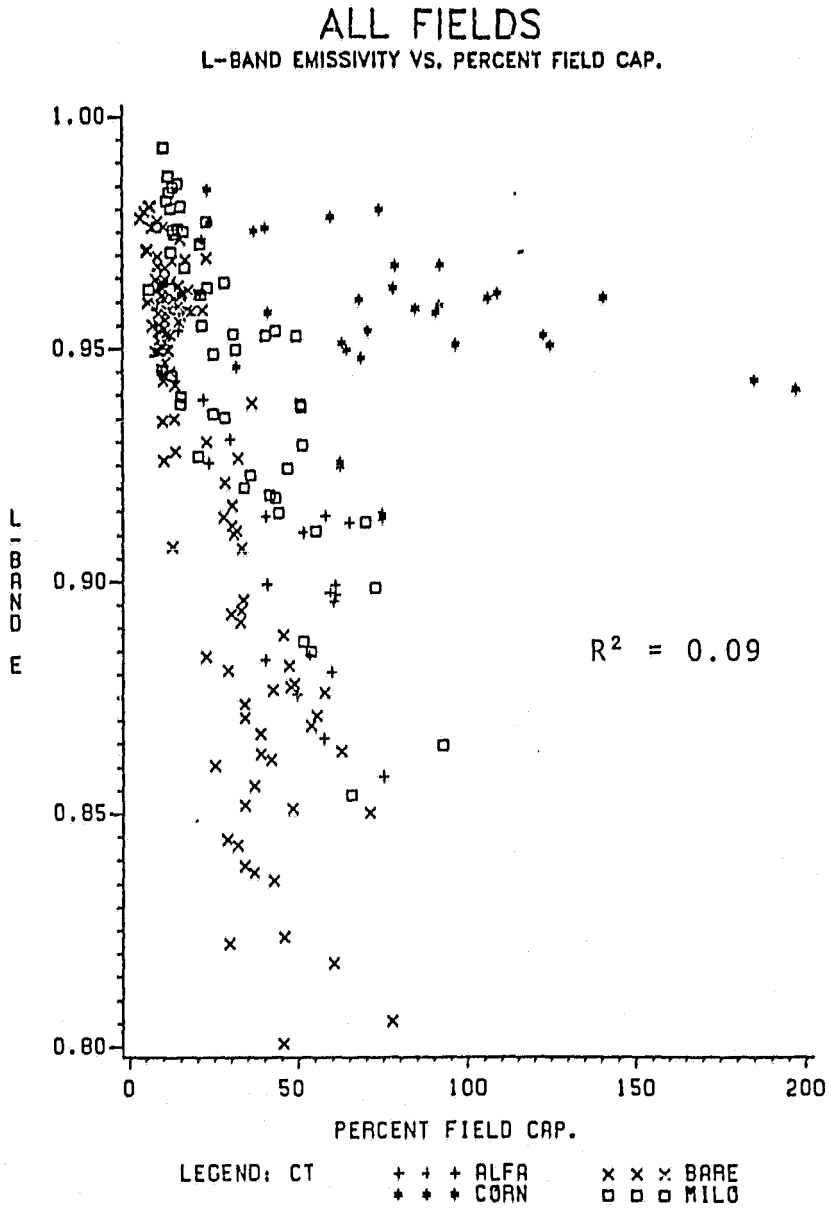

FIG. 32 Scatterplot of L-band emissivity vs. percent field capacity for all crop types.

$$\varepsilon_m = \varepsilon_s e^{-\tau} + (1 - \varepsilon_s)\, \varepsilon_v (1 - e^{-\tau})\, e^{-\tau} + \varepsilon_v (1 - e^{-\tau}) \qquad (32)$$

where τ = vegetation index

ε_m = measured emissivity

ε_s = emissivity of the soil (function of soil moisture)

ε_v = emissivity of vegetation

The first term on the right is the contribution from the soil surface as attenuated by the vegetation. The second term is the contribution from the vegetation as reflected by the soil surface $(1-\varepsilon_s)$ and again attenuated by the vegetation. The third term is the direct contribution from the vegetation. By rearranging terms:

$$\varepsilon_m = \varepsilon_v - \varepsilon_v e^{-2\tau} + \varepsilon_s (e^{-\tau} - \varepsilon_v e^{-\tau} + \varepsilon_v e^{-2\tau}) \qquad (33)$$

and solving for ε_s, the resulting equation is:

$$\varepsilon_s = \frac{\varepsilon_m - \varepsilon_v + \varepsilon e_v^{-2\tau}}{e^{-\tau} - \varepsilon_v e^{-\tau} + \varepsilon_v e^{-2\tau}} \qquad (34)$$

There is always an error in the measurement of ε_m. ε_m was replaced with $\varepsilon_m + \varepsilon_{er}$ (ε_{er} is the error in measurement) yielding

$$\varepsilon_s = \frac{\varepsilon_m + \varepsilon_{er} - \varepsilon_v + \varepsilon_v e^{-2\tau}}{e^{-\tau} - \varepsilon_v e^{-\tau} + \varepsilon_v e^{-2\tau}} \qquad (35)$$

In a similar fashion, the error term can be applied to the emissivity of the soil ε_s resulting in the following equation

$$\varepsilon_m = \varepsilon_v - \varepsilon_v e^{-2\tau} + (\varepsilon_s + \varepsilon_{er})(e^{-\tau} - \varepsilon_v e^{-\tau} + \varepsilon_v e^{-2\tau}) \qquad (36)$$

The soil moisture information is contained in ε_s. Choudhury reported values of ε_v to be 0.97. Using the value $\varepsilon_{er} = 0.01$, the sensitivity of ε_s and ε_r to different values of τ was investigated in Fig. 33. It was noted that as τ increases from 0 to 1.5 the error in ε_s increases from 0.01 to 0.18 while the error of ε_m decreases from 0.01 to 0.0006. This indicates that these equations can predict the emissivity measured at the radiometer well, but cannot estimate the ε_s or emissivity of the soil accurately when the vegetation becomes dense.

Coefficients of the linear regression equations for the calculation of ε from percent field capacity for each crop type are tabulated in Table 5.

Table 5. Coefficients of linear prediction equations for estimation of emissivity as a function of percent field capacity.

Crop Type	Intercept	Slope
Bare	0.9801	-.00253
Alfalfa	0.9638	-.00125
Milo	0.9869	-.00136
Corn	0.9657	-.000121

These coefficients were used to predict the value of emissivity. The calculated values of emissivity resulting from these equations are

C-2

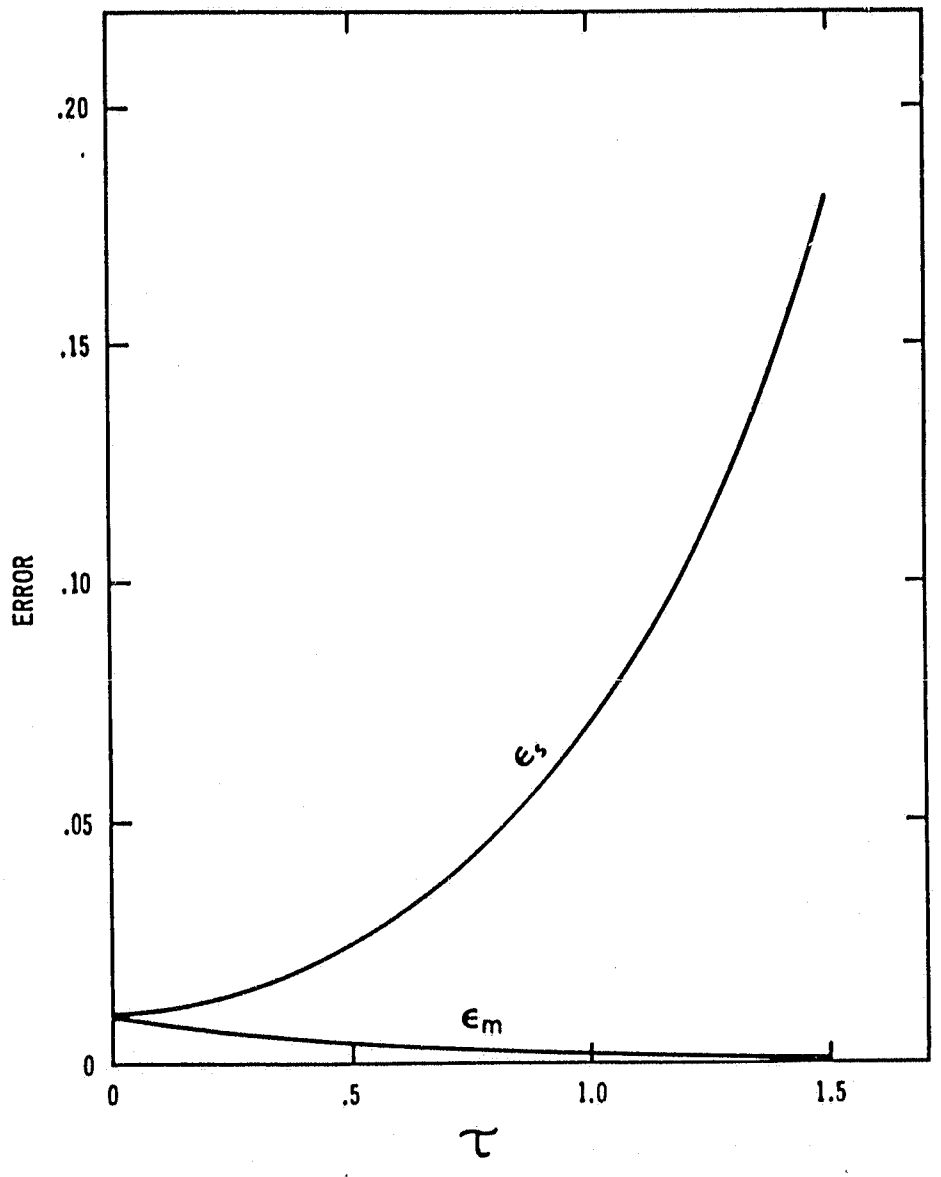

FIG. 33 Illustration of the sensitivity of Choudhury's model to errors in measurement vs. a vegetation index (τ). The curve denoted by ε_S is the error in the predicted emissivity of the soil that would be incurred with a 0.01 error in the measured emissivity. The curve denoted by ε_m is the error in the predicted measured emissivity with a 0.01 error in ε_S.

compared to the measured emissivity in Fig. 34. The R^2 value of measured versus predicted emissivity using this approach is 0.74.

Soil Moisture Determination with Multiple Sensors

The remainder of this study considers the soil moisture parameter as the dependent variable. Regression lines for percent field capacity versus emissivity for the four major crop types along with mean vegetation index values are shown in Fig. 35. This figure introduces two approaches to estimate soil moisture by using visible/infrared data with passive microwave sensors. The first approach uses visible/infrared sensors to classify the crop and crop class to estimate moisture. The second approach bypasses classification by using the PVI values (obtained from visible/infrared sensor) and microwave response in a direct relationship.

Classification Technique

The classification technique approach assumes that all fields within a particular crop type have equal biomass and thus the same vegetation effect on the passive microwave radiometer. This assumption was tested by investigating the effect of different biomass (as indicated by PVI) within crop types for corn and milo. Regression lines for each field group with the corresponding average PVI values are presented in Fig. 36. Significantly different regression lines within both crop types were observed. The sensitivity of the percent field capacity to changes in emissivity was directly related to PVI. That is, as PVI increased, the sensitivity of PFC to ε increased. This increased sensitivity dictates that errors in the measurement of ε have greater effects on the accuracy of estimates of the percent

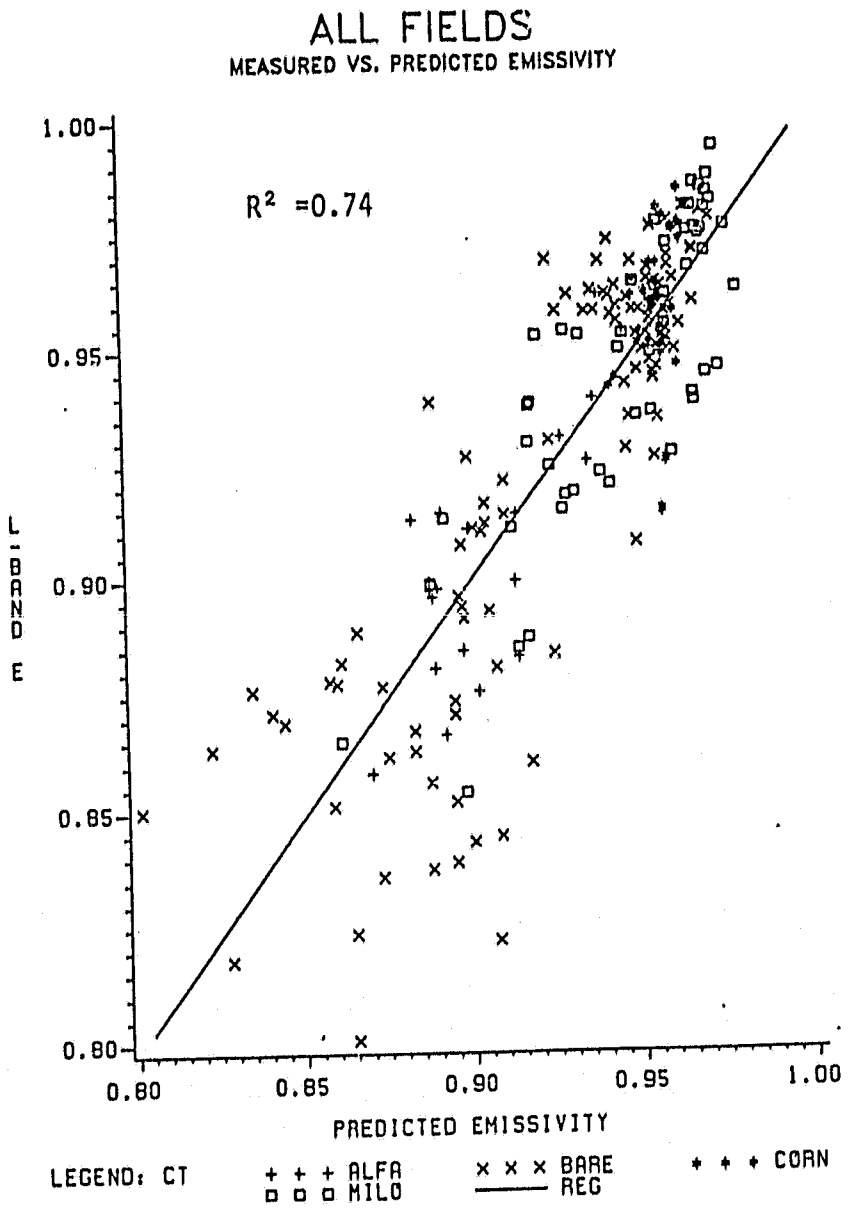

FIG. 34 Scatterplot and regression line for measured vs. predicted emissivity for all fields.

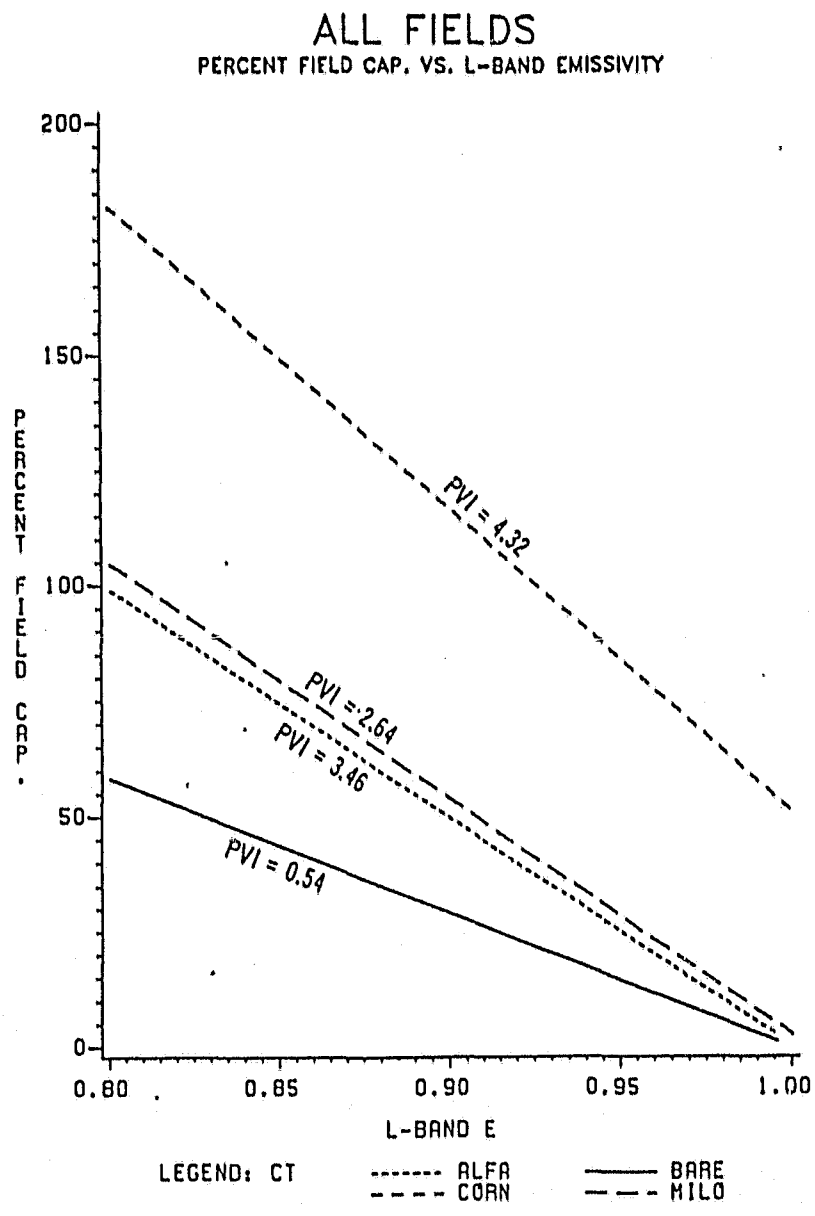

FIG. 35 Regression lines relating percent field capacity to emissivity and the corresponding PVI values for each crop type.

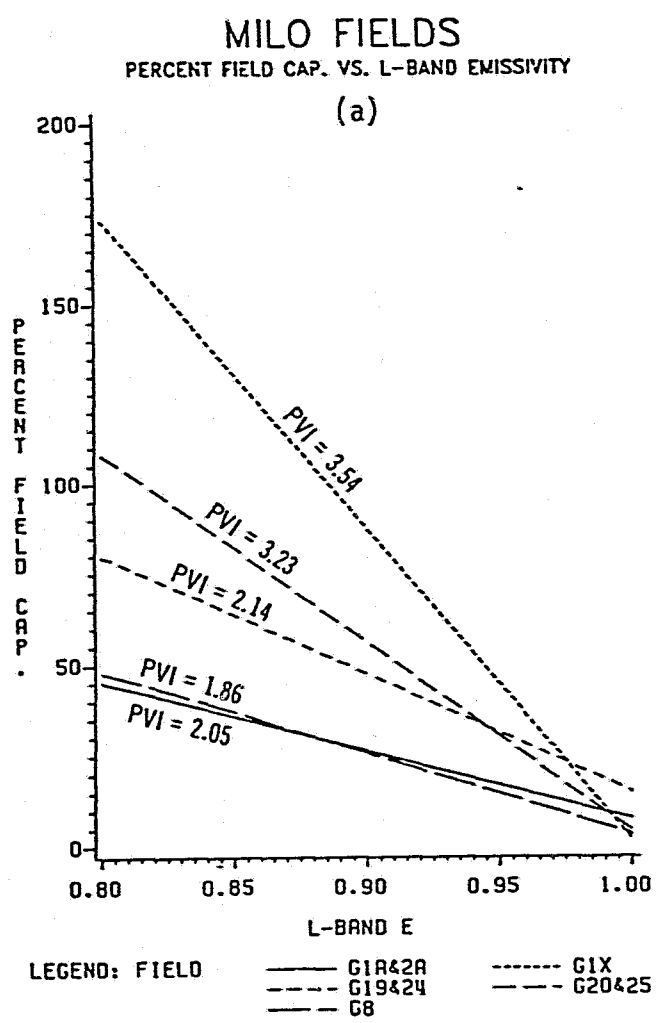

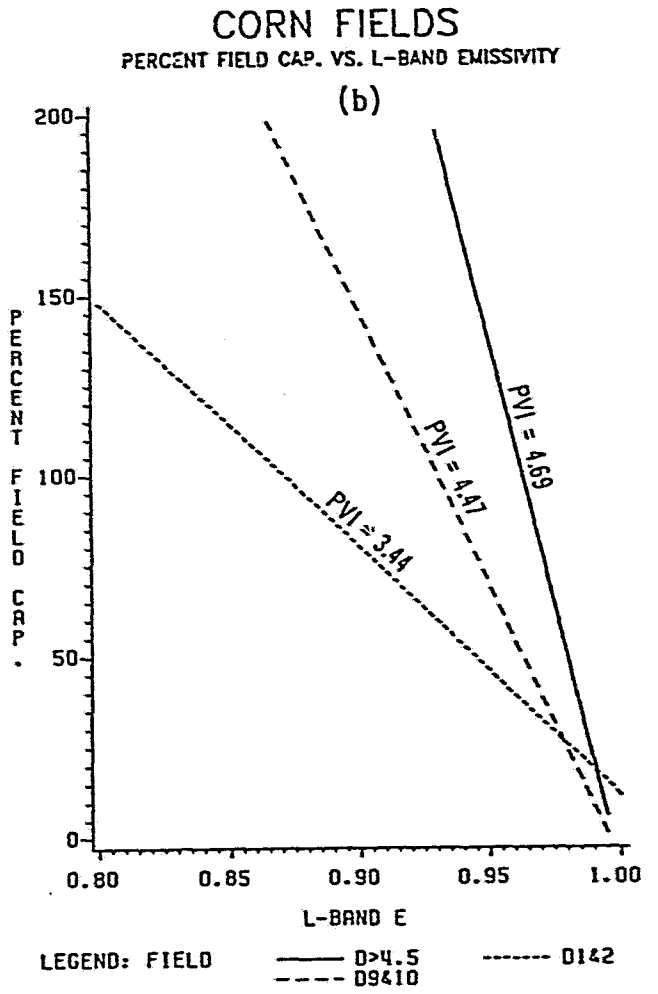

FIG. 36 Regression lines relating percent field capacity to emissivity and the PVI values for each field group in a) milo and b) corn.

field capacity at high PVI values. This same relation is the controlling element in the sensitivity analysis of the Choudhury equation that was discussed in the previous section.

Coefficients for the linear regression equations used for estimating percent field capacity as a function of measured emissivity are presented in Table 6. The regression lines defined by these values were illustrated in Fig. 35.

Table 6: Coefficients of linear prediction equations for estimation of percent field capacity as a function of emissivity

Crop Type	Intercept	Slope
Bare	291.86	-291.97
Alfalfa	493.61	-493.65
Milo	512.70	-510.19
Corn	707.31	-656.58

Measured percent field capacity was plotted against the predicted values obtained from these equations (Fig. 37a). This illustration points out the failure of using one set of linear coefficients per crop type (especially in corn) to predict soil moisture for an entire set of fields inside that crop type. The most significant R^2 value which can be expected using classification technique on this data set with corn included is 0.67. When the corn fields were not considered the R^2 value increased to 0.76 (Figure 37b). Thus, if the severe attenuation from corn can be avoided we may be able to estimate percent field capacity from measured emissivity reasonably well.

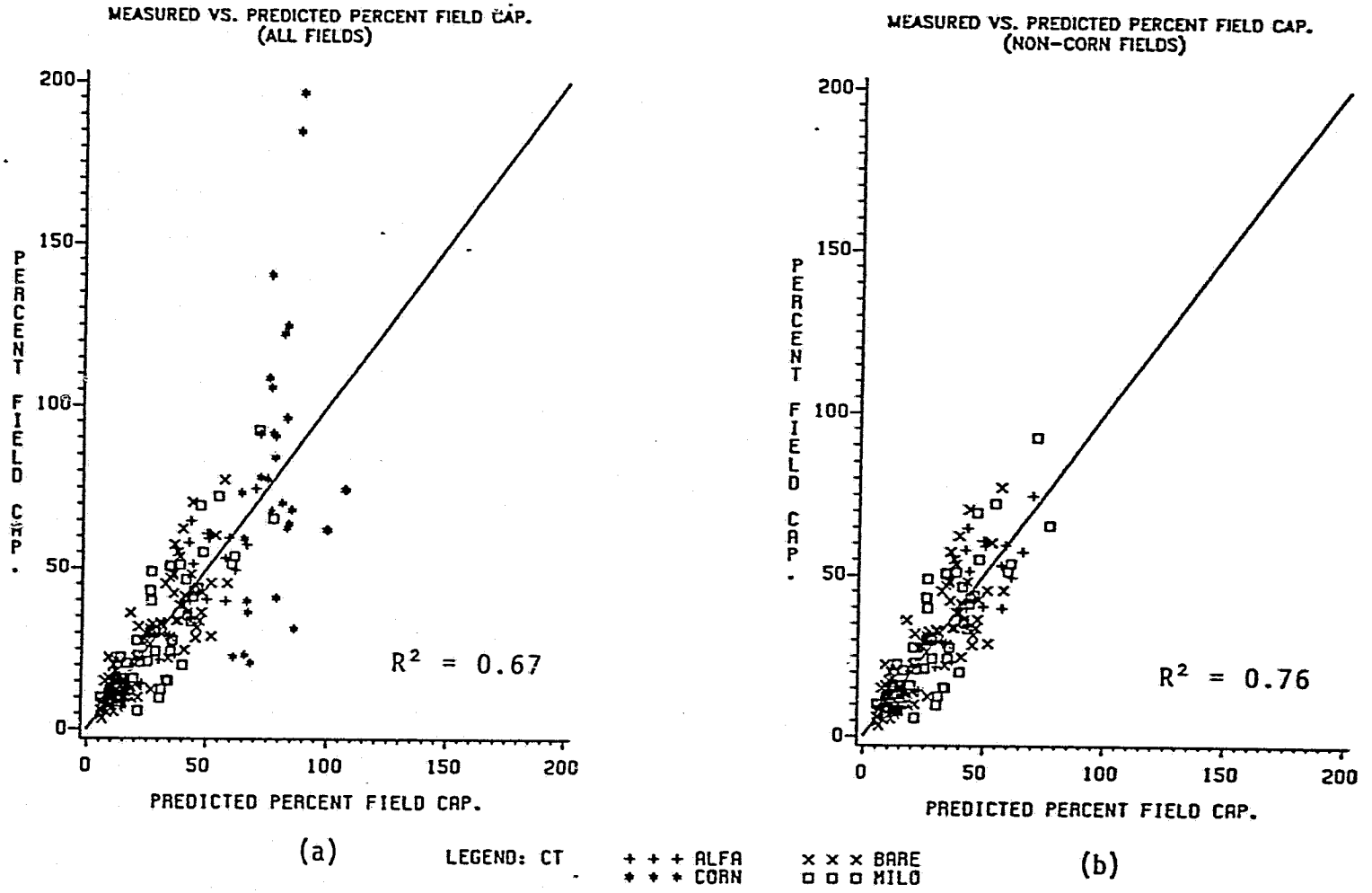

FIG. 37 Scatterplots and regression lines for measured vs. predicted percent field capacity for a) all fields and b) non-corn fields.

Direct Combination

The estimation of percent field capacity with a combination of sensors required the development of an equation that defines percent field capacity as a function of both microwave emissivity and vegetation index data (PVI). This technique should be more flexible than the classification technique described earlier since it can accommodate differences in biomass within each crop class.

The regression lines for the different crop types and the corresponding values of PVI are presented in Fig. 38 with the corn subdivided into three field groups. The slopes of these regression lines were then plotted against the average PVI values in Fig. 39. The form of the relation appears to be a straight line function when fields D9&10 and D>4.5 are not considered. The linear form of the relationship between percent field capacity and emissivity is:

$$PFC = A - B * \varepsilon \tag{37}$$

If biomass (PVI) is considered to linearly affect both A and B then:

$$A = A1 + A2 * PVI \tag{38}$$

$$B = B1 + B2 * PVI \tag{39}$$

Substituting into equation (37) and expanding the form, the equation becomes:

$$PFC = A1 + (A2 * PVI) - (B1 * \varepsilon) - (B2 * \varepsilon * PVI) \tag{40}$$

Applying this to all fields except those with average PVI value greater than 4.3 (D9&10 and D>4.5) yields the equation:

$$PFC = 279.53 + (51.20 * PVI) - (281.22 * \varepsilon) - (48.41 * \varepsilon * PVI) \tag{41}$$

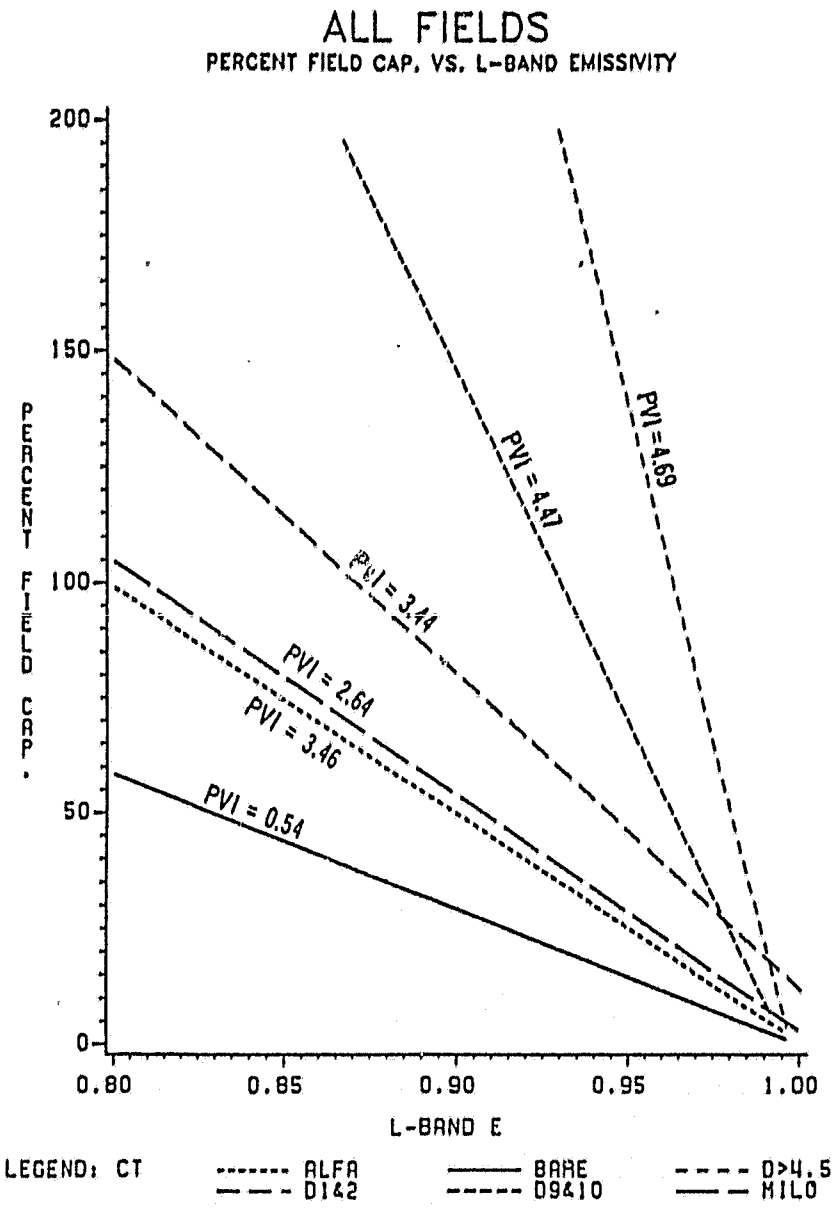

FIG. 38 Regression lines relating percent field capacity to emissivity for all fields (corn divided into individual field groups).

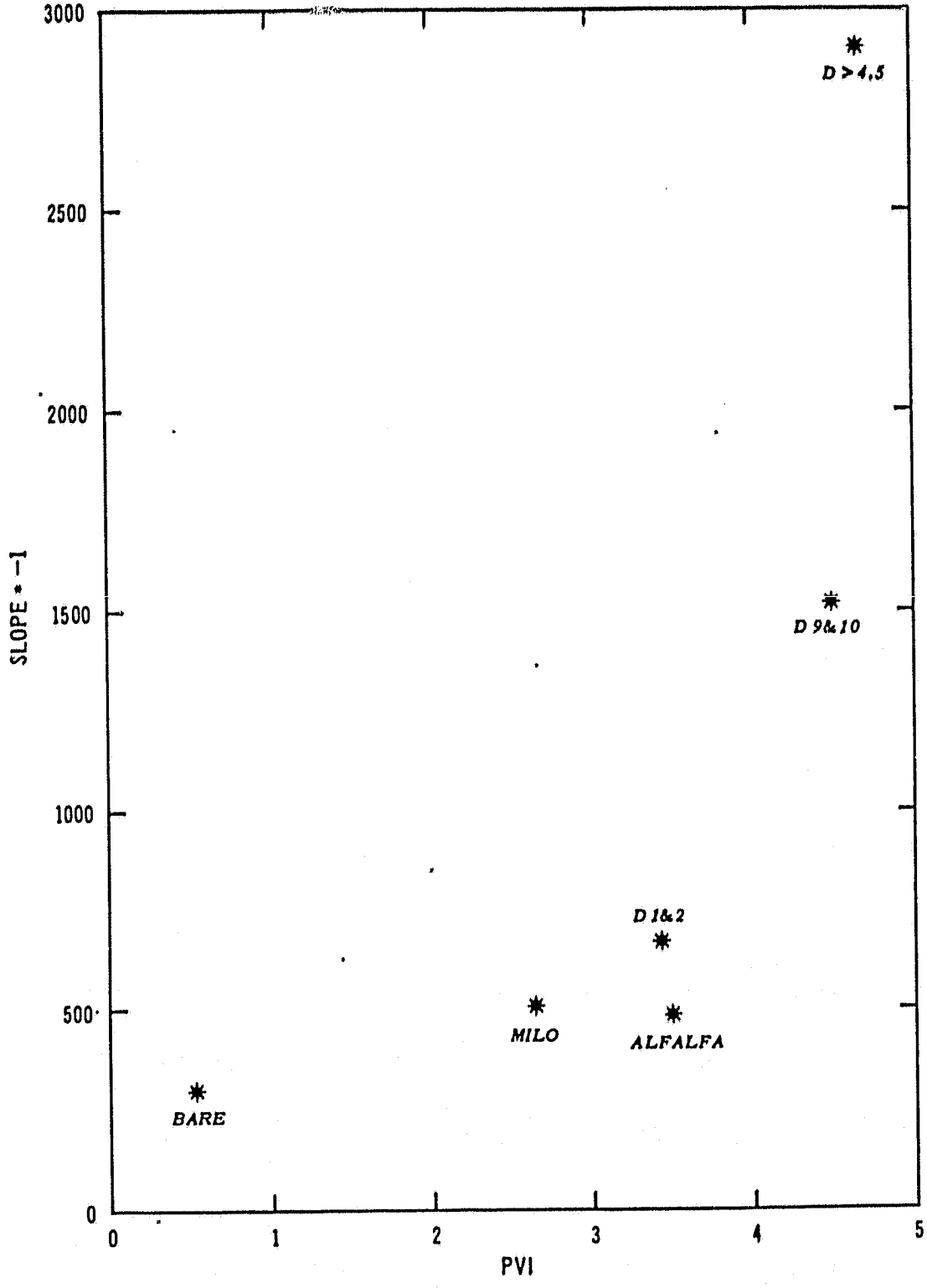

FIG. 39 Slopes of regression lines in Fig. 38 vs. corresponding PVI values.

It is significant to note the values of A1 and B1 in equation (41) are comparable to the values of A and B obtained for bare fields (291.86 and 291.97, respectively) (Table 6). This indicates that the influence of vegetation was compensated for by the increased values of PVI obtained over the non-bare fields. Comparisons of the capability of the L-band radiometer to estimate percent field capacity are presented in Fig. 40 when it is used:

1) alone
2) with a classification technique which excludes all corn
3) in direct combination with PVI excluding fields with average values of PVI greater than 4.3.

This illustrates that passive microwave alone cannot estimate soil moisture when several crop types are considered. The classification technique works reasonably well when the variation of biomass within a crop type are small. This technique also requires perfect classification. The direct combination technique shows the greatest potential to detect soil moisture because it:

1) is able to discern difference in biomass within crop types
2) will vary as the crop matures
3) is not hindered by misclassification
4) provides a means to determine a threshold value of biomass beyond which the radiometer is unable to accurately estimate soil moisture.

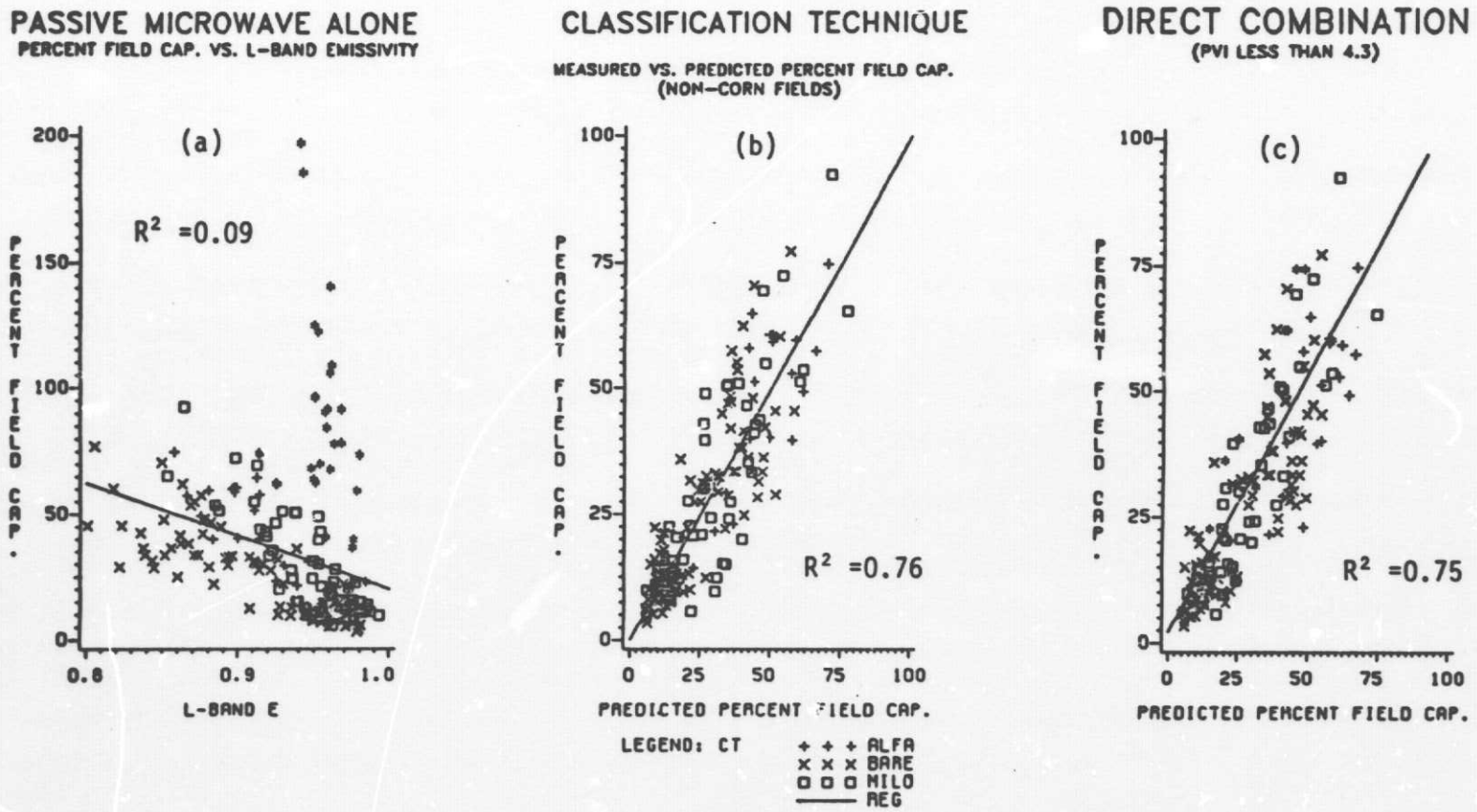

FIG. 40 The ability of the L-band radiometer to predict percent field capacity when used a) alone, b) with classification technique (no corn), and c) with direct combination technique (excluding fields with PVI greater than 4.3).

CONCLUSIONS AND RECOMMENDATIONS

The principal objective of this research was twofold. The first objective was to select the most useful single sensor from the array of sensors available for the estimation of soil moisture. The second objective was the development of a linear combination of sensor data that would provide an improvement in estimation of soil moisture over estimates made with a single sensor.

The L-band passive microwave radiometer was found to be the most suitable single system. Several subordinate conclusions led to the selection of this sensor. First the L-band system was found to be the most sensitive to soil moisture differences in terms of the range of return from the full range of soil moisture. Secondly, the error in measurement in relation to the range of sensor response was small in relation to the active microwave systems. Third, it became obvious that with the passive microwave systems it was possible to get a relative calibration while with the active microwave systems this could not be done. Fourth, the L-band horizontal passive microwave responded less to variations in roughness than the C-band passive microwave. In the preliminary analysis leading to these conclusions, it was shown that the L-band passive microwave measured emissivity relationship to soil moisture was more significant when moisture was expressed as percent of field capacity.

All previous experiments analyzed the microwave return, whether it was the passive microwave antenna temperature or the active microwave scattering coefficient, as a function of the moisture measurements. A more useful but more difficult modeling effort is required

to predict moisture from remote sensing inputs. Due to the nature of the influence of surface roughness and vegetation on the transmission of microwave energy from the surface soil volume to the antenna, significant errors in estimated soil moisture will occur unless the systems used can provide a reliable measure of surface roughness and vegetation attenuation. No practical satisfactory measure of roughness was found in these data; however, the perpendicular vegetation index was found to be useful as a measure of vegetation effects for agricultural crops other than dense corn. A linear equation was developed to predict percent field capacity as a function of L-band emissivity and the vegetation index. The prediction algorithm improved the estimation of moisture significantly over predictions from L-band emissivity alone.

The results of this experiment infer that effective estimation of soil moisture will require as a minimum a combination of a dual polarized L-band radiometer (at some incident angle greater than 15 degrees) and a visible/infrared imager with at least two bands that are suitable for developing the perpendicular vegetation index. Most importantly all of the sensors must have a satisfactory means for calibration. An active microwave system could also be used for the roughness measurement if such a system is calibrated. Further experiments along these lines should be conducted with truck systems in order to maintain more control of the site and better calibration of instruments, while collecting and processing the data at lower cost.

REFERENCES

1. Barrick, D. E. 1968. Rough surface scattering band on the specular point theory. IEEE Trans. on Antennas and Prop. Ap-16 (4):449-454.

2. Basharinov, A. Ye and H. M. Shutko. 1978. Determination of the moisture content of the earth's cover by superhigh frequency (microwave) radiometric methods: a review. Radio Engineering and Electronic Physics, 23:1-12, translation.

3. Basharinov, A. Ye, L. F. Borodin and A. M. Shutko. 1974. Passive microwave sensing of moist soils. Preprints, 9th Int. Symp. Remote Sensing of Environ. April 15-19. Environmental Research of Michigan, Ann Arbor, MI. p. 363-367.

4. Beckman, P. 1965. Scattering by composite rough surfaces. Proc. IEEE 53:1012-1015.

5. Beckman, P. and A. Spizzichino. 1963. The scattering of electromagnetic waves from rough surfaces. Macmillan Co. New York.

6. Berger, D. H. 1970. Texture as a discriminant of crops on radar imagery, IEEE Trans., Geosci. Elect. GE-8(4):344-348.

7. Blanchard, A. J. 1977. Volumetric effects in the depolarization of electromagnetic waves scattered from rough surfaces. Ph.D. Dissertation. Dept. of Electrical Engineering, Texas A&M University, College Station, TX. 192 p.

8. Blanchard, B. J. 1972. Measurements from aircraft to characterize watershed, 4th Annual Earth Resources Program Review, NASA, Manned Spacecraft Center, Houston, TX. Jan, 17-21, V(118):1-14.

9. Blanchard, B. J. 1978. Measurement of soil moisture trends with airborne scatterometers. Progress Rep. 3458-2, Remote Sensing Center. Texas A&M University, College Station, TX. 102 p.

10. Blanchard, B. J. 1979. Soil moisture. Proc. Fifth Annual William T. Pecora Memorial Symp. on Remote Sensing. American Water Resources Association, Sioux Falls, SD. June 10-15, p. 331-332.

11. Blanchard, B. J. 1980. Measurements of soil moisture trends with airborne scatterometers. Progress Rep. RSC 3458-4. Remote Sensing Center. Texas A&M University, College Station, TX. 67 p.

12. Blanchard, B. J. 1981. Personal Communications.

13. Blanchard, B. J., J. L. Nieber and A. J. Blanchard. 1979. Continuation of measurements of hydrologic soil cover complex with airborne scatterometers. Final Rep. 3496. NSG-5156, Remote Sensing Center, Texas A&M University, College Station, TX. 43 p.

14. Blinn, J. C. and J. G. Quade. 1972. Microwave properties of geological materials: studies of penetration depth and moisture effects. 4th Annual Earth Resources Program Review NASA Manned Spacecraft Center, Houston, TX. Jan. 17-21. II:53-1 to 53-12.

15. Brady, N. C. 1978. The nature and properties of soils. 8th edition McMillan Publ. Co. New York. 639 p.

16. Burke, W. J. and J. F. Paris. 1975. A radiative transfer model for microwave emission from bare agricultural soils. NASA Tech. Memo. TMX-58166. NASA/JSC. Houston, TX.

17. Bush, T. F. and F. T. Ulaby. 1978. An evaluation of radar as a crop classifier. Remote Sensing Environ. 7:15-36.

18. Casey, K. F. 1972. Application of Hill's Functions to problems of propagation in stratified media. IEEE Trans. on Antennas and Propa. AP-20(3):368-374.

19. Choudhury, B. J. 1981. Personal Communication.

20. Choudhury, B. J., T. J. Schmugge. R. W. Newton, and A. Chang. 1979. Effect of surface roughness on the microwave emission from soils. J. Geophys. Res. 84:5699-5706.

21. Cihlar, J. and F. T. Ulaby. 1974. Dielectric properties of soils as a function of moisture content. RSL Tech. Rep. 177-47. The University of Kansas Center for Research, Lawrence, Kansas. 61 p.

22. Clark, B. V. and R. W. Newton. 1979. JSME scatterometer data processing. Final Report 3337. NAS9-14875, Remote Sensing Center, Texas A&M University, College Station, TX. 110 p.

23. Claassen, J. P., R. O. Stroud, B. V. Clark, B. R. Jean and R. W. Newton. 1979. The system and hardware design of real-time fan beam scatterometer data processors. Final Report 3556, Remote Sensing Center, Texas A&M University, College Station, TX. 275 p.

24. Cosgriff, R. L., W. H. Peake and R. C. Taylor, 1960. Terrain scattering properties for sensor system design (terrain handbook II) Engineering Experiment Station. College of Engineering, The Ohio State University, Columbus. Bulletin Vol. 29, No. 3, 118 p.

25. Dellwig, L. F. and R. K. Moore, 1966. The geological value of simultaneously produced like- and cross-polarized radar imagery, J. Geophys. Res. 71(14):3597-3601.

26. Du, L. 1969. Scattering and absorption by large leaves at microwave frequencies. Tech. Rep. 2440-6 Electro. Science Laboratory. Ohio State University, Columbus, OH.

27. Eagleman, J. R. and W. C. Lin. 1976. Remote sensing of soil moisture by a 21 cm passive radiometer. J. Geophys. Res. 81: 3660-3666.

28. Ellermeier, R. D., D. S. Simonett and L. F. Dellwig. 1967. The use of multi-parameter radar imagery for the discrimination of terrain characteristics. IEEE, International Convention Record, Part 2, New York, p. 127-135.

29. Fung, A. K. 1966. On depolarization waves backscattered from a rough surface. Planetary Space Sciences 14:563-568.

30. Gates, D. M. 1980. Biophysical ecology. Springer-Verlag. New York. 611 p.

31. Hess, S. L. 1959. Introduction to theoretcal meteorology. Holt, Rinehard and Winston. New York. 355 p.

32. Hoekstra, P., and A. Delaney. 1974. Dielectric properties of soils at UHF and microwave frequencies. J. Geophys. Res. 79: 1699-1709.

33. Jackson, T. J., A. Chang, and T. J. Schmugge, 1981a. Aircraft active microwave measurements for estimating soil moisture, Photogram. Eng. and Remote Sensing 47:801-805.

34. Jackson, T. J., T. J. Schmugge and J. R. Wang. 1981b. Effects of vegetation on passive microwave estimates of soil moisture. Intern. Geosci. and Remote Sensing Symp., IEEE, Washington, D. C., June 8-10, I:375-387.

35. Kirdiashev, K. P., A. A. Chukhlantsev and A. M. Shutko. 1979. Microwave radiation of the earth's surface in the presence of vegetation cover. Radiotecknika i Elecktronika 24: 256-264 (translation).

36. Kodis, R. 1966. A note on the theory of scattering from an irregular surface. IEEE Trans. on Antennas and Propa. AP-14:77-82.

37. Leader, J. C. and W. Dalton. 1972. Bidirectional scattering of electromagnetic waves from the volume of dielectric materials. J. Appl. Physics 43:3080.

38. Lee S. L. 1974. Dual frequency microwave radiometer measurements of soil moisture for bare and vegetated rough surfaces. Tech. Rep. RSC-56. Remote Sensing Center, Texas A&M University, College Station, TX. 211 p.

39. Lintz, J. and D. S. Simonett. 1976. Remote sensing of environment. Addison-Wesley Publ. Co. Reading, Mass. 694 p.

40. Lundien, J. R. 1966. Terrain analysis by electromagnetic means, Report 2, Radar responses to laboratory prepared soil samples, Technical Report No. 3-693, U. S. Army Corps of Engineers, U. S. Army Engineer Waterways Experiment Station, Vicksburg, Mississippi, September, 55 p.

41. MacDonald, H. C. and W. P. Waite. 1971. Soil moisture detection with imaging radars. Water Resources Research 7:100-110.

42. McFarland, M. J. 1976. The correlation of Skylab L-band brightness temperatures with antecedent precipitation. Preprints Conf. on Hydrometeorology. Amer. Met. Soc. Ft. Worth. p. 60-65.

43. McFarland, M. J. and B. J. Blanchard. 1977. Temporal correlations of antecedent precipitation with Nimbus 5 ESMR brightness temperatures. Preprints 2nd Conf. Hydrometeorology. Toronto, Ontario Canada. Amer. Meteor. Soc. p. 311-315.

44. McFarland, M. J., C. Jones, S. W. Theis and W. D. Rosenthal. 1981. Measurement of soil moisture with airborne scatterometers. Progress Rep. RSC 3458-5. Remote Sensing Center. Texas A&M University. College Station, TX. 46 p.

45. Marion, J. B. 1975. Classical electromagnetic radiation. Academic Press. New York. 479 p.

46. Moore, R. K. and D. S. Simonett. 1967. Radar remote sensing in biology. Bioscience 17(6):384-390.

47. Morain, S. A. and D. S. Simonett, 1966. Vegetation analysis with radar imagery. Proceedings, Fourth Symposium on Remote Sensing of the Environment, Report No. 4864-11-X, Willow Run Laboratories of the Institute of Science and Technology, The University of Michigan, Ann Arbor, April, p. 605-622.

48. Newton, R. W. 1977. Microwave remote sensing and its applications to soil moisture detection. Tech. Rep. RSC-81, Remote Sensing Center, Texas A&M University, College Station, TX. 500 p.

49. Newton, R. W. 1981. Personal Communication.

50. O'Neill, P. 1981. Personal Communication.

51. Paris, J. F. 1969. Microwave radiometry and its application to marine meteorology and oceanography. Ref No. 69-11. Contract No. 2119(04). Dept. of Oceanography. Texas A&M University, College Station, TX. 210 p.

52. Paris, J. F. 1971. Transfer of thermal microwave in the atmosphere. NASA Grant NGR-44-001-098. Dept. of Meteorology Rpt. Texas A&M University, College Station, TX. 257 p.

53. Peake, W. H. 1959a. Interaction of electromagnetic waves with some natural surfaces. IRE Trans. on Antennas and Propa. AP-7: 5324-5329.

54. Peake, W. H. 1959b. Theory of radar return from terrain. IRE Convention Record, 7:27-41.

55. Poe, G. A., A. Stogryn and A. T. Edgerton. 1971. Determination of soil moisture content using microwave radiometry. Final Tech. Rep. 1684-1. Aerojet General Corp. El Monte, California.

56. Priestley, C. H. B. and R. J. Taylor. 1972. On the assessment of surface heat flux and evaporation using large-scale parameters. Mon. Weather Rev. 100:81-92.

57. Richardson, A. J. and C. L. Wiegand. 1977. Distinguishing vegetation from soil background information. Photogram. Eng. and Remote Sensing. 48:1541-1552.

58. Richerson, J. A. 1971. An experimental evaluation of a theoretical model of the microwave emission of a natural surface. Tech. Rpt. RSC-27. Remote Sensing Center, Texas A&M University, College Station, TX.

59. Rosenthal, W. D. 1981. Development of visible/infrared/microwave agricultural classification and biomass models. Ph.D. Dissertation. Dept. of Agricultural Engineering, Texas A&M University. College Station, TX. 214 p.

60. Rouse, J. W. Jr. 1972. The effect of the subsurface on the depolarization of rough-surface backscatter. Radio Sci. 7: 889-895.

61. Rouse, J. W. Jr., H. C. MacDonald and W. P. Waite. 1969. Geoscience applications of radar sensors. IEEE Trans. Geosci. Elect. GE-7(1):1-19.

62. Rouse, J. W. Jr., R. H. Haas, J. A. Schell and D. W. Deering. 1973. Monitoring vegetation systems in the great plains with ERTS. Third ERTS Symp. NASA SP-351. I:309-317.

63. Schmugge, T. J. 1976. Preliminary results from the March 1975 soil moisture flight. Goddard Space Flight Center Rep. 913-76-216. Greenbelt, MD 23 p.

64. Schmugge, T. J. 1978. Remote sensing of surface soil moisture. J. Appl. Meteorology 17:1549-1557.

65. Schmugge, T. J. 1980a. Effect of texture on microwave emission from soils. IEEE Trans. on Geosci. and Remote Sensing GE-18:353-361.

66. Schmugge, T. J. 1980b. Microwave approaches in hydrology. Photogram. Eng. and Remote Sensing 46(4):495-507.

67. Schmugge, T. J. 1980c. Soil moisture sensing with microwave radiometers. Reprints, 1980 Machine Processing of Remote Sensed Data Symp., June, p. 346-354.

68. Schmugge, T., P. Gloesen, T. Wilheit, and F. Geiger. 1974. Remote sensing of soil moisture with microwave radiometers. J. Geophys. Res. 79(2):317-323.

69. Schmugge, T. J., J. M. Meneely, A. Rango, and R. Neff. 1977. Satellite microwave observations of soil moisture variations. Water Resources Bull. 13:265-281.

70. Schwarz, D. E. and F. Caspall. 1968. The use of radar in the discrimination and identification of agricultural land use. Proceedings, Fifth Symp. on Remote Sensing of the Environment. Report No. 4864-18-X, Willow Run Laboratories of the Institute of Science and Technology The University of Michigan, Ann Arbor. p. 233-247.

71. Semenov, B. 1966. An approximate calculation of scattering of electromagnetic waves from a rough surface. Radioteknika Electronika (USSR) 11:1351-1361.

72. Sibley, R. 1973. Microwave emission and scattering from vegetated terrain. Tech. Rep. RSC-44 Remote Sensing Center, Texas A&M University, College Station, TX.

73. Simonett, D. S. 1970. Remote sensing with imaging radar: a review. Geoforum, No. 2:61-74.

74. Stogryn, A. 1970. The brightness temperature of a vertically structured medium. Radio Sci. 5(12):1397-1406.

75. Taylor, R. C. 1959. Terrain return measurements at X, Ku and Ka band. IRE Convention Record, 7:19-26.

76. Taylor, S. A. and G. L. Ashcroft. 1972. Physical edaphology-the physics of irrigated and non-irrigated soils. Freeman and Co., San Francisco. 533 p.

77. Theis, S. W. 1979. Surface soil moisture estimation with the electrically scanning microwave radiometer (ESMR). M.S. Thesis. Dept. of Meteorology, Texas A&M University, College Station, TX.

78. Tsang, L., E. Njoku and J. A. Kong. 1975. Microwave thermal emission from a stratified medium with non-uniform temperature distribution. J. Appl. Physics 46(2):5127-5133.

79. Ulaby, F. T. 1974. Radar measurement of soil moisture content. IEEE Trans. Antenna Propa. AP-22(2)257-265.

80. Ulaby, F. T., M. C. Dobson, and G. A. Bradley. 1977. If you want to remotely sense soil moisture, use a C-band radar. Proc. Microwave Remote Sensing Symp. Dec. 6-7, 1977, NASA JSC, Houston, TX. pp 51-74.

81. Ulaby, F. T., G. A. Bradley and M. C. Dobson. 1979. Microwave backscatter dependence on surface roughness, soil moisture, and soil texture: Part II, Vegetation--covered soil. IEEE Trans. Geosci. Elect. GE-17(2):33-40.

82. Ulaby, F. T., G. A. Bradley and M. C. Dobson. 1978. Microwave backscatter dependence on surface roughness, soil moisture, and soil texture: Part I, bare soil. IEEE Trans. Geosci. Elect. GE-16(4):286-295.

83. Ulaby, F. T., and P. P. Batlivala. 1976. Optimum radar parameters for mapping soil moisture. IEEE Trans. Geosci. Elect. GE-14(2):81-93.

84. Waite, W. P. and K. R. Cook. 1974. Broad spectrum microwave systems for remotely measuring ecological parameters. Final Rpt. NSF-31515. Department of Electrical Engineering, University of Arkansas, Fayetteville, AK.

85. Wang, J. R., J. Shiue, E. Engman, J. McMurtrey, P. Lawlass, T. Schmugge, T. Jackson, W. Gould, J. Fuchs, C. Calhoon, T. Carnahan, E. Hirschmann, and W. Glazar. 1980. Remote measurements of soil moisture by microwave radiometers at BARC test site, Technical Memorandum 80720, NASA Goddard Space Flight Center, Greenbelt, MD.

APPENDIX A DATA PROCESSING PROCEDURES

DATA PROCESSING PROCEDURES

The processing of the Guymon and Dalhart data sets was accomplished through joint effort at Texas A&M University. This appendix summarizes the work and can also be found in Blanchard (1980), McFarland et al. (1981), and Rosenthal (1981).

Scatterometer Processing

Scatterometer data were collected aboard the NASA C-130 in analog form on a 14-track tape. Copies of the tape were later sent to Texas A&M University/Remote Sensing Center for individual processing, which consisted of three phases. The initial processing converted the analog data to digital and copied the digital data onto 9-track magnetic tapes. The second phase processed the digital data using software which calculated sigma (σ^0) values for each look angle at given time intervals. Data were processed so that a cell size roughly had a length of 25 m for 13.3 GHz, 38 m for 4.75 GHz, 50 m for 1.6 GHz, and 75 m for 0.4 GHz. The processing software was described by Claassen et al. (1979) and Clark and Newton (1979).

After processing scatterometer data, field start and stop times were determined for each frequency and polarization from line plots of σ^0 versus time, and aerial photographs. Times were adjusted by shifting the start/stop times at least 0.5 seconds to insure full scatterometer coverage within the field. The final start and stop times defined the field boundary and were used in determining field averages for each frequency, polarization, and look angle. Time frames during excessive aircraft roll and drift (roll greater than 3.5°; drift

greater than 9°) were noted and data from affected look angles were deleted from further analysis.

No known technique or mechanism was available to calibrate all of the scatterometers. Consequently, any temporal variation in σ° could indicate either soil moisture, roughness, or vegetation changes, or unstable sensors.

Due to excessive aircraft roll and drift, several look angles had to be eliminated at Dalhart and Guymon due to the uncertainty of the cell being within the field. At Dalhart, data from only one field had to be eliminated--field 16 on 8/18/80. Also, data at 40° and 45° look angles off nadir from several other fields on 8/18/80 were eliminated due to excessive drift (Table A1). At Guymon, flying conditions were much worse; consequently, data from more fields needed to be deleted. A complete list of omitted look angles is given in Table A2. Data from 8/11, 8/14, and 8/17/78 were most questionable.

Passive Microwave Processing

The raw analog data collected aboard the aircraft were converted to digital uncorrected brightness temperatures at NASA/Goddard Space Fight Center (GSFC). Corrected brightness temperatures were calculated from an equation developed at NASA/JSC (O'Neill, 1981):

$$T_B = \frac{1}{t}\left[T_U\left(\frac{L}{1-r^2}\right) - \frac{r^2(T_\sigma)(L)}{1-r^2} - T_L(L-1) - e\,T_R\right] \qquad (A1)$$

where t is the transmittance of the radome, e is the emissivity of the radome, T_U is the uncorrected brightness temperature based on raw digital counts, L is antenna cable loss factor, T_L is an antenna

TABLE A1. QUESTIONABLE SCATTEROMETER DATA FOR DALHART AS OF 5-6-81

Date	Field #	Questionable Analysis
8/14/80	All data is good	
8/16/80	All data is good	
8/18/80	L12 R2 20,8,18	45° (drift 9°)
	L12 R2 14	40, 45° (drift 11°)
	L11 R3 16	All Angles

TABLE A2. QUESTIONABLE SCATTEROMETER DATA FOR GUYMON

Date	Field #		Questionable Analysis
8/2/78	L1 R1	2,4,6,7,8,2x,1x	40°,45° (-8° drift, 2° roll)
	L2 R1	10,13,14,15,2a,2x,1x	45° (-9° drift)
	L1 R2	2,4,6,7,1a,2x,1x	45° (-9° drift)
	L2 R2	15,17,2a	45° (-8° drift)
8/8/78	L2 R1	17, 1x	all angles
	L2 R2	2A	all angles
	L4 R1	26	all angles
	L1 R2	2,6,7	all angles
8/11/78	L1 R1	6,8,2x	all angles
	L3 R1	19,22,1x	all angles
	L2 R1	2x,	all angles
	L4 R1	24,25,27	all angles
	L1 R2	4,6,7,1A	all angles
	L3 R2	22	all angles
	L2 R2	10,17	45° (-4° drift, 4° roll)
		2A, 2X	all angles
	L4 R2	24,26,27	all angles
8/14/78	L1 R2	4	all angles
	L3 R2	19	40°,45° (-8° drift, 3° roll)
	L2 R2	13	45° (9° drift)
		10	40°,45° (9° drift, 3° roll)
	L1 R3	all fields	40°,45° (11° drift)
	L3 R3	1x	all angles
	L2 R3	13,14	all angles
		15	45° (9° drift)
8/17/78	L3 R1	21,22	35°,40°,45° (-12° drift)
	L4 R1	2x,24,25,26,27	35°,40°,45° (-12° drift)
	L3 R2	21,22	all angles
		1x,19,20	40°,45° (-10° drift)
	L4 R2	24,25,2x	45° (-9° drift)
8/5/78	L1 R1	2	40°,45°
	L4 R1	2x	40°,45°
	L2 R2	2x	40°,45°
	L4 R2	2x	40°,45°

These fields were deleted from the MFMR plots due to excessive roll; drift was not a factor.

temperature factor, T_R is the radome temperature factor, r^2 is an internal parameter for each frequency, and T_σ is the self-emission of the receiver. The various constants used in the equation were determined from flights over homogeneous areas. Once brightness temperatures were calculated, line plots of T_B versus time were produced and field start and stop times were determined from the plots. The times defined field boundaries and were used in calculating field averages for each frequency and polarization.

Since the passive microwave radiometer was oriented at a constant angle (3° from nadir), any excessive roll would imply questionable MFMR data. Consequently, any time the airplane had roll greater than 3.5°, the field average MFMR data were deleted. Table A3 lists the deleted data. With the exception of data from one flight line at Guymon (1.6 GHz data on 8/11/78 had highly erratic brightness temperatures), brightness temperatures were quite stable. The highly variable brightness temperatures indicated local unmeasured variations in the field. Therefore, the following fields at Guymon were deleted from further analysis: fields 10, 13, 14, 15 and 17.

NS001/M^{2}S Processing

Raw data collected on the NASA C-130 were in analog form. The data were converted to digital onto 9-track tapes at NASA/Johnson Space Center. Included with the surface data were calibration data consisting of digital counts from looks at constant radiance targets aboard the plane. The calibration data were then used to convert digital counts to radiance.

TABLE A3. Guymon and Dalhart Questionable MFMR Data

Date	Field #	% Roll
8/8/78	L2 R1 1X	5.3
8/11/78	L3 R1 1X	4.9
	L1 R2 6	-5.1
	L4 R2 24	4.9
8/14/78	L2 R1 10,17,2a	5.4,-8,-5.6 respectively
	L4 R1 27	4.9
	L3 R3 1X	-4.8
8/17/78	L3 R2 22	5.0
8/18/78	L1 R1 16	6.3

Since radiance is a function of the solar angle, a correction factor was needed before comparing crop radiance differences. All the Dalhart data were normalized to August 18, the day with the smallest solar zenith angle; Guymon data were adjusted to August 11 zenith angle conditions. The correction factor used was

$$R_c = \frac{R_i}{\cos \theta} \qquad (A2)$$

where R_i and R_c are the non-normalized and normalized radiance values, respectively, and θ is the solar zenith angle.

Most of the visible/infrared data were good quality at Dalhart and Guymon. One of the exceptions was the excessively noisy water absorption bands (channels 6 and 7) on 8/14/80 at Dalhart. Since no means was possible to correct the bands, they were eliminated from further data analysis. Also, channel 1 data for fields 6, 8, 10, 12 and 22 were deleted due to unstable calibration.

With the exception of channel 9 (770-863 nm) MMS data at Guymon, the calibration information proved to be quite stable. Table A4a lists the equations used to convert raw digital counts to radiance values. Note channel 9 had three different equations applicable at different periods of the experiment.

All of the working NS001 bands had less stable calibration information at Dalhart. Table A4b lists the equations used to convert digital counts to radiance values. Note several channels had different calibration values on each flight day.

Calibration of the thermal band proved to be different for Guymon and Dalhart. The calibration, using the PRT-5 data, showed that

TABLE A4. Equations Used to Convert Raw NSOO1/MMS Digital Counts (DC) to Radiance Values, R, (watts $cm^{-2}ster^{-1}$) for Guymon (a) and Dalhart (b)

a.	channel	4	$R = \frac{10.46 \times 10^{-4}}{233} * (DC-12)$
		7	$R = \frac{9.61 \times 10^{-4}}{230} * (DC-13)$
		8	$R = \frac{8.14 \times 10^{-4}}{230} * (DC-14)$
		9	$R = \frac{6.98 \times 10^{-4}}{232} * (DC-12)$ (8/2, 8/5, and 8/8)
		9	$R = \frac{6.98 \times 10^{-4}}{100} *(DC-10)$ (8/11)
		9	$R = \frac{6.98 \times 10^{-4}}{160} *(DC-17)$ (8/14)
b.	channel	1	$R = \frac{1.96 \times 10^{-4}}{207} *(DC-1)$ (8/14 & 8/16 (Flt 1))
		1	$R = \frac{1.96 \times 10^{-4}}{151} *(DC-1)$ (8/16 (Flt 2))
		1	$R = \frac{1.96 \times 10^{-4}}{70} *(DC-1)$ (8/18)
		2	$R = \frac{4.63 \times 10^{-4}}{210} *(DC-21)$ (8/14 - 8/16)
		2	$R = \frac{4.63 \times 10^{-4}}{140} *(DC-21)$ (8/18)
		3	$R = \frac{5.61 \times 10^{-4}}{224} *(DC-29)$ (8/14-8/16)
		3	$R = \frac{5.61 \times 10^{-4}}{172} *(DC-29)$ (8/18)
		4	$R = \frac{11.42 \times 10^{-4}}{232} *(DC-9)$ (8/14-8/6 (Flt 1))
		4	$R = \frac{11.42 \times 10^{-4}}{171} *(DC-9)$ (8/16 (Flt 2))
		4	$R = \frac{11.42 \times 10^{-4}}{107} *(DC-8)$ (8/18)

TABLE A4. (Continued)

5	$R = \frac{5.43\times10^{-4}}{232}$	*(DC-8) (8/14-8/16 (Flt 1))
5	$R = \frac{5.43\times10^{-4}}{147}$	*(DC-9) (8/16 (Flt 2))
5	$R = \frac{5.43\times10^{-4}}{107}$	*(DC-9) (8/18)
6	$R = \frac{2.8\times10^{-4}}{222}$	*(DC-12) (8/16)
6	$R = \frac{2.8\times10^{-4}}{166}$	*(DC-12) (8/18)
6	$R = \frac{1.43\times10^{-4}}{110}$	*(DC-16) (8/16 & 8/18)

at Guymon the low temperature calibration black box aboard the plane was too high while the high temperature calibration black box was measuring the proper temperature. This implied that low surface temperatures were as much as 5 K too high. At Dalhart, the opposite condition occurred. The low temperature calibration box was reading the proper temperature while the high temperature calibration box was reading 5 K too low, suggesting that high surface temperatures were as much as 5 K too low.

The normalization solar correction factors ($\cos \theta_i$) for Dalhart are as follows: August 14, 5.7; August 16 (flight 1), 2.0; and (flight 2), 1.1 and August 18, 1.0. For Guymon, the normalization solar correction factors are August 2, 1.7; August 5, 1.6; August 8, 5.0; August 11, 1.0; August 14, 1.6 and August 17, 1.6. To normalize the two data sets, the Guymon data set required a multiplication factor of 1.3 to roughly match the radiance values at Dalhart.

Soil Moisture

Each sensor has a different cell size. Consequently, to compare data, field averages were determined for each sensor and compared to ground data field averages. Unfortunately, in some cases, averaging point locations of soil moisture proved not to be a reliable field average. For instance, several rows were irrigated and seen by the sensors but not sampled within the field. Also rainfall events occurred at Guymon between sampling periods--on 8/2 and 8/8/78. An attempt was made to correct the soil moisture by adding the amount of rainfall or irrigation, assuming complete infiltration. In some cases, this correction did a good job. But in the end the question-

able soil moisture data were deleted from the data set. The fields at Guymon with deleted soil moisture data were for 8/2: 22, 27, 20, 25, 19, 24, 8/8: 1x, 2x, 2, 10 and 8/17: 1x, (line 2).

With the deletions, calibrations, and normalizations the Guymon and Dalhart data sets were as complete as possible.

APPENDIX B SCATTEROMETER RESPONSES TO SOIL MOISTURE

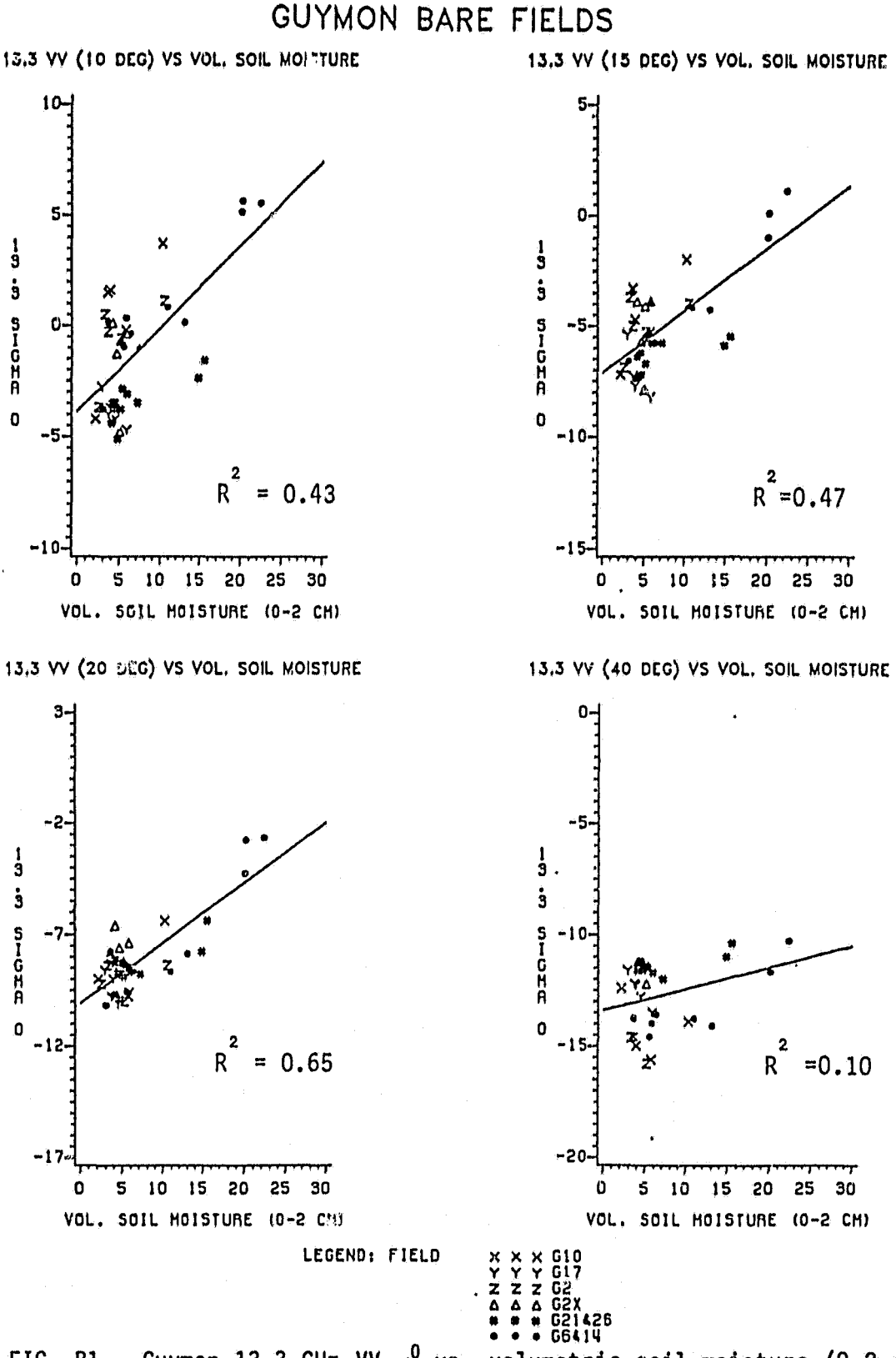

FIG. B1 Guymon 13.3 GHz VV σ^0 vs. volumetric soil moisture (0-2 cm) at 10, 15, 20, and 40 degree incident angles.

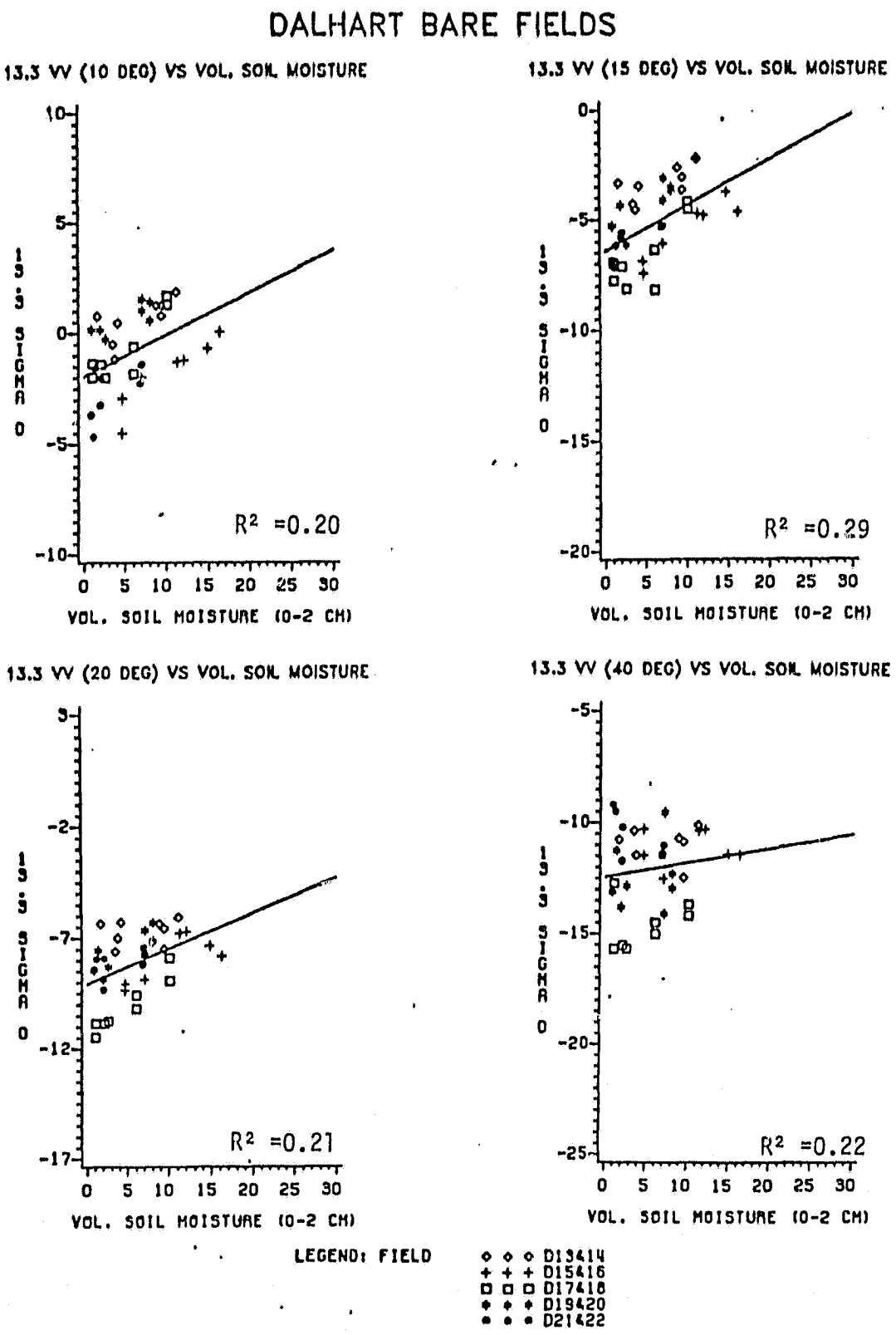

FIG. B2 Dalhart 13.3 GHz VV σ^0 vs. volumetric soil moisture (0-2 cm) at 10, 15, 20, and 40 degree incident angles.

GUYMON BARE FIELDS

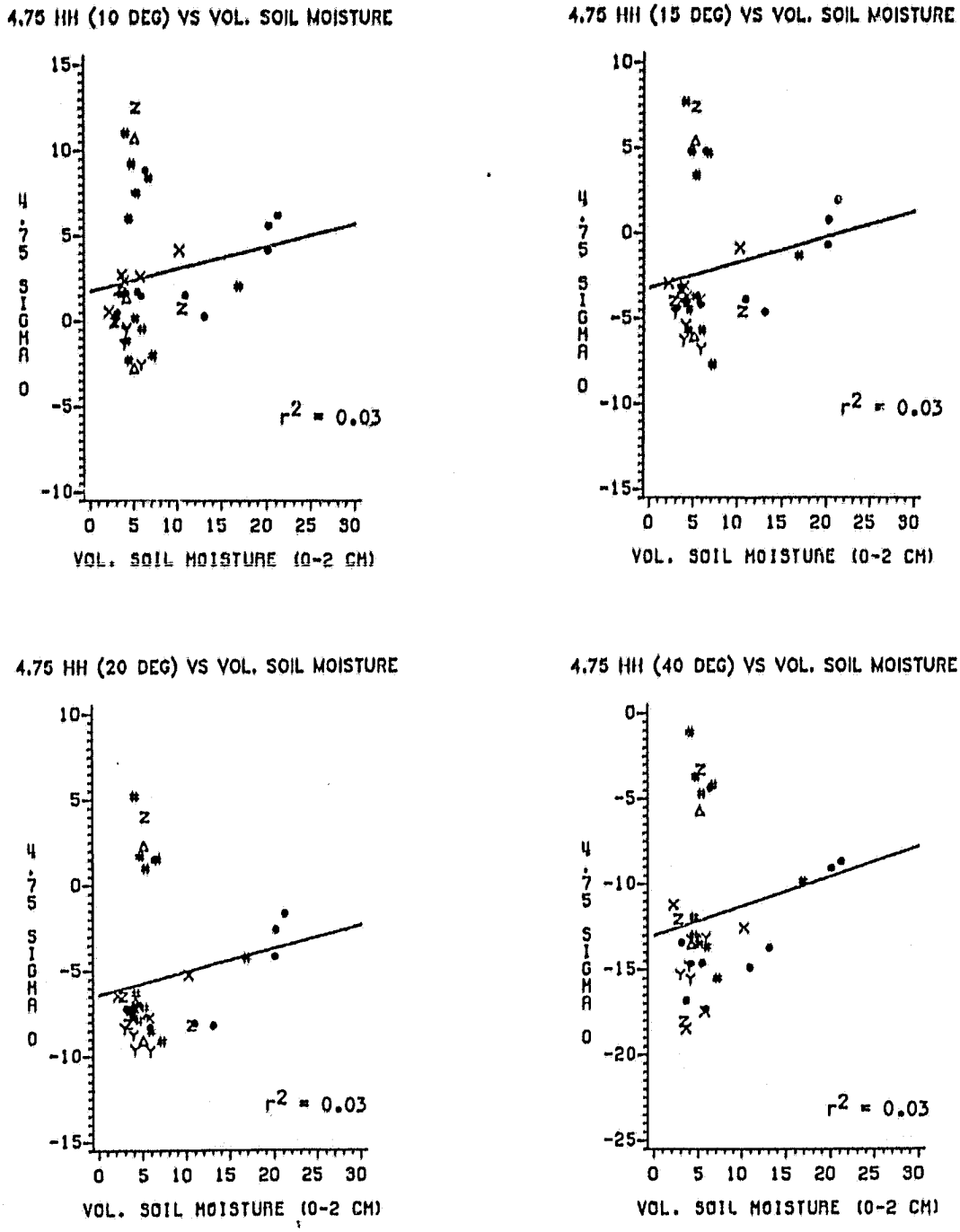

FIG. B3 Guymon 4.75 HH σ^0 vs. volumetric soil moisture (0-2 cm) at 10, 15, 20, and 40 degree incident angles.

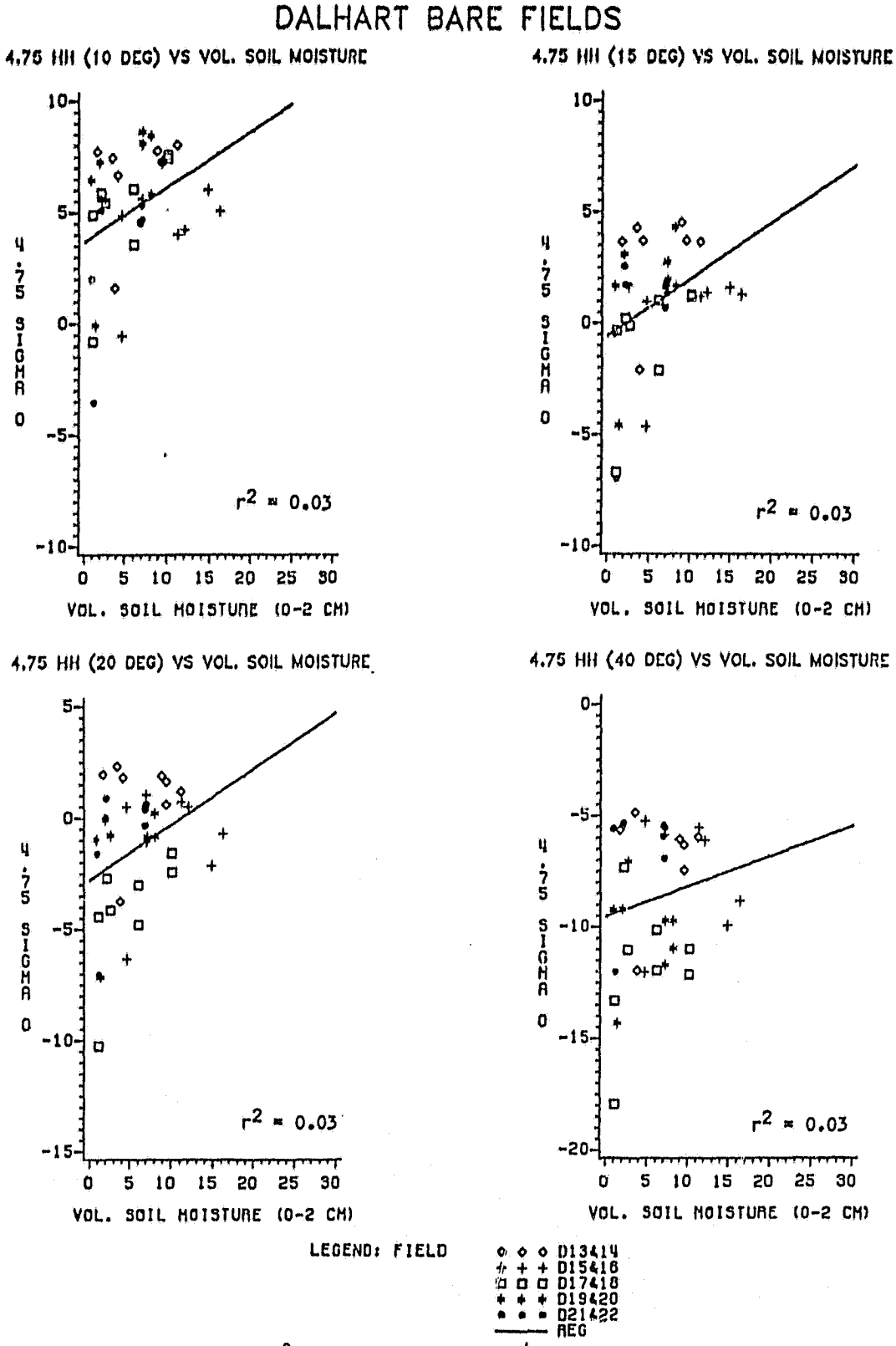

FIG. B4 Dalhart 4.75 HH σ^0 vs. volumetric soil moisture (0-2 cm) at 10, 15, 20, and 40 degree incident angles.

GUYMON BARE FIELDS

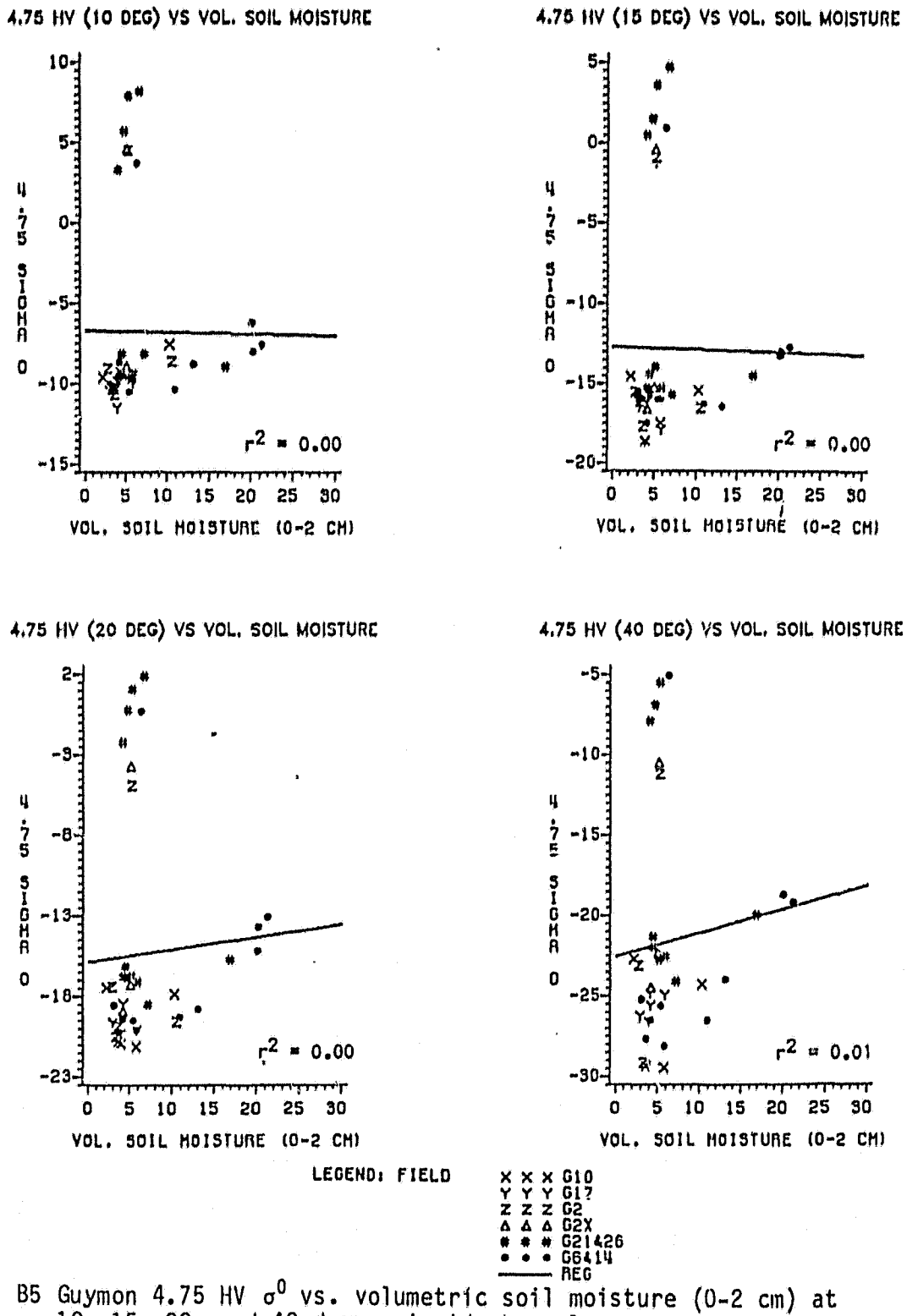

FIG. B5 Guymon 4.75 HV σ^0 vs. volumetric soil moisture (0-2 cm) at 10, 15, 20, and 40 degree incident angles.

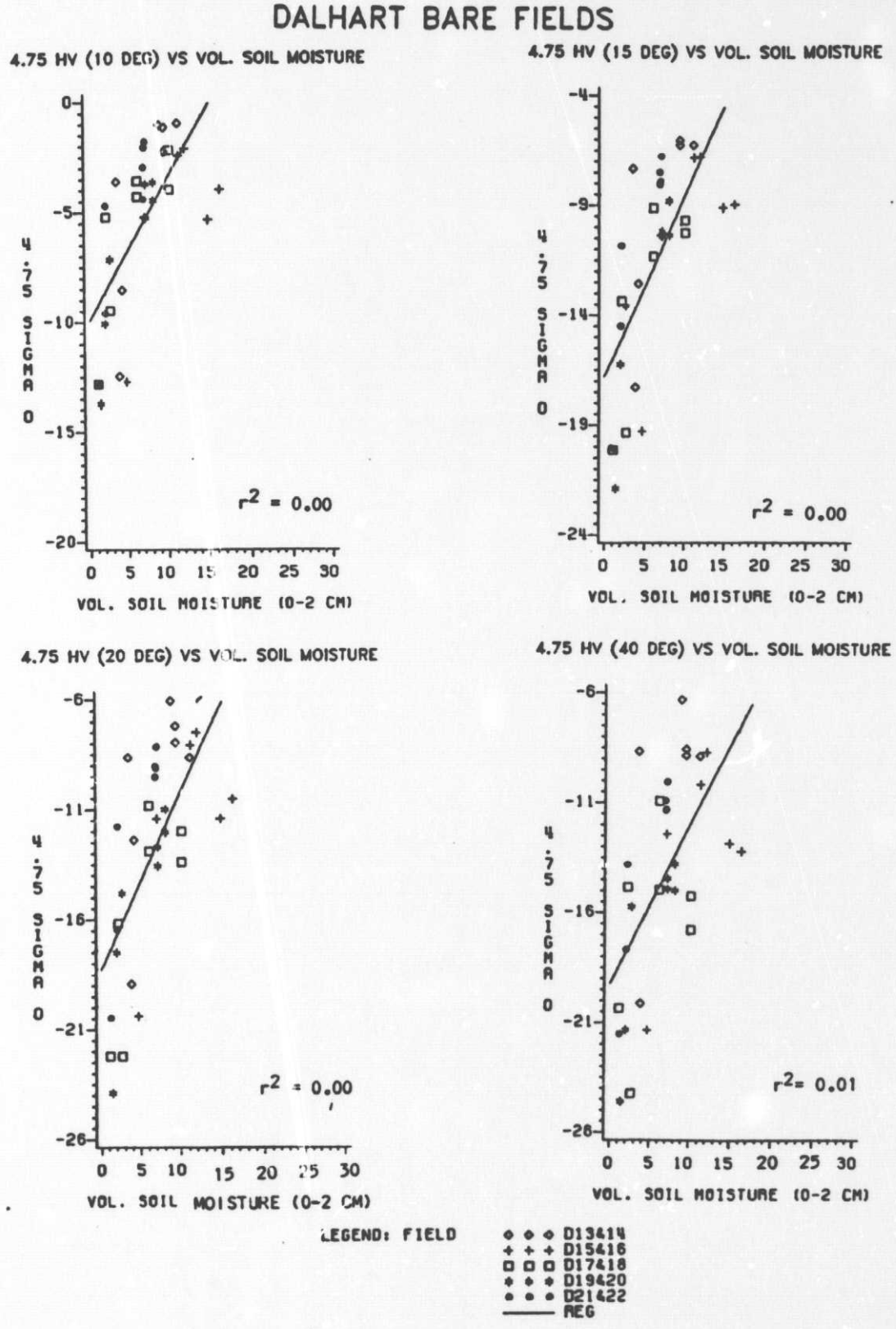

FIG. B6 Dalhart 4.75 HV σ^0 vs. volumetric soil moisture (0-2 cm) at 10, 15, 20, and 40 degree incident angles.

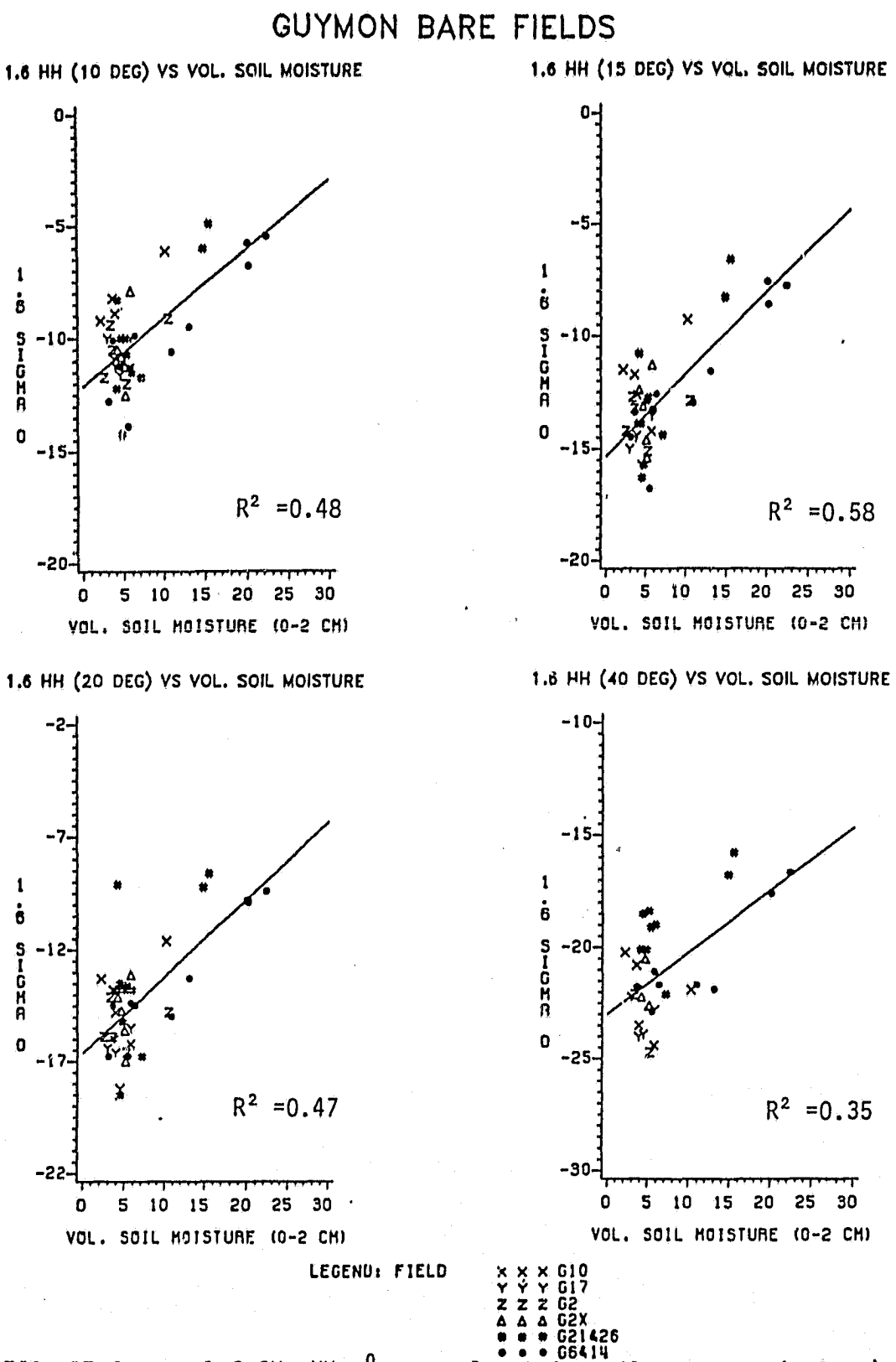

FIG. B7 Guymon 1.6 GHz HH σ^0 vs. volumetric soil moisture (0-2 cm) at 10, 15, 20, and 40 degree incident angles.

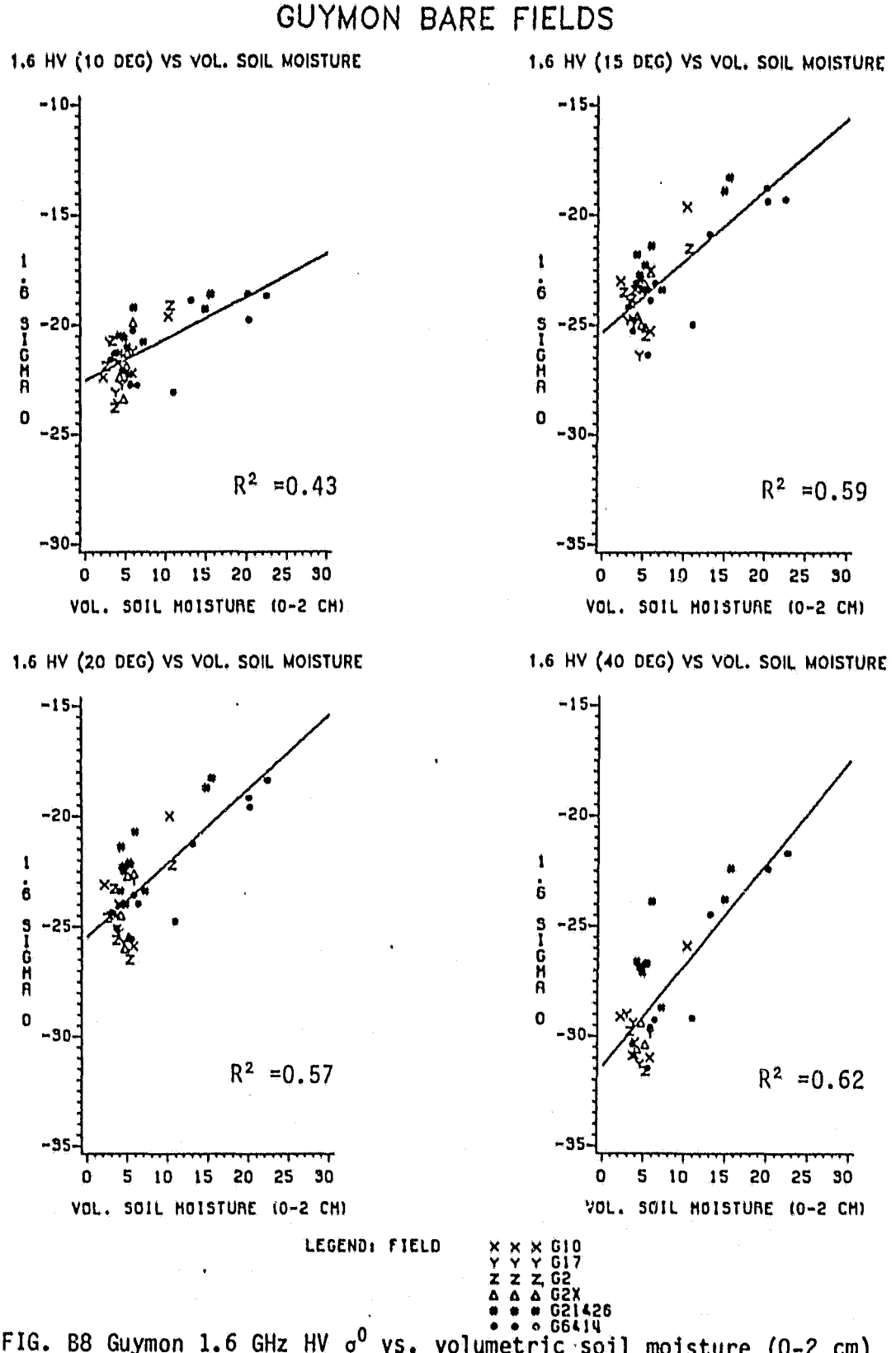

FIG. B8 Guymon 1.6 GHz HV σ^0 vs. volumetric soil moisture (0-2 cm) at 10, 15, 20, and 40 degree incident angles.

DALHART BARE FIELDS

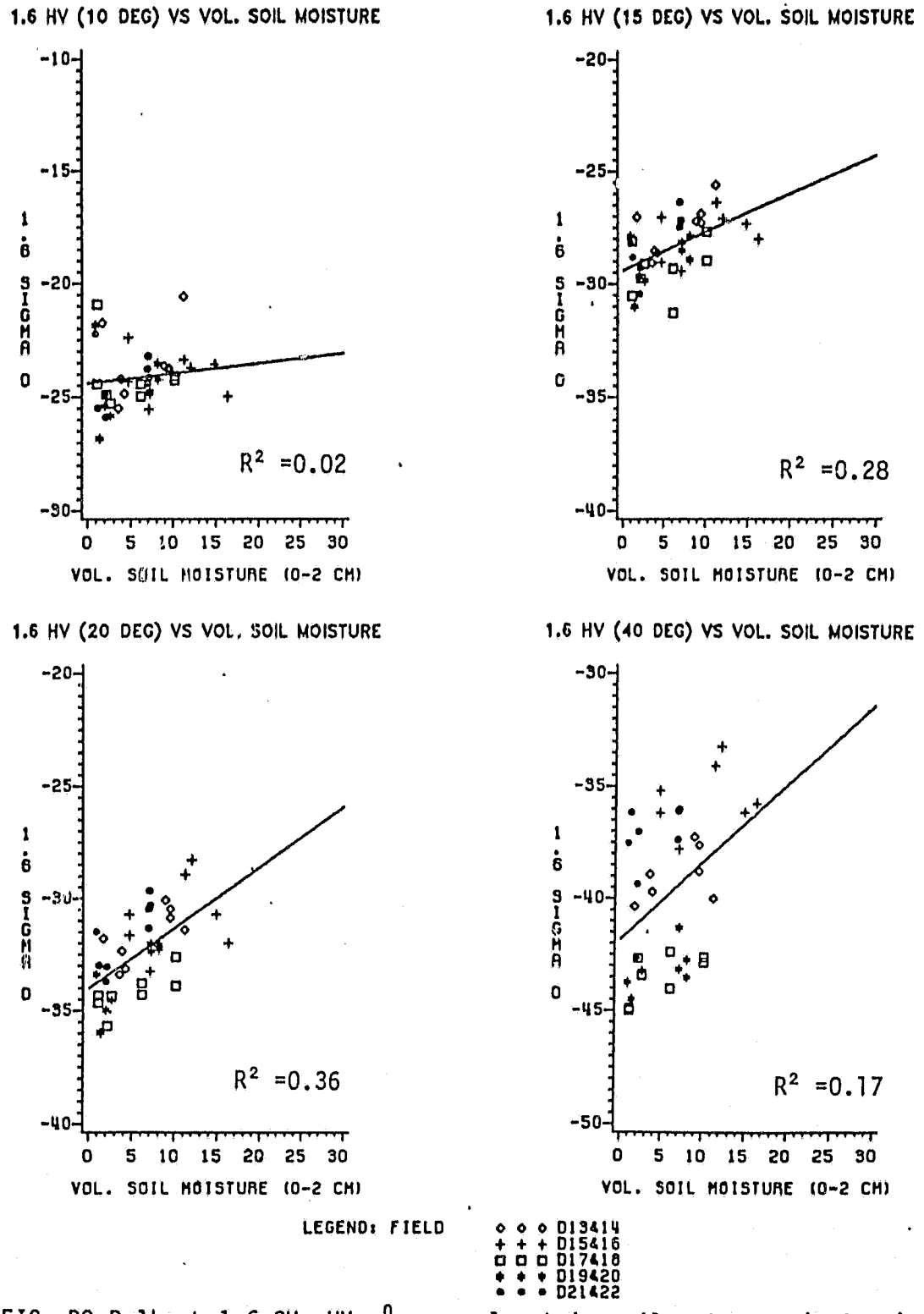

FIG. B9 Dalhart 1.6 GHz HV σ^0 vs. volumetric soil moisture (0-2 cm) at 10, 15, 20, and 40 degree incident angles.

GUYMON BARE FIELDS

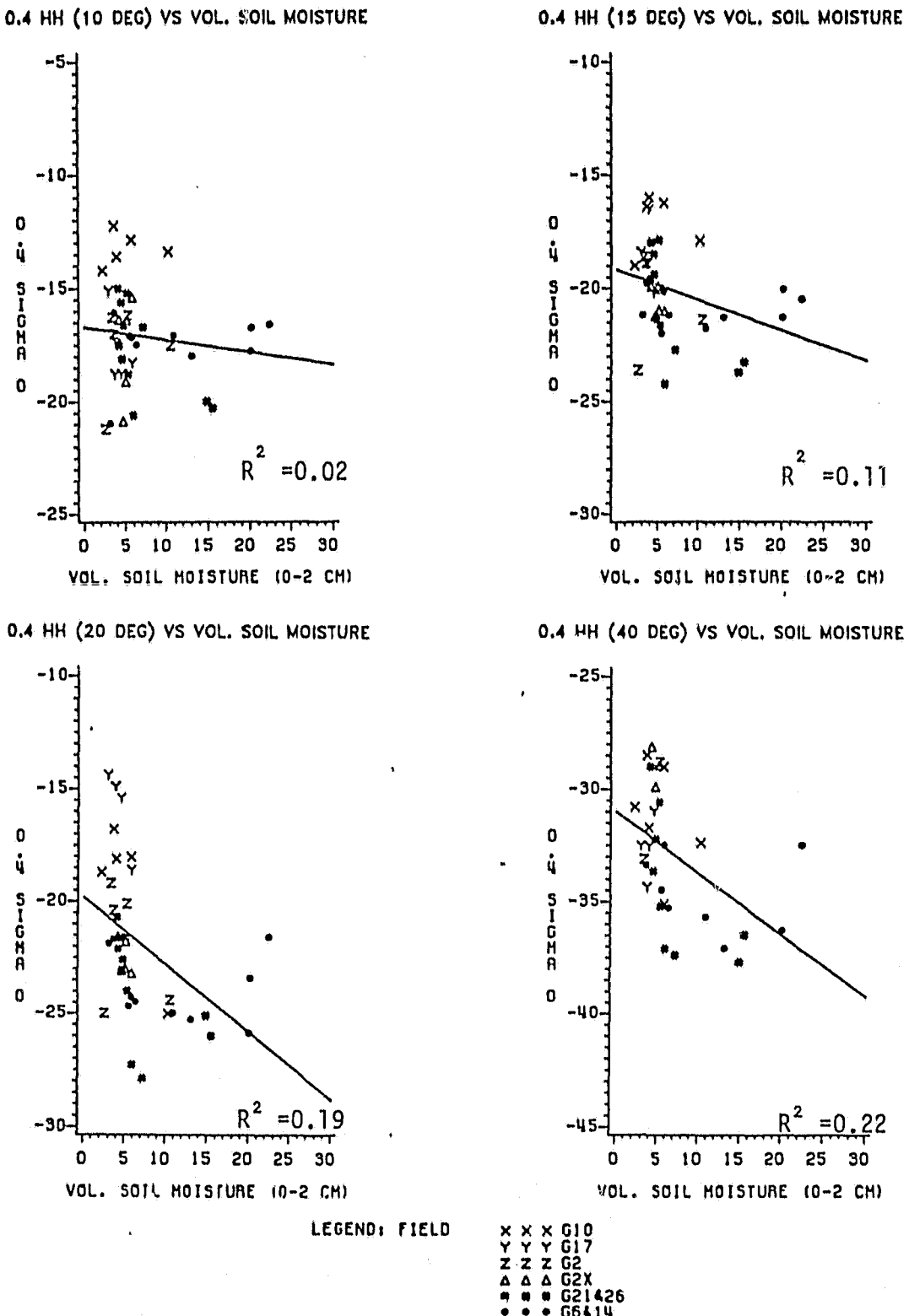

FIG. B10 Guymon 0.4 GHz HH σ^0 vs. volumetric soil moisture (0-2 cm) at 10, 15, 20, and 40 degree incident angles.

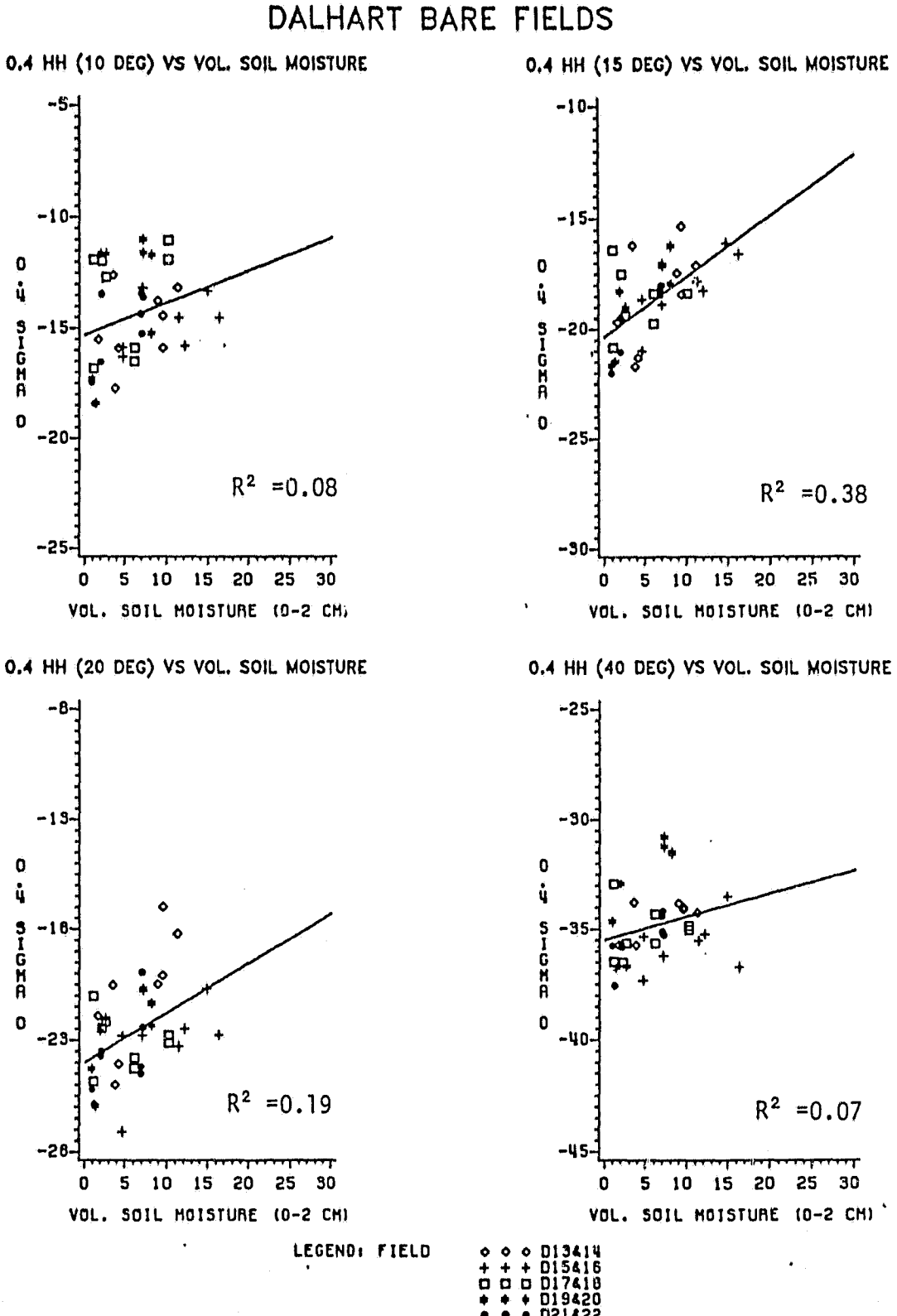

FIG. B11 Dalhart 0.4 GHz HH σ^0 vs. volumetric soil moisture (0-2 cm) at 10, 15, 20, and 40 degree incident angles.

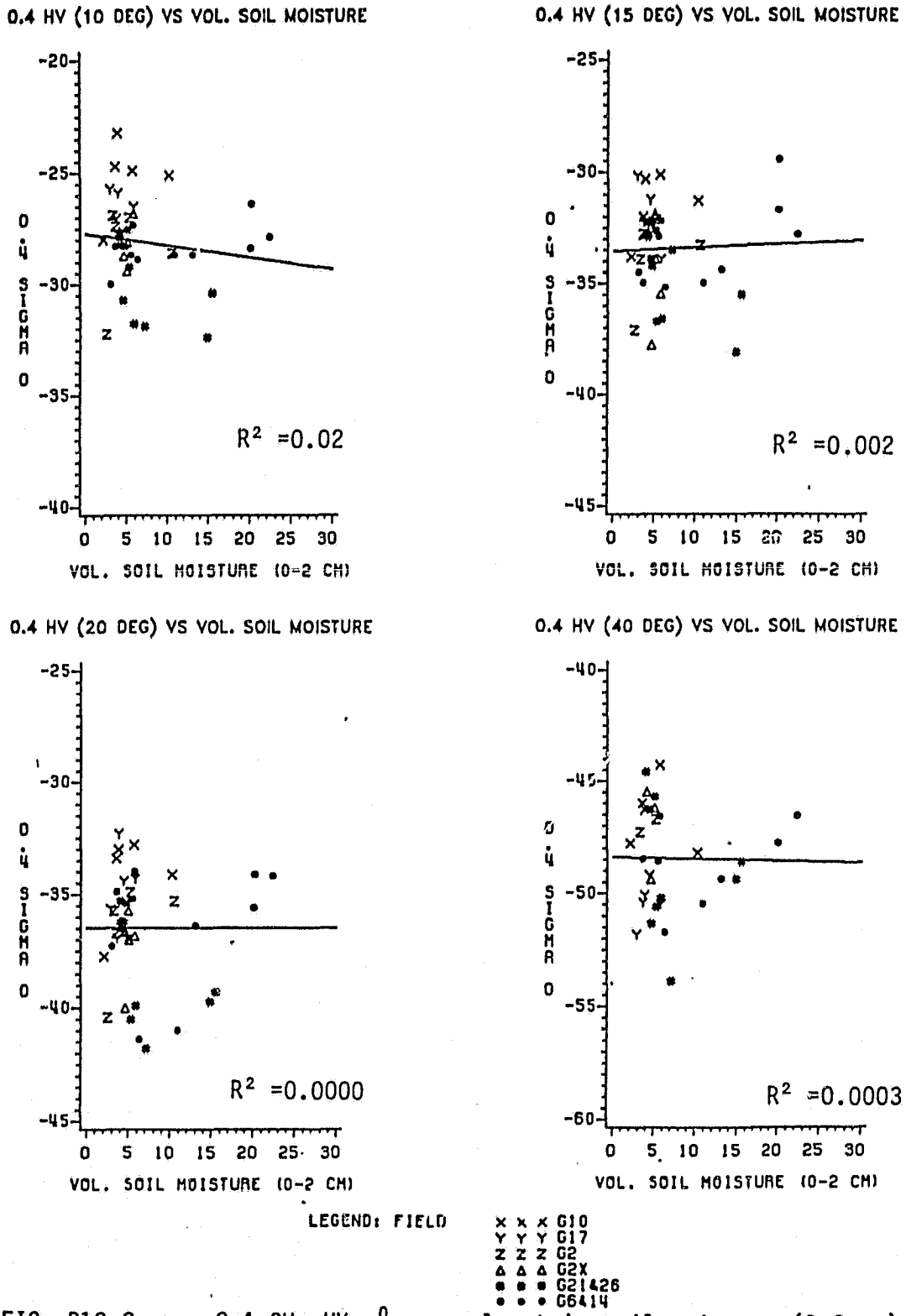

FIG. B12 Guymon 0.4 GHz HV σ^0 vs. volumetric soil moisture (0-2 cm) at 10, 15, 20, and 40 degree incident angles.

DALHART BARE FIELDS

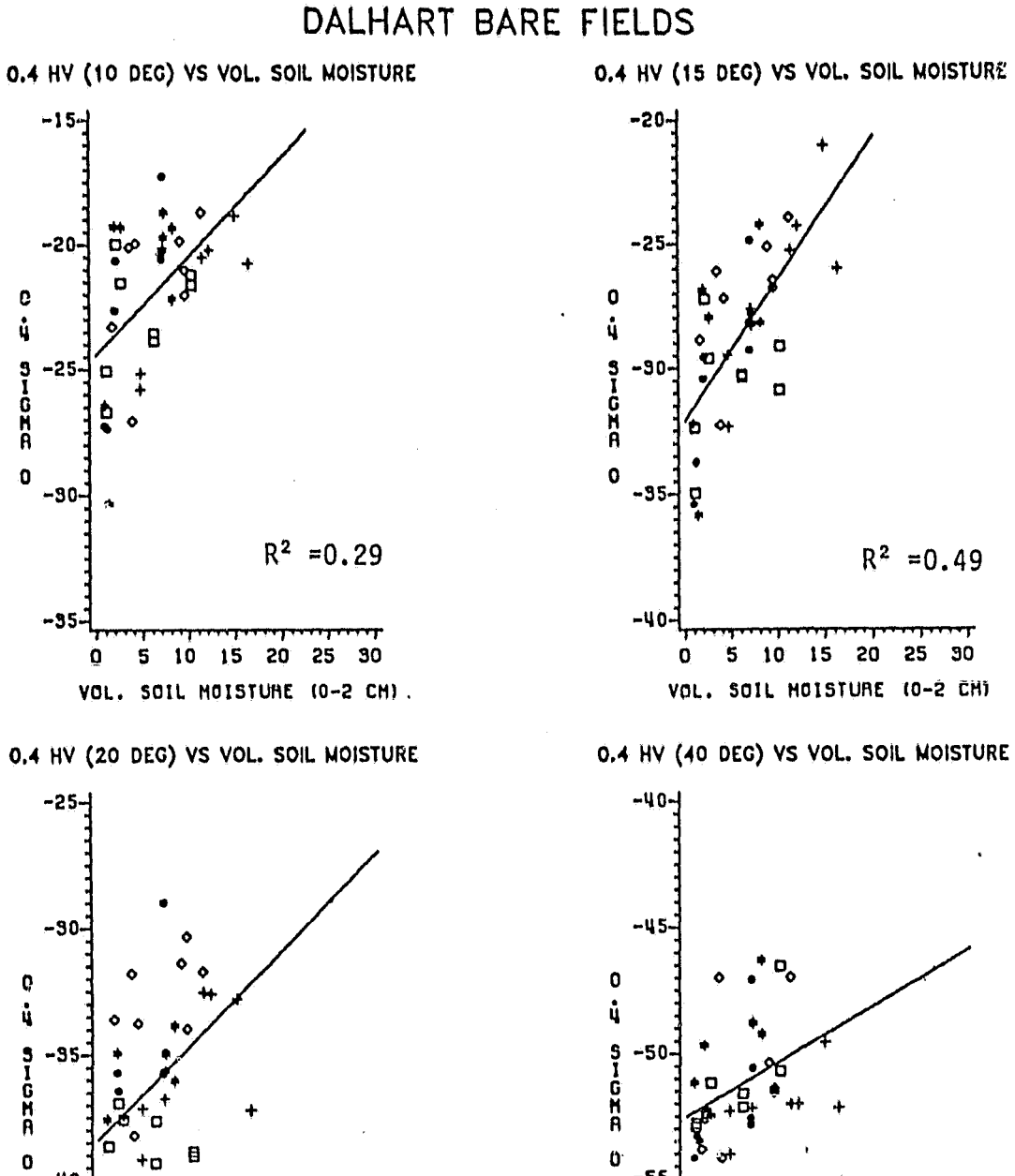

FIG. B13 Dalhart 0.4 GHz HV σ^0 vs. volumetric soil moisture (0-2 cm) at 10, 15, 20, and 40 degree incident angles.